Appendix 2 Experimental Geometry

A. Catcher Foil counting geometry

Jaffey (Ja-54) gives an expression for the average geometry of a finite source as seen by an aperture:

$$G_s = \frac{1}{A_s} \iint_S G_p \, dS \qquad (1)$$

G_p = point source geometry expression

A_s = source area

Generally this must be determined by numerical integration. However, if the source is coaxial with the aperture (detector) and symmetrically distributed about the axis, Eq. (1) can in some cases be explicitly integrated.

In this work the source is rectangular to elliptical in shape and symmetrical about the axis to the detector center. It is assumed that it is a uniformly spread source.

Both rectangular and elliptical geometries are derived, although there is only an insignificant difference.

For a rectangular the following schematic diagram is appropriate.

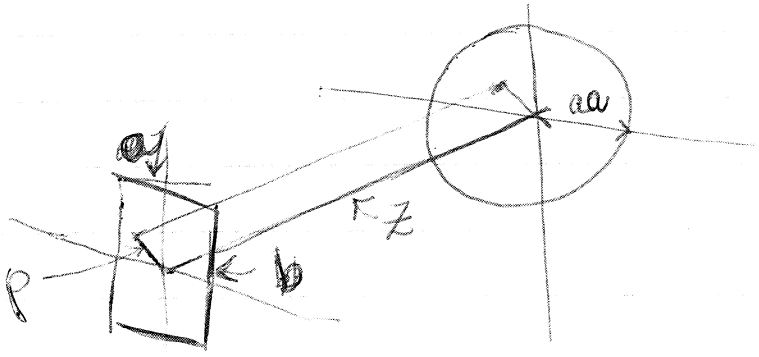

To calculate the geometry, we must evaluate the expression

$$\frac{1}{A}\int_{-a}^{+a}\int_{-b}^{+b} G_p \, dx\, dy, \text{ where}$$

$$G_p = \frac{1}{2}\left\{1 - \frac{1}{(1+\beta)^{1/2}}\right\} - \frac{1}{2}\left\{\gamma\left[\frac{3/4\,\beta}{(1+\beta)^{5/2}}\right] - \gamma^2\left[\frac{15/16\,\beta}{(1+\beta)^{7/2}} - \frac{105/64\,\beta^2}{(1+\beta)^{9/2}}\right]\right.$$

$$\left. + \gamma^3\left[\frac{35/32\,\beta}{(1+\beta)^{9/2}} - \frac{315/64\,\beta^2}{(1+\beta)^{11/2}} + \frac{1155/256\,\beta^3}{(1+\beta)^{13/2}}\right] + \cdots\cdots\right\} \quad (2)$$

$$\beta = \frac{a^2}{Z^2} \qquad \frac{\rho^2}{Z^2} = \gamma = \frac{x^2+y^2}{Z^2}$$

G_p is derived in (Ja-54). It is an expression for a point source viewing a circular aperture, but the source can be off the perpendicular axis drawn from the aperture center by the distance ρ. To simplify, write Eq. (2) as a sum of constants $\times$:

$$\frac{1}{A}\iint_{y\,x}\left\{\frac{1}{2}C_1 - \frac{1}{2}C_2\frac{(x^2+y^2)}{Z^2} + \frac{1}{2}C_3\frac{(x^2+y^2)^2}{Z^4} - \frac{1}{2}C_4\frac{(x^2+y^2)^3}{Z^6} + \cdots\right\} dx\,dy$$

Integrating term by term first with respect to x yields:

$$\frac{1}{A}\int_{y=-a}^{+a}\left[C_1 b - \frac{1}{2}\frac{C_2}{Z^2}\left(\frac{2}{3}b^3 + 2y^2 b\right) + \frac{1}{2}\frac{C_3}{Z^4}\left(\frac{2}{5}b^5 + \frac{4}{3}y^2 b^3 + 2y^4 b\right) - \right.$$

$$\left. \frac{1}{2}\frac{C_4}{Z^6}\left(\frac{2}{7}b^7 + \frac{6}{5}y^2 b^5 + 2y^4 b^3 + 2y^6 b\right) + \cdots\right] dy$$

finally,

$$G_s = \frac{1}{A}\left[\frac{A}{2}\left(C_1 - \frac{C_2}{3Z^2}b^2 - \frac{C_2}{3Z^2}a^2 + \frac{C_3(a^4+b^4)}{5Z^4} + \frac{C_3}{9Z^4}\frac{A^2}{8} - \frac{C_4}{7Z^6}(b^6+a^6)\right.\right.$$

$$\left.\left. - \frac{C_4}{5Z^6}\frac{A^2}{8}(a^2+b^2) + \cdots\cdots\right)\right] \quad (3)$$

since $A_s = 4ab$

For the ellipse geometry, we have

$$y^2/a^2 + x^2/b^2 = 1$$

$$\rho^2 = x^2 + y^2$$

$$A_S = \pi a b$$

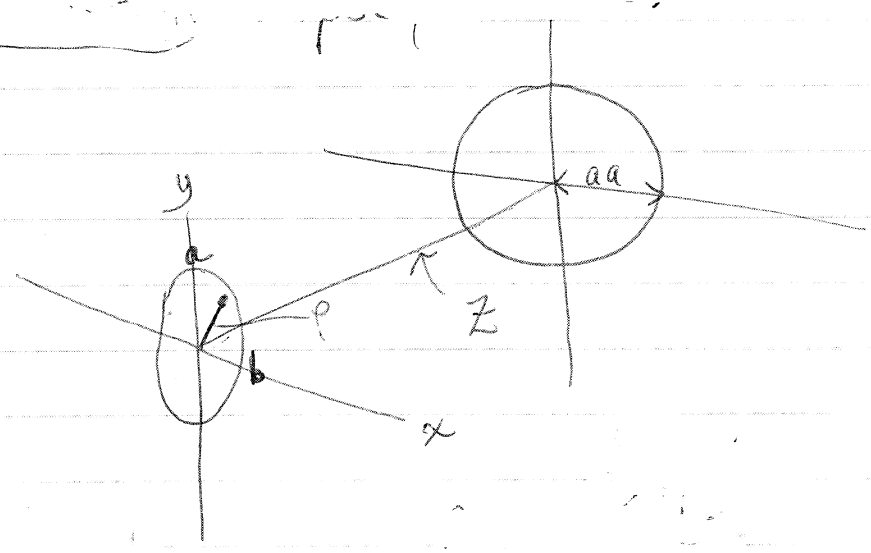

For this case, Eqn. (1) becomes

$$G_S = \frac{1}{\pi a b} \iint_S G_\rho \, dS \qquad \text{where } G_\rho \text{ is as above.}$$

$$G_S = \frac{1}{\pi a b} \int_{-b}^{+b} \int_{-\frac{a}{b}\sqrt{b^2-x^2}}^{+\frac{a}{b}\sqrt{b^2-x^2}} \left(\frac{1}{2} C_1 - \frac{(x^2+y^2)}{2Z^2} C_2 + \frac{(x^2+y^2)^2}{2Z^4} C_3 - \frac{(x^2+y^2)^3}{2Z^6} + \cdots \right) dx\,dy$$

Integrating first with respect to y yields

$$G_S = \frac{1}{\pi a b} \int_{-b}^{+b} \Big(C_1 \frac{a}{b}(b^2-x^2)^{1/2} - \frac{C_2}{Z^2} x^2 \frac{a}{b}(b^2-x^2)^{1/2} - \frac{C_2}{3Z^2} \frac{a^3}{b^3}(b^2-x^2)^{3/2}$$

$$+ \frac{C_3}{Z^4} x^4 \frac{a}{b}(b^2-x^2)^{1/2} + \frac{2}{3} \frac{C_3}{Z^4} x^2 \frac{a^3}{b^3}(b^2-x^2)^{3/2}$$

$$+ \frac{C_3}{5Z^4} \frac{a^5}{b^5}(b^2-x^2)^{5/2} - \frac{C_4}{Z^6} x^6 \frac{a}{b}(b^2-x^2)^{1/2}$$

$$- \frac{C_4}{Z^6} x^4 \frac{a^3}{b^3}(b^2-x^2)^{3/2} - \frac{3}{5} \frac{C_4}{Z^6} x^2 \frac{a^5}{b^5}(b^2-x^2)^{5/2}$$

$$- \frac{C_4}{7Z^6} \frac{a^7}{b^7}(b^2-x^2)^{7/2} + \cdots \Big) dx$$

These term by term integrals are easely integrated by using the trigonometric substitution:

$$x = b \sin u$$
$$dx = b \cos u \, du$$
$$u = \sin^{-1} \frac{x}{b}$$
$$\sqrt{b^2 - x^2} = b \cos u$$

With x varying from $-b$ to $+b$, u varies from $-\frac{\pi}{2}$ to $+\frac{\pi}{2}$

$$G_s = \frac{1}{\pi a b} \left[C_1 \frac{\pi a b}{2} - \frac{C_2}{Z^2} \frac{\pi a b}{2} \frac{b^2}{4} - \frac{C_2}{Z^2} \frac{\pi a b}{2} \frac{a^2}{4} + \frac{C_3}{Z^4} \frac{\pi a b}{2} \frac{b^4}{8} + \cdots\cdots \right]$$

This becomes finally

$$G_s = \frac{1}{2} \left\{ C_1 - \frac{C_2}{4Z^2}(b^2+a^2) + \frac{C_3}{8Z^4}(a^4+b^4) + \frac{C_3}{12Z^4}(a^2b^2) - \frac{5}{64}\frac{C_4}{Z^6}(a^6+b^6) - \frac{3}{64}\frac{C_4}{Z^6}(a^2b^4+a^4b^2) + \cdots\cdots \right\} \quad (4)$$

The difference between the geometries calculated for the average dimensions of the source mentioned in Section II.A is less than 0.5%. Refer to Table II.4.1

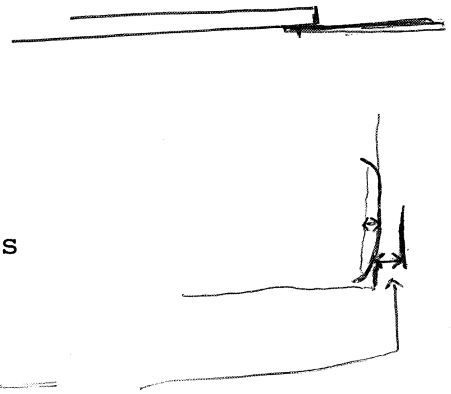

Table II.4.1

Detector geometries

avg. source size: 1.98 mm x 4.37 mm

wheel face to holder tube end equals 5.556 mm

$100mm^2$ active area assumed	fractional relative Geometry	fractional absolute Geometr
(.07%)*	1.0000	.08564
$150mm^2$ active area (1.22%)*	1.5071	
$75mm^2$ active area (11.7%)*	1.0766	

average source size = 4 times above value gives

G_{100mm^2} = 7.346%

if source were maximum beam burn dimensions (2.78 x 6.75 mm)

G_{100mm^2} = 8.326%

Δ = 2.8% of .08564

Assigned Absolute Errors

$100mm^2$	G ± (3%G + $^+$)
$150mm^2$	" (3%G + $^+$)
$75mm^2$	" (12%G + $^+$)

* errors from detector placement in counting mounts, and difficulty of measuring detector face recession due to casing design.

\+ errors from active areas uncertainties.

Appendix 2 gives a complete explanation of the spread source geometry calculation. For the calculation it is assumed that the source is uniformly and symmetrically distributed about a line from the detector center to the source center. Table II.4.1 gives the counting geometries. The catcher foil source to detector distance varied because of the differences in the depth of recession of the detector faces into their permanent mountings. From table II.4.1 it should be noted that the source size has only a marginal effect on the geometry, so that the exact recoil distribution size on the catcher is not critical.

A.H. Jaffey Rev. Sci Instr 25 (1954) 349 for geometry of spread source

75 μg/cm² Th on 30 μg/cm² degrader foil + ? vyns
? μg/cm² ThF_4

ANL-4875
Physics

ARGONNE NATIONAL LABORATORY
P. O. Box 299
Lemont, Illinois

SOLID ANGLE SUBTENDED BY A CIRCULAR APERTURE AT POINT AND SPREAD SOURCES: FORMULAE AND SOME TABLES

by

Arthur H. Jaffey

CHEMISTRY DIVISION

September 1952

Operated by The University of Chicago
under
Contract W-31-109-eng-38

The denominator can be transformed into a form suitable for binomial expansion in powers of $\frac{H}{F^2}$:

$$\left[z^2 + r^2 + \rho^2 - 2\rho r \cos\phi\right]^{3/2} = F^3 \left[1 + \frac{H(\rho, r, \phi)}{F^2}\right]^{3/2} \tag{5}$$

Integration of the individual double integrals leads to an infinite series for G_P. The form of the series is determined by the choice of F. F = z is one possible choice,[3] but this leads to a particularly clumsy form, in which a and ρ are not readily separable. While this result can be used for calculating G_P, it is difficult to integrate it further, e.g., in the case of a spread source of known uniformity.

The choice of $F = \sqrt{z^2 + r^2}$ leads to a simpler expansion which is suitable for further integration when a spread source is considered. The sum of integrals may be evaluated by first integrating with respect to $\phi\left(\int_0^{2\pi} \cos^K \phi \, d\phi\right)$ and then evaluating integrals of the form $\int_0^a \frac{r^n \, dr}{(z^2 + r^2)^{m/2}}$. While the calculations are quite tedious, the results are straightforward, giving

$$G_P = \frac{1}{2}\left[1 - \frac{z}{D}\right] - \frac{3}{8}\rho^2 \frac{a^2 z}{D^5} + \frac{15}{32}\rho^4 \frac{a^2 z}{D^9}\left(z^2 - \frac{3}{4}a^2\right) - \frac{35}{64}\rho^6 \frac{a^2 z}{D^{13}}\left(z^4 - \frac{5}{2}z^2 a^2 + \frac{5}{8}a^4\right) + \ldots \tag{6}$$

off axis

Equation (6) reduces to (3) when P is on the axis ($\rho = 0$).

Essentially the same method has been used by Blachman,[4] who calculated the geometry of a spread source (see Equation (27)). It can be shown that the same method gives, for a point source, a formula which is of different form, but equivalent (i.e., directly transformable) to Equation (6):

point source

$$G_P = \frac{1}{2}\left\{1 - \frac{1}{\sqrt{1+\beta}}\right\} - \frac{1}{2}\left\{\gamma\left[\frac{3/4\,\beta}{(1+\beta)^{5/2}}\right] - \gamma^2\left[\frac{15/16\,\beta}{(1+\beta)^{7/2}} - \frac{105/64\,\beta^2}{(1+\beta)^{9/2}}\right] + \gamma^3\left[\frac{35/32\,\beta}{(1+\beta)^{9/2}} - \frac{315/64\,\beta^2}{(1+\beta)^{11/2}} + \frac{1155/256\,\beta^3}{(1+\beta)^{13/2}}\right] + \ldots\right\}$$

---

[4]Nelson Blachman, private communication to B. J. Burtt (Nucleonics 5, 28-43 (August, 1949), Appendix C).

$$= \frac{1}{2}\left[1 - \frac{z}{D}\right] - \frac{3}{8}\rho^2 \frac{a^2 z}{D^5} + \rho^4 \left[\frac{15}{32}\frac{a^2 z}{D^7} - \frac{105}{128}\frac{a^4 z}{D^9}\right] \tag{7}$$

$$- \rho^6 \left[\frac{35}{64}\frac{a^2 z}{D^9} - \frac{315}{128}\frac{a^4 z}{D^{11}} + \frac{1155}{512}\frac{a^6 z}{D^{13}}\right] + \cdots$$

The mode of calculation used for (6) and (7) has the disadvantage that there is no evident method for writing down the general term, hence requiring increasingly complex integrations and tedious algebraic manipulations as more terms are required. Another method of derivation can be used, which reduces the calculation difficulties by enabling the development of the general term.

When a function is symmetrical around an axis and its value is known on the axis, i.e., $G(z,\rho) = f(z)$ for $\rho = 0$, G may be formally expanded in the form

$$G(z,\rho) = f(z) + \rho^2 f_2(z) + \rho^4 f_4(z) + \cdots$$

where $f_{2n}(z)$ are as yet unspecified functions. Utilizing the fact that the solid angle obeys Laplace's equation, i.e., $\nabla^2 G = 0$, a recursion formula can be determined:

$$f_{2n}(z) = -\frac{1}{(2n)^2} f''_{2n-2}(z) = (-1)^n \frac{1}{(2n)^2}\frac{1}{(2n-2)^2}\cdots\frac{1}{6^2}\frac{1}{4^2}\frac{1}{2^2} f^{(2n)}(z)$$

where

$$f''_{2n-2}(z) = \frac{d^2}{dz^2}\left[f_{2n-2}(z)\right] \quad \text{and} \quad f^{(2n)}(z) = \frac{d^{2n}}{dz^{2n}} f(z)$$

Then[5]

$$G(z,\rho) = f(z) - \frac{\rho^2}{2^2} f''(z) + \frac{\rho^4}{2^2 \cdot 4^2} f^{IV}(z) - \frac{\rho^6}{2^2 \cdot 4^2 \cdot 6^2} f^{VI}(z) + \cdots$$

$$= f(z) - \frac{\rho^2}{2^2} f''(z) + \frac{\rho^4}{2^4 (2!)^2} f^{IV}(z) - \cdots + (-1)^n \frac{\rho^{2n}}{2^{2n}(n!)^2} f^{(2n)}(z) + \cdots \tag{8}$$

Taking f(z) from (3) and calculating successive derivatives, one gets equation (6). However, this method also involves extensive algebraic manipulation for higher terms. A general term was derived to simplify the calculation and, it was hoped, to make possible the determination of the region of

---

[5]This is a method to be found in treatments of Laplace's equation, e.g., H. Bateman, Partial Differential Equations of Mathematical Physics (Dover Publications, 1944), p. 406.

convergence. The derivation may be found in Appendix A; the results are:

$$\frac{(-1)^n \rho^{2n}}{2^{2n}(n!)^2} f^{(2n)}(z) = \tag{9}$$

$$(-1)^n \rho^{2n} \frac{(2n+1)!}{2^{4n}(n!)^2} \frac{z}{(z^2+a^2)^{2n+1/2}} \left\{ -(z^2)^n \left[\frac{(4n-1)!}{(2n-1)!\ (2n+1)!}\right] \right.$$

$$+ (a^2+z^2)(z^2)^{n-1} \left[\frac{(4n-3)!}{(2n-2)!\ (2n-1)!}\right]$$

$$- 1/2!\ (a^2+z^2)^2 (z^2)^{n-2} \left[\frac{(4n-5)!}{(2n-3)!\ (2n-3)!}\right]$$

$$+ 1/3!\ (a^2+z^2)^3 (z^2)^{n-3} \left[\frac{(4n-7)!}{(2n-4)!\ (2n-5)!}\right]$$

$$+ \cdots$$

$$\left. \mp \frac{1}{n!} (a^2+z^2)^n \frac{(2n)!}{2(n!)} \right\}$$

- for n even
+ for n odd

The coefficients in (8) have been evaluated to the terms in ρ^{12} giving equation (10), which is evidently the same as (6):

$$G_P = \frac{1}{2}\left[1 - \frac{z}{D}\right] - \frac{3}{8}\rho^2 \frac{a^2 z}{D^5} + \frac{15}{32}\rho^4 \frac{a^2 z}{D^9}\left(z^2 - \frac{3}{4}a^2\right) \tag{10}$$

$$- \frac{35}{64}\rho^6 \frac{a^2 z}{D^{13}}\left(z^4 - \frac{5}{2}z^2a^2 + \frac{5}{8}a^4\right)$$

$$+ \frac{315}{512}\rho^8 \frac{a^2 z}{D^{17}}\left(z^6 - \frac{21}{4}z^4a^2 + \frac{35}{8}z^2a^4 - \frac{35}{64}a^6\right)$$

$$- \frac{693}{1024}\rho^{10} \frac{a^2 z}{D^{21}}\left(z^8 - 9z^6a^2 + \frac{63}{4}z^4a^4 - \frac{105}{16}z^2a^6 + \frac{63}{128}a^8\right)$$

$$+ \frac{3003}{4096}\rho^{12} \frac{a^2 z}{D^{25}}\left(z^{10} - \frac{55}{4}z^8a^2 + \frac{165}{4}z^6a^4 - \frac{1155}{32}z^4a^6 + \frac{1155}{128}z^2a^8 - \frac{231}{512}a^{10}\right)$$

$$+ \cdots$$

We have not been successful in determining the region of convergence analytically, but numerical calculation indicates that convergence occurs for $\rho/D<1$, for any z and a.

large point source off axis

The evaluation of G_P' (3) as the first term in (10) is simple, except where $\frac{z}{a}$ is large, in which case G_P' appears as a small difference of large numbers. G_P' can be expanded by the binomial theorem in powers of $\frac{a}{z}$ (in (14b), set $\ell = z$, $P_n = 1$) and can be adequately calculated with the use of only a few terms, since the series converges rapidly in the region where it is needed at all. Alternatively $[1 - \frac{z}{D}]$ may be transformed[6] into a form eliminating the difference of two large numbers.

$$G_P' = \frac{1}{2}\left[1 - \frac{z}{D}\right] = \frac{1}{2}\left[\frac{a^2}{D(D+z)}\right] \tag{11}$$

Zumwalt[7] has used another method of integration leading to an expansion in other variables, although similar in form. Integration of (4) with respect to r leads to (see Figure 1):

$$G_P = \frac{1}{2} - \frac{1}{4\pi}\,\frac{2z}{\sqrt{a^2+\ell^2}}\int_0^{\pi} \frac{\left(1 + \frac{\rho}{\ell}\frac{a}{\ell}\cos\phi\right)d\phi}{\left[1 - \left(\frac{\rho}{\ell}\right)^2\cos^2\phi\right]\sqrt{1 + \frac{2a\ell}{\ell^2+a^2}\left(\frac{\rho}{\ell}\right)\cos\phi}}$$

The two terms in the integrand denominator are expanded in separate binomial series in ρ/ℓ, the two series multiplied out, and each resulting term then is integrated with respect to ϕ. The resulting series is:

$$\begin{aligned} G_P = \frac{1}{2}\left\{1 - \frac{2}{\sqrt{\ell^2+a^2}}\right\} - \frac{1}{2}\frac{z}{\ell}\Bigg\{ & \frac{1}{2}\left(\frac{\rho}{\ell}\right)^2 \frac{1}{\lambda^5}\left(1 + \frac{5}{2}y^2\right) \\ & + \frac{3}{8}\left(\frac{\rho}{\ell}\right)^4 \frac{1}{\lambda^9}\left(1 + \frac{9}{2}y^2 + \frac{63}{8}y^4\right) \\ & + \frac{5}{16}\left(\frac{\rho}{\ell}\right)^6 \frac{1}{\lambda^{13}}\left(1 + \frac{13}{2}y^2 + \frac{143}{8}y^4 + \frac{429}{16}y^6\right) \\ & + \frac{35}{128}\left(\frac{\rho}{\ell}\right)^8 \frac{1}{\lambda^{17}}\left(1 + \frac{17}{2}y^2 + \frac{255}{8}y^4 + \frac{1105}{16}y^6 + \frac{12155}{128}y^8\right) + \cdots\Bigg\} \end{aligned} \tag{12}$$

where $y = \frac{a}{\ell}$ and $\lambda = \sqrt{1+y^2}$.

Since $\ell^2 = \rho^2 + z^2$, (12) is not easily integrated over ρ when the sample is distributed and hence is less useful in this case than (10). Convergence presumably obtains for conditions under which the binomial expansions hold, i.e., $\frac{\rho}{\ell} < 1$. Since this is always true, (12) should converge in regions where (10) will not.

---

[6] We wish to thank Herman P. Robinson for informing us of this transformation.

[7] Lloyd R. Zumwalt, "Absolute beta-counting using end-window GM counters and experimental data on beta-particle scattering effects," Appendix B, Oak Ridge National Laboratory Report Mon C-397 (Sept., 1949).

The fact that G_P satisfies Laplace's equation has led[8] to another kind of expansion in the Legendre polynomials, $P_n(\cos\theta)$. Since G_P is axially symmetric, the general solution is:

$$G_P = \frac{1}{2}\sum_0^\infty \left[A_n \ell^n + \frac{B_n}{\ell^{n+1}} \right] P_n(x)$$

It is possible to evaluate A_n and B_n by noting that on the axis: $\ell = z$, $\cos\theta = 1$, and $P_n(1) = 1$, and the form of G_P is known explicitly (G_P' in (3)). Binomial expansions of G_P' in powers of $\frac{a}{z}$ and in powers of $\frac{z}{a}$ give the values of both sets of coefficients.

For $\frac{\ell}{a} < 1$,

$$A_0 = 1;\ A_1 = -\frac{1}{a};\ A_{2n} = 0\ (n \geq 1);\ B_n \equiv 0$$

$$A_{2n+1}\,\ell^{2n+1}\,P_{2n+1} = (-1)^{n+1}\,\frac{1.3\cdots 2n-1}{2.4\cdots 2n}\left(\frac{\ell}{a}\right)^{2n+1} P_{2n+1} \tag{13a}$$

For $\frac{a}{\ell} < 1$,

$$B_{2n} = 0\ (n \geq 0);\ A_n \equiv 0$$

$$B_{2n-1}\,\frac{P_{2n-1}}{\ell^{2n}} = (-1)^{n+1}\,\frac{1.3\cdots 2n-1}{2.4\cdots 2n}\left(\frac{a}{\ell}\right)^{2n} P_{2n-1} \tag{13b}$$

The coefficients are explicitly calculated to terms in $P_{17}(\cos\theta)$ in (14). With $\frac{\ell}{a} = w$, $\frac{a}{\ell} = y$, $P_n = P_n(\cos\theta)$,

For $\frac{\ell}{a} < 1$,

$$G_P = \frac{1}{2}\left[1 - wP_1 + \frac{w^3}{2}P_3 - \frac{3}{8}w^5P_5 + \frac{5}{16}w^7P_7 - \frac{35}{128}w^9P_9 + \frac{63}{256}w^{11}P_{11} - \frac{231}{1024}w^{13}P_{13} + \frac{429}{2048}w^{15}P_{15} - \frac{6435}{32768}w^{17}P_{17} + \cdots \right] \tag{14a}$$

For $\frac{a}{\ell} < 1$,

$$G_P = \frac{1}{2}\left[\frac{1}{2}y^2P_1 - \frac{3}{8}y^4P_3 + \frac{5}{16}y^6P_5 - \frac{35}{128}y^8P_7 + \frac{63}{256}y^{10}P_9 - \frac{231}{1024}y^{12}P_{11} + \frac{429}{2048}y^{14}P_{13} - \frac{6435}{32768}y^{16}P_{15} + \frac{12155}{65536}y^{18}P_{17} + \cdots \right] \tag{14b}$$

---

[8] For example, see Sir James Jeans, Mathematical Theory of Electricity and Magnetism (Cambridge University Press, 1948), fifth edition, p. 431.

In contrast to (10) and (12), the use of (14) has the advantage that the values of the polynomial parts of each term (P_n) are listed in tables.[9,10,11] On the other hand, integration with respect to ρ is not simple, since it is contained in both P_n and the expansion variable in an inconvenient form. The series (14a) and (14b) are complementary in that one converges within the sphere $\ell = a$ and the other outside of it. As is generally true near the convergence boundaries of series, convergence of either series is quite slow for values of ℓ close to a. For this region the use of (10) or (12) is preferable.

III. GEOMETRY OF POINT SOURCE OFF THE AXIS - NUMERICAL METHODS

Other methods have been developed which require numerical integrations. In general, these are less convenient than the series described in Section II but are included here for completeness.

If (4) is integrated first with respect to ϕ, using the de Haan integral table,[12]

$$G_P = \frac{z}{4\pi} \int_0^a \int_0^{2\pi} \frac{r\,dr\,d\phi}{[z^2 + r^2 + \rho^2 + 2\rho r \cos\phi]^{3/2}}$$

$$= \frac{z}{\pi} \int_0^a \frac{r\,E'(p)\,dr}{\sqrt{z^2 + (r+\rho)^2}\,[z^2 + (r-\rho)^2]} = \frac{z}{2\pi} \int_0^a \frac{r\,p\,E'(p)\,dr}{\sqrt{\rho r}\,[z^2 + (r-\rho)^2]} \tag{15}$$

$$\text{where } p = \sqrt{\frac{4\rho r}{z^2 + (r+\rho)^2}} \text{ and } E'(p) = \int_0^{\frac{\pi}{2}} dx \sqrt{1 - p^2 \sin^2 x}, \ (p^2 < 1)$$

---

[9] H. Tallqvist, "Six-place Tables of the Legendre Functions. Part I. $P_n(x)$ at 0.001 intervals for n = 1 to 16; Part II. $P_n(\cos\theta)$ at 10′ intervals for n = 1 to 32," Acta Soc. Sci. Fennicae (Nova Series A) 2, No. 4 (1937); 2, No. 11 (1938).

[10] Other tables listed in A. Fletcher, J. C. P. Miller, and L. Rosenhead, Index of Mathematical Tables (McGraw-Hill, 1946).

[11] If tables are not available, the explicit form of the polynomials is available in mathematics texts and compendia which contain treatments of spherical harmonics. E.g., Jahnke and F. Emde, Tables of Functions with Formulae and Curves (Dover Publications, 1945); E. Madelung, Mathematischen Hilfsmittel der Physikers (Dover Publications, 1943).

[12] D. Bierens de Haan (translated by J. F. Ritt), Nouvelles Tables D'Integrales Definies (G. E. Stechert and Co., 1939) Table 68, Equation 26.

is the complete elliptic integral of the second kind. Since values of $E'(p)$ are available from tables,[10] (15) may be evaluated by numerical integration. The relationship is valid for all values of a, ρ, z.

Another kind of numerical method has been independently reported in two papers.[13,14] Consider the cone formed by joining the point P (Figure 1) with the boundary of aperture A. The cone intersects the unit sphere with center at P in a space curve whose equation may be determined by solving the simultaneous equations of cone and sphere. The area on the unit sphere cut off by the cone (i.e., the desired solid angle) may be determined by integrating over the sphere, with integration limits set by the equation of the space curve. According to Berne,[13]

$$G_P = \frac{1}{2\pi} \int_{-\frac{\pi}{2}}^{\frac{\pi}{2}} \int_0^{\eta(\phi)} \frac{r\,dr\,d\phi}{\sqrt{1 - r^2}} = \frac{1}{2\pi} \int_{-\frac{\pi}{2}}^{\frac{\pi}{2}} \left[1 - \sqrt{1 - \eta^2}\right] d\phi \qquad (16)$$

where $r = \eta(\phi)$ is determined by solving for r in the relationship:

$$\sin\phi = -\frac{z}{2\rho} \frac{r}{\sqrt{1 - r^2}} + \frac{a^2 - \rho^2}{2\rho z} \frac{\sqrt{1 - r^2}}{r}$$

G_P may be evaluated by numerical integration.

According to Healy, et al.,[14] using a sphere of radius t (rather than the unit sphere),

$$G_P = \frac{1}{4\pi t^2} \int_{\rho - t}^{\epsilon} \int_{\alpha(x)}^{\sqrt{t^2 - x^2}} \frac{t\,dy\,dx}{\sqrt{t^2 - x^2 - y^2}}$$

$$= \frac{1}{4\pi t} \int_{\rho - t}^{\epsilon} \left[\frac{\pi}{2} - \arcsin \frac{\alpha(x)}{t^2 - x^2}\right] dx \qquad (17)$$

Where

$$\alpha(x) = \frac{\rho x \pm \sqrt{\rho^2 x^2 - K}}{K/t^2 z}, \quad K = t^2(\rho^2 - a^2 - z^2), \quad \epsilon = \frac{t}{\sqrt{1 + \left(\frac{z}{\rho + t}\right)^2}}$$

---

[13] E. Berne, Rev. Sci. Instr. 22, 509-12 (1951).

[14] J. W. Healy, L. C. Schwendiman, and R. C. Thorburn, "Counter Calibrations in the Health Instrument Methods Group," Hanford Works Report HW-18258 (July, 1950).

Here too, G_P may be evaluated by numerical integration. Both references have tables and graphs calculated for a range of values of z, a, ρ. (Since only the ratios enter, only two parameters are involved.)

A formula whose evaluation involves the numerical integration of only a correction term has been derived by Henrich.[15] Considering the origin to lie vertically above the point P (Figure 2), from (4), for $a > \rho$

$$G_P = \frac{z}{2\pi} \int_0^{a-\rho} \int_0^{\pi} \frac{r\, d\phi\, dr}{(z^2 + r^2)^{3/2}} + \frac{z}{2\pi} \int_{a-\rho}^{a+\rho} \int_0 \frac{r\, d\phi\, dr \; \arccos \frac{r^2 + \rho^2 - a^2}{2\rho r}}{(z^2 + r^2)^{3/2}}$$

$$= \frac{1}{2} \left[1 - \frac{z}{\sqrt{(a-\rho)^2 + z^2}} \right] + \frac{z}{2\pi} \int_{a-\rho}^{a+\rho} \arccos \left(\frac{r^2 + \rho^2 - a^2}{2\rho r} \right) \frac{r\, dr}{(z^2 + r^2)^{3/2}} \tag{18}$$

The integral may be evaluated by numerical integration. The magnitude of the integral relative to the first term depends upon the difference $(a - \rho)$. When the difference is small, the integral is the larger component; for ρ relatively small, the integral need not be calculated very accurately, since it is then only a correction term.

IV. SOME APPROXIMATE FORMULAE FOR THE GEOMETRY OF AN OFF-AXIS POINT SOURCE

Since the difference between G_P and G_P' is approximately second order in ρ, the geometry of an off-axis point may often be sufficiently approximated by G_P' (3) for small displacement. It is sometimes of interest to know how much error may be introduced by shift of the source from the axis. It is useful, therefore, to have a simple relationship which gives the percentage deviation of G_P from G_P'.

Robinson[16] has used an approximate method suitable for small $\frac{a}{z}$ and $\frac{\rho}{z}$. The geometry of a point off the axis (G_P) is less than that of a point on the axis (G_P') primarily because of two factors: (1) increased average

---

[15] L. R. Henrich, Appendix IV in Isotopic Carbon by Calvin, Heidelberger, Reid, Tolbert, and Yankwich (Wiley, 1949).

[16] Herman P. Robinson, University of California Radiation Laboratory, Berkeley, California, private communication.

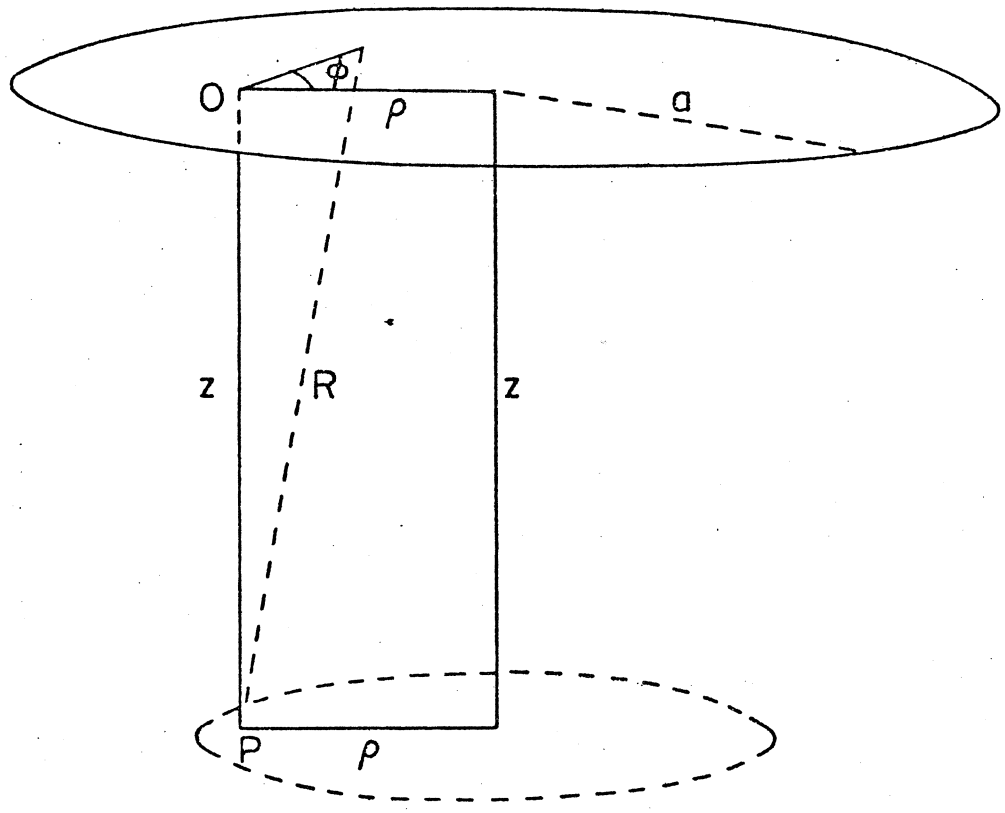

Figure 2

SOURCE-APERTURE DIAGRAM
FOR HENRICH NUMERICAL METHOD

source-aperture distance (which enters in as the inverse square), and (2) smaller effective aperture area, entering in as cos θ or z/ℓ (Figure 1). Thus approximately,

$$G_P = G_P' \left(\frac{z}{\ell}\right)^2 \left(\frac{z}{\ell}\right) = G_P' \frac{z^3}{\ell^3} = G_P' \frac{1}{\left(1 + \frac{\rho^2}{z^2}\right)^{3/2}} \tag{19}$$

where G_P' is defined in (3) and (11).

Using (11) and the first two terms of (10), approximately, for small $\frac{\rho}{z}$,

$$G_P = G_P' \left\{ 1 - \frac{3}{4} \rho^2 \left[\frac{z\,(z + D)}{D^4} \right] \right\} \tag{20}$$

Using a binomial expansion, either (19) or (20) leads to a more approximate relationship, for small $\frac{a}{z}$,

$$G_P = G_P' \left(1 - \frac{3}{2} \frac{\rho^2}{z^2}\right) \tag{21}$$

It is interesting to consider the effect of variations of ρ or z on G_P/G_P'. The term in ρ^2 (20) has a maximum value with respect to z at $z = \frac{a}{4} \sqrt{7 + \sqrt{17}} = 0.8338a$.

It is evident from this that the geometry is most sensitive to displacements of the source from the axis when z is approximately equal to the aperture radius. For evaluation of the effect of variation of z on G_P, it is sufficient to calculate it for G_P'. From the relation

$$\frac{dG_P'}{G_P'} = -\frac{D + z}{D^2}\, dz$$

it is evident that the percentage change in G_P' due to a vertical source shift, dz, increases slowly from z = 0 (change proportional to $\frac{1}{a}$) to a maximum at $z = \frac{a}{\sqrt{3}} = 0.58a$ (change proportional to $\frac{1.3}{a}$) and then decreases with increasing z. The region of greatest sensitivity to shifts in z and ρ corresponds to a region of operation commonly used with mica end-window GM tubes.

For $\frac{\ell}{a}$ small, from (14a), approximately,

$$G_P = \frac{1}{2} \left[1 - \frac{\ell}{a} \cdot \frac{z}{\ell} \right] = \frac{1}{2} \left[1 - \frac{z}{a} \right] \tag{22}$$

Near the aperture, the geometry does not vary appreciably with displacement from the axis. From (21), it is evident that the same is true for large z.

For $\frac{a}{\ell}$ small, from (14b), approximately,

$$G_P = \frac{1}{4}\frac{a^2}{\ell^2}\cos\theta = \frac{1}{4}\frac{a^2}{z^2}\cos^3\theta \tag{23}$$

and $G_P' = \frac{1}{4}\frac{a^2}{z^2}$

This relation is equivalent to approximating the area of a small section of a sphere by the area of its projection on the tangent plane.

The effect of particular percentage errors in the measurement of the dimensions z and a on the percentage error in the calculation of G_P is smallest close to the aperture (22) and at a maximum for small $\frac{a}{z}$. In the latter case,

$$\frac{dG_P}{G_P} = 2\left(\frac{da}{a} - \frac{dz}{z}\right)$$

V. UNIFORMLY SPREAD SOURCE COAXIAL WITH APERTURE - INFINITE SERIES EXPANSIONS

If the area of a source is too large to approximate it as a point, an average value (G_S) of the geometry may be calculated (A_S = source area):

$$G_S = \frac{1}{A_S}\iint_S G_P \, dS \tag{24a}$$

In general, this can be determined only by numerical integration, using one of the G_P formulae for evaluating the integrand. If the source is circular, parallel to and coaxial with the aperture, and the intensity distribution is simple, (24a) can be integrated explicitly. The simplest case, one for which most of the G_P formulae above may be integrated, involves a uniformly spread source, for which

$$G_S = \frac{1}{\pi b^2}\int_0^b G_P \cdot 2\pi\rho d\rho = \frac{2}{b^2}\int_0^b G_P \, \rho d\rho \tag{24b}$$

$$\frac{2}{b^2}\int_0^b G_\rho \, \rho \, d\rho$$

$$\int\left(\frac{1}{2}\left[1-\frac{z}{D}\right] - \frac{3}{8}\rho^2 c_1 + \frac{15}{32}\rho^4 c_2 - \cdots\cdots\right)\rho \, d\rho$$

$$\int_0^b\left(\frac{1}{2}\rho - \frac{1}{2}\frac{z}{D}\rho - \frac{3}{8}\rho^3 c_1 + \frac{15}{32}\rho^5 c_2 - \cdots\cdots\right)d\rho$$

$$\frac{1}{2}\frac{\rho^2}{2}\Big|_0^b - \frac{1}{2}\frac{z}{D}\frac{\rho^2}{2} - \frac{3}{8}\frac{\rho^4}{4}c_1\Big|_0^b + \frac{15}{32}\frac{\rho^6}{6}c_2\Big|_0^b - \cdots\cdots\Big)$$

$$\frac{2}{b^2}\left(\frac{b^2}{4} - \frac{1}{4}\frac{z}{D}b^2 - \frac{3}{32}b^4 c_1 + \frac{15}{192}b^6 c_2 - \cdots\cdots\right)$$

$$= \frac{1}{2} - \frac{1}{2}\frac{z}{D} - \frac{3}{16}b^2 c_1 + \frac{15}{96}b^4 c_2 - \cdots\cdots$$

$$= G_s$$

explicit integration for circular source of radius b uniformly spread

$$\frac{1}{2}\left[1-\frac{z}{D}\right]-\frac{3}{8}\rho^2 c_1+\frac{15}{32}\rho^4 c_2-\rho^6 c_3 \quad \text{etc.} \qquad (10)$$

The simplest integration occurs with G_P defined by (10), each term in G_S being identical to that in G_P, except that ρ^{2n} is replaced* by $\frac{b^{2n}}{n+1}$. Thus,

$$G_S = \frac{1}{2}\left[1-\frac{z}{D}\right] - \frac{3}{16}b^2\,\frac{a^2 z}{D^5} + \frac{5}{32}b^4\,\frac{a^2 z}{D^9}\left(z^2-\frac{3}{4}a^2\right)+\cdots \qquad (25)$$

Since (7) is equivalent to (10), it may be integrated in the same way to give Blachman's equation.[4] It is also possible to get the same result by starting from (4) and (24b); this method suggests[17] another type of expansion for G_S.

$$G_S = \frac{1}{4\pi(\pi b^2)}\int_A\int_S \frac{z\,dA\,dS}{R^3} = \frac{z}{2\pi b^2}\int_0^b\int_0^a\int_0^{2\pi}\frac{r\rho\,d\phi\,dr\,d\rho}{R^3}$$

$$= \frac{1}{8\pi\Gamma}\int_0^\Gamma\int_0^\beta\int_0^{2\pi}\frac{d\phi\,dt\,ds}{P^3} \qquad (26)$$

Spread Source

where $t=\frac{r^2}{z^2}$, $s=\frac{\rho^2}{z^2}$, $\Gamma=\frac{b^2}{z^2}$, $\beta=\frac{a^2}{z^2}$

and $P^3=\frac{R^3}{z^3}=[(1+t)+(s-\sqrt{ts}\cos\phi)]^{3/2}$.

Expanding $\frac{1}{P^3}$ in a binomial series with $(1+t)$ as the first term and $(s-\sqrt{ts}\cos\phi)$ as the second, the three integrations relative to (ϕ, s, t) may be performed as discussed in calculating (6). Terms are then arranged in ascending powers of Γ, giving

$$G_S = \frac{1}{2}\left\{1-\frac{1}{\sqrt{1+\beta}}\right\} - \frac{1}{2}\left\{\frac{3}{8}\Gamma\,\frac{\beta}{(1+\beta)^{5/2}} - \Gamma^2\left[\frac{5}{16}\,\frac{\beta}{(1+\beta)^{7/2}} - \frac{35}{64}\,\frac{\beta^2}{(1+\beta)^{9/2}}\right]\right.$$

$$\left. + \Gamma^3\left[\frac{35}{128}\,\frac{\beta}{(1+\beta)^{9/2}} - \frac{315}{256}\,\frac{\beta^2}{(1+\beta)^{11/2}} + \frac{1155}{1024}\,\frac{\beta^3}{(1+\beta)^{13/2}}\right] - \cdots\right\} \qquad (27)$$

Presumably (25) and (27) will converge under the same conditions that (7) and (10) do, i.e., $\frac{b}{D}<1$, for any (z, a). If Γ is large and β is not, it is possible to expand G_S in powers of β, since the roles of t and s in P and (26) are almost

---

$$^*\frac{2}{b^2}\int_0^b \rho^{2n}\,\rho\,d\rho = \frac{2}{b^2}\,\frac{b^{2n+2}}{2n+2} = \frac{b^{2n}}{n+1}$$

$\gamma = \frac{\rho^2}{z^2} = \Gamma$ $\quad \frac{1}{2}\left\{ \quad 3/4\ \beta \right.$

[17] Nelson Blachman, private communication.

symmetrical, i.e., $P = [(1 + s) + (t - \sqrt{st}\cos\phi)]^{1/2}$. Then

$$G_S = \frac{1}{2}\frac{\beta}{\Gamma}\left\{1 - \frac{1}{\sqrt{1+\Gamma}}\right\} - \frac{1}{2}\frac{\beta}{\Gamma}\left\{\frac{3}{8}\beta\frac{\Gamma}{(1+\Gamma)^{5/2}}\right. \tag{28a}$$

$$- \beta^2\left[\frac{5}{16}\frac{\Gamma}{(1+\Gamma)^{7/2}} - \frac{35}{64}\frac{\Gamma^2}{(1+\Gamma)^{9/2}}\right]$$

$$+ \beta^3\left[\frac{35}{128}\frac{\Gamma}{(1+\Gamma)^{9/2}} - \frac{315}{256}\frac{\Gamma^2}{(1+\Gamma)^{11/2}} + \frac{1155}{1024}\frac{\Gamma^3}{(1+\Gamma)^{13/2}}\right] + \cdots$$

or

$$G_S = \frac{1}{2}\frac{a^2}{b^2}\left[1 - \frac{z}{L}\right] - \frac{3}{16}\frac{a^4 z}{L^5} + \frac{5}{32}\frac{a^6 z}{L^9}\left(z^2 - \frac{3}{4}b^2\right)$$

$$- \frac{35}{256}\frac{a^8 z}{L^{13}}\left(z^4 - \frac{5}{2}b^2 + \frac{5}{8}b^4\right) + \cdots \tag{28b}$$

If a large number of terms are required for the desired accuracy, further expansion of (27) or (28) becomes quite inconvenient owing to the increasing complexity of the integrations and subsequent algebraic manipulations.

The integration of (12) with respect to ρ is excessively complicated, since ρ enters into both ℓ and λ. No attempt has been made to perform the integration except for the approximation containing only the first two terms.[7]

The expansions in Legendre polynomials, (14a) and (14b), may be integrated by substituting $\frac{z}{\ell} = \cos\theta$ in each Legendre polynomial and integrating term by term. Then, for $\frac{a}{\ell} < 1$

$$G_S = \frac{2}{b^2}\int_0^b G_P\,\rho d\rho = \frac{1}{b^2}\int_z^L \ell d\ell\left\{\frac{1}{2}\frac{a^2}{\ell^2}\frac{z}{\ell} - \frac{3}{16}\frac{a^4}{\ell^4}\left(5\frac{z^3}{\ell^3} - 3\frac{z}{\ell}\right)\right.$$

$$\left. + \frac{5}{128}\frac{a^6}{\ell^6}\left(63\frac{z^5}{\ell^5} - 70\frac{z^3}{\ell^3} + 15\frac{z}{\ell}\right) + \cdots\right\} \tag{29a}$$

$$= \frac{1}{2}\frac{a^2}{b^2}\left\{\left(1 - \frac{z}{L}\right) + \frac{3}{8}Y^2 X(X^2 - 1) - \frac{5}{64}Y^4 X(7X^4 - 10X^2 + 3) + \cdots\right\}$$

Equation (29a) is similar to the equation calculated by Kovarik and Adams,[2] except that $a \neq b$ (they treated the case $a = b$). It can also readily be shown that (29a) is equivalent to (28b) and hence to (28a).

For small $\frac{b}{L}$, the polynomials in X involve small differences between large numbers and hence are awkward to calculate. This difficulty may be eliminated by dividing through by $1 - X^2$:

$$G_S = \frac{1}{2}\frac{a^2}{L^2}\left\{\frac{1}{1+X} - \frac{3}{8}Y^2X + \frac{5}{64}Y^4X(7X^2-3) + \frac{35}{1024}Y^6X(33X^4 - 30X^2 + 5) - \cdots\right\} \tag{29b}$$

Similarly, for $\frac{\ell}{a} < 1$,

$$G_S = \frac{1}{b^2}\int_z^L \ell\, d\ell \left\{1 - \frac{\ell}{a}\frac{z}{\ell} + \frac{1}{4}\frac{\ell^3}{a^3}\left(5\frac{z^3}{\ell^3} - 3\frac{z}{\ell}\right) - \cdots\right\}$$

$$= \frac{1}{2}\frac{L^2}{b^2}\left\{\left(1 - \frac{z}{a}\right)(1 - X^2) - \frac{1}{8}W^3X(7X^4 - 10X^2 + 3) + \frac{3}{64}W^5X(33X^6 - 63X^4 + 35X^2 - 5) - \cdots\right\} \tag{30a}$$

where $\frac{L^2}{b^2}$ may also be written as $\frac{1}{1 - X^2}$.

Again, for small $\frac{b}{L}$, divide through by $(1 - X^2)$ and

$$G_S = \frac{1}{2}\left\{\left(1 - \frac{z}{a}\right) + \frac{1}{8}W^3X(7X^2 - 3) - \frac{3}{64}W^5X(33X^4 - 30X^2 + 5) + \cdots\right\} \tag{30b}$$

It may be noted that the polynomials in X in (29a) and (30a) and in (29b) and (30b), respectively, are identical. The general terms for these equations are described in Appendix B.

The labor of calculating the polynomials in X would be decreased if it were possible to show relationships between them and the Legendre polynomials, whose values have been tabulated.[9,10] Such relationships do indeed exist. While it is possible to deduce these directly from (29) and (30), it is simpler to start from (24b) and certain recursion properties of the Legendre polynomials. The derivation is given in Appendix C. The results are:

For $\frac{a}{\ell} < 1$

$$G_S = \frac{1}{2}\frac{a^2}{b^2}\left\{\left(1 - \frac{z}{L}\right) - \frac{1}{4}Y^2(P_1 - XP_2) + \frac{1}{8}Y^4(P_3 - XP_4) - \cdots\right\} \tag{31a}$$

With a general term ($n \geq 2$)

$$(-1)^{n+1}\ 2\frac{1.3 \cdots 2n-3}{2.4 \cdots 2n}\ Y^{2n-2}\left[P_{2n-3}(X) - XP_{2n-2}(X)\right] \tag{31b}$$

As before, for $\frac{b}{L}$ small, the polynomials in (31) are small differences between large numbers. An alternative form without this awkwardness is (see Appendix C):

$$G_S = \frac{1}{2}\frac{a^2}{L^2}\left\{\frac{1}{1+X} - \frac{1}{8}Y^2\frac{dP_2}{dx} + \frac{1}{32}Y^4\frac{dP_4}{dx} - \frac{5}{384}Y^6\frac{dP_6}{dx} + \cdots\right\} \tag{32a}$$

With the general term ($n \geq 2$):

$$(-1)^{n+1}\ \frac{1.3 \cdots 2n-3}{2.4 \cdots 2n}\ \frac{1}{n-1}\frac{d}{dx}P_{2n-2}(X) \tag{32b}$$

Unfortunately, the precision and detail of the available tables[18] of the derivative function are not as extensive as those of the P_n tables themselves.

For $\frac{\ell}{a} < 1$,

$$G_S = \frac{1}{2}\frac{L^2}{b^2}\left\{(1 - X^2)\left(1 - \frac{z}{a}\right) + \frac{1}{5}W^3(P_3 - XP_4) - \frac{3}{28}W^5(P_5 - XP_6) + \cdots\right\} \tag{33a}$$

With a general term

$$(-1)^{n+1}\ \frac{1.3 \cdots 2n-1}{2.4 \cdots 2n}\ \frac{2}{2n+3}\ W^{2n+1}\ [P_{2n+1} - XP_{2n+2}] \tag{33b}$$

and for small $\frac{b}{\ell}$, from [C - 2d]

$$G_S = \frac{1}{2}\left\{\left(1 - \frac{z}{a}\right) + \frac{1}{20}W^3\frac{dP_4}{dx} - \frac{1}{56}W^5\frac{dP_6}{dx} + \frac{5}{576}W^7\frac{dP_8}{dx} - \cdots\right\} \tag{34a}$$

With a general term

$$(-1)^{n+1}\ \frac{1.3 \cdots 2n-1}{2.4 \cdots 2n-2}\ \frac{1}{(n+1)(2n+3)}\ W^{2n+1}\frac{d}{dx}P_{2n+2}(X) \tag{34b}$$

---

[18] H. Tallqvist, "Tables of Legendre Functions and Associated Functions," Acta Soc. Sci. Fennicae 32, No. 6 (1904); 33, No. 9 (1906).

Owing to the regions of convergence of the forms of G_P used, none of the equations (29) through (34) may be used for a source which intersects the sphere $\ell^2 = z^2 + \rho^2 = a^2$.

VI. UNIFORMLY SPREAD SOURCES - NUMERICAL METHODS

Any of the results for G_P (Sec. II to IV) may be used in a numerical integration for evaluation of G_S (24a). In fact, for a spread source whose distribution is not suitably simple (or uniform), this is the only method that can be used.

Henrich's[15] method (Sec. IV) may also be applied to a uniformly spread source. For $\frac{a}{b} > 1$,

$$G_S = \frac{1}{2}\left\{1 - \frac{1}{2}\left[\frac{z}{\sqrt{z^2 + (a-b)^2}} + \frac{z}{\sqrt{z^2 + (a+b)^2}}\right]\right\} \tag{35a}$$

$$+ \frac{z}{\pi b^2}\int_{a-b}^{a+b}\left\{\frac{a^2}{2}\arccos\left(\frac{r^2 + a^2 - b^2}{2ar}\right) - \frac{b^2}{2}\arcsin\left(\frac{r^2 + b^2 - a^2}{2br}\right)\right.$$

$$\left. - \frac{1}{4}\sqrt{4a^2r^2 - (r^2 + a^2 - b^2)^2}\right\}\frac{r\,dr}{(z^2 + r^2)^{3/2}}$$

For $\frac{b}{a} > 1$,

$$G_S = \frac{1}{2}\left\{\frac{a^2}{b^2}\left[1 - \frac{z}{\sqrt{z^2 + (b-a)^2}}\right] + \frac{1}{2}\left[\frac{z}{\sqrt{z^2 + (b-a)^2}} - \frac{z}{\sqrt{z^2 + (b+a)^2}}\right]\right.$$

$$+ \frac{z}{\pi b^2}\int_{b-a}^{b+a}\left\{\quad\right\}\frac{r\,dr}{(z^2 + r^2)^{3/2}} \tag{35b}$$

The integrands in (35a) and (35b) are the same. As in the case of (18), this method is chiefly of value where the integral is small, so that its numerical integration need be performed only to modest accuracy.

VII. SOME APPROXIMATE FORMULAE FOR SPREAD SOURCES

Robinson's approximate equation (Sec. IV) for G_P may be easily integrated[16] in (24b) to give (using (11))

$$G_S = \frac{2G_P'}{b^2}\int_0^b \frac{\rho\,d\rho}{\left(1 + \frac{\rho^2}{z^2}\right)^{3/2}} = \frac{2z^2G_P'}{b^2}\left\{1 - \frac{1}{\sqrt{1 + \frac{b^2}{z^2}}}\right\} \tag{36}$$

(36 cont'd.)

$$G_S = \frac{2G_P'}{\left(1 + \frac{b^2}{z^2}\right) + \sqrt{1 + \frac{b^2}{z^2}}} = \frac{a^2}{z^2}\left[\frac{1}{1 + \frac{b^2}{z^2} + \sqrt{1 + \frac{b^2}{z^2}}}\right]\left[\frac{1}{1 + \frac{a^2}{z^2} + \sqrt{1 + \frac{a^2}{z^2}}}\right]$$

This may be expanded in binomial series in $\frac{a^2}{z^2}$ and $\frac{b^2}{z^2}$. It is, however, more convenient to calculate F_S, where

$$F_S = \frac{1}{G_S} = \frac{z^2}{a^2}\left(1 + \frac{a^2}{z^2} + \sqrt{1 + \frac{a^2}{z^2}}\right)\left(1 + \frac{b^2}{z^2} + \sqrt{1 + \frac{b^2}{z^2}}\right) \tag{37a}$$

Expanding F_S to the first few terms in the binomial series,

$$F_S = \left(4\frac{z^2}{a^2} + 3 + 3\frac{b^2}{a^2} + \frac{9b^2 - a^2}{4z^2}\right) - \left(\frac{1}{4}\frac{b^4}{a^2z^2} + \frac{3}{16}\frac{b^4 + a^2b^2}{z^4}\right) \tag{37b}$$

For the conditions of validity of (37b), namely small $\frac{a}{z}$ and $\frac{b}{z}$, the first term dominates, and the succeeding terms need be calculated with only limited accuracy. Comparison of (37b) results with accurate values calculated from (29a) shows the error in the approximation to be $<0.1\%$, for ($\frac{b}{z} < 0.15$, $\frac{a}{z} < 0.19$) and ($\frac{b}{z} < 0.2$, $\frac{a}{z} < 0.14$) and ($\frac{b}{z} < 0.5$, $\frac{a}{z} < 0.07$).

Some of the formulae of Sec. IV can be extended, with little modification, to spread sources. For example, close to the aperture (i.e., $\frac{L}{a}$ small), from (30b) or (34a),

$$G_S = \frac{1}{2}\left[1 - \frac{z}{a}\right] \tag{38}$$

which is the same as (22). The same result comes from direct integration of (22) in (24b). Similarly from direct integration of (20), or from (25),

$$G_S = G_P'\left\{1 - \frac{3}{8}b^2\left[\frac{z(z+D)}{D^4}\right]\right\} \tag{39}$$

VIII. SOME TABLES OF G_P VALUES

Some preliminary calculations were made in a program of setting up tables of G_P and G_S. Although this program was only partially completed, the resulting tables, incomplete as they are, have some usefulness in the region covered, and are presented in this section.

Tables I and II give the results of the calculation of G_P from (14b) over a range of $(\frac{z}{a}, \frac{\rho}{a})$ values, for $\frac{\ell}{a} > 1$. In order to simplify interpolation, (14b) was rewritten so as to make the tabulated portion a slowly varying function of the parameters. From (14b)

$$G_P = \frac{1}{4}\frac{a^2}{z^2}\left[x^2 P_1 - \frac{3}{4}y^2 x^2 P_3 + \frac{5}{8} y^4 x^2 P_5 - \cdots\right] = \frac{1}{4}\frac{a^2}{z^2} S_P = G_o S_P \quad (40a)$$

In Table I are tabulated values of S_P over a range of $\frac{z}{a}$ and $\frac{\rho}{a}$ values. The second and third columns contain

$$G_o = \frac{1}{4}\frac{a^2}{z^2} \text{ and } \frac{1}{G_o}$$

For small $\frac{z}{a}$, S_P varies too rapidly for accurate interpolation, and another method of tabulation was attempted. In this

$$G_P = \frac{1}{4} y^2 \left[P_1 - \frac{3}{4}y^2 P_3 + \frac{5}{8} y^4 P_5 - \cdots\right] = \frac{1}{4}\frac{a^2}{\ell^2} S'_P = G'_o S'_P \quad (40b)$$

The results are shown in Table II, with $\frac{\ell}{a}$ and $\frac{z}{a}$ as parameters. It is evident that the function S'_P varies too rapidly for accurate interpolation, although there is some improvement over Table I.

We wish to thank Professor Norman I. Adams of Yale University for informing us of Jeans's solid angle calculation. We are grateful to Marion Greene for having performed much of the calculation of the tables and to Jerome Lerner, Robert Keyes, and Lawrence Sjoblom for checking the manuscript and parts of the tables for errors.

APPENDIX A. DETERMINATION OF GENERAL TERM FOR (8).

$$\frac{d^n}{dz^n}(uv) = \frac{d^n u}{dz^n} v + \binom{n}{1}\frac{d^{n-1}u}{dz^n}\frac{dv}{dz} + \binom{n}{2}\frac{d^{n-2}u}{dz^{n-2}}\frac{d^2 v}{dz^2} + \cdots + u\frac{d^n v}{dz^n} \quad (A\text{-}1)$$

$$\text{Now } f(z) = \frac{1}{2}\left[1 - \frac{z}{\sqrt{z^2 + a^2}}\right]$$

$$\text{If we set } uv = \frac{-\frac{1}{2} z}{\sqrt{z^2 + a^2}}$$

$$\text{Then } \frac{d^n f(z)}{dz^n} = \frac{d^n(uv)}{dz^n} \quad (A\text{-}2)$$

Table I

GEOMETRY VALUES FOR $\frac{\ell}{a}>1$. S_p VALUES LISTED, WHERE $G_p = G_o S_p$

$\frac{z}{a}$	G_o	$1/G_o$	ρ/a									
			0	0.25	0.5	0.75	1.0	1.5	2.0	3.0	4.0	5.0
100	0.00002500	40,000	.9999	.9999	.9999	.9998	.9998	.9996	.9993	.9986	.9975	.9962
80	0.00003906	25,600	.9999	.9999	.9998	.9998	.9996	.9994	.9989	.9976	.9961	.9941
60	0.00006944	14,400	.9998	.9998	.9997	.9996	.9994	.9989	.9981	.9961	.9932	.9895
50	0.00010000	10,000	.9997	.9997	.9996	.9994	.9991	.9984	.9973	.9943	.9902	.9849
40	0.00015625	6400	.9995	.9995	.9993	.9990	.9986	.9974	.9958	.9912	.9847	.9766
35	0.00020408	4900	.9994	.9993	.9991	.9987	.9982	.9966	.9945	.9885	.9801	.9696
30	0.00027778	3600	.9992	.9991	.9988	.9982	.9975	.9954	.9926	.9844	.9732	.9590
27.5	0.00033058	3025	.9990	.9989	.9985	.9979	.9970	.9946	.9912	.9815	.9682	.9515
25	0.0004000	2500	.9988	.9987	.9982	.9975	.9964	.9934	.9893	.9777	.9617	.9419
23.75	0.0004432	2256.3	.9987	.9985	.9980	.9972	.9960	.9927	.9882	.9753	.9578	.9360
22.5	0.0004938	2025	.9985	.9983	.9978	.9969	.9956	.9919	.9868	.9726	.9531	.9291
21.25	0.0005536	1806.3	.9983	.9981	.9975	.9965	.9950	.9910	.9853	.9693	.9477	.9211
20	0.0006250	1600	.9981	.9979	.9972	.9960	.9944	.9898	.9834	.9655	.9413	.9117
19	0.0006927	1444	.9979	.9977	.9969	.9956	.9938	.9887	.9816	.9619	.9354	.9030
18	0.0007716	1296	.9977	.9974	.9965	.9951	.9931	.9874	.9796	.9577	.9284	.8929
17	0.0008651	1156	.9974	.9971	.9961	.9945	.9923	.9859	.9772	.9528	.9204	.8813
16	0.0009766	1024	.9971	.9967	.9956	.9938	.9913	.9842	.9743	.9470	.9109	.8632
15	0.0011111	900	.9967	.9963	.9950	.9930	.9901	.9820	.9709	.9401	.8998	.8519
14	0.0012755	784	.9962	.9957	.9943	.9920	.9887	.9794	.9667	.9318	.8864	.8332
13	0.0014793	676	.9956	.9950	.9934	.9907	.9869	.9762	.9616	.9217	.8704	.8109
12	0.0017361	576	.9948	.9942	.9923	.9891	.9847	.9722	.9552	.9093	.8508	.7843
11	0.0020661	484	.9938	.9931	.9908	.9871	.9818	.9671	.9472	.8937	.8268	.7523
10	0.0025000	400	.9926	.9916	.9889	.9844	.9781	.9605	.9368	.8740	.7970	.7134
9.5	0.0027701	361	.9918	.9908	.9877	.9827	.9758	.9565	.9304	.8621	.7794	.6909
9.0	0.0030864	324	.9908	.9897	.9864	.9808	.9731	.9517	.9231	.8485	.7596	.6660
8.5	0.0034602	289	.9897	.9885	.9847	.9786	.9700	.9462	.9145	.8330	.7373	.6386
8.0	0.0039063	256	.9884	.9870	.9828	.9759	.9663	.9398	.9046	.8151	.7122	.6082
7.5	0.0044444	225	.9869	.9853	.9805	.9727	.9619	.9321	.8928	.7944	.6838	.5748
7.0	0.005102	196	.9850	.9831	.9777	.9688	.9565	.9229	.8789	.7704	.6516	.5379
6.5	0.005917	169	.9826	.9805	.9743	.9640	.9500	.9117	.8621	.7424	.6152	.4975
6.0	0.006944	144	.9796	.9772	.9700	.9581	.9419	.8980	.8419	.7096	.5741	.4535
5.5	0.008264	121	.9759	.9730	.9645	.9507	.9318	.8811	.8173	.6710	.5277	.4058
5.0	0.010000	100	.9710	.9676	.9575	.9411	.9189	.8599	.7870	.6257	.4758	.3548
4.5	0.012346	81	.9644	.9603	.9482	.9286	.9021	.8329	.7493	.5725	.4183	
4.0	0.015625	64	.9554	.9504	.9356	.9118	.8799	.7980	.7021	.5102	.3555	
3.5	0.020408	49	.9427	.9364	.9180	.8886	.8497	.7522	.6426	.4383	.2886	
3.0	0.027778	36	.9237	.9157	.8925	.8557	.8078	.6915	.5676	.3581	.2198	
2.75	0.033058	30.25	.9106	.9016	.8753	.8339	.7807	.6539	.4815	.3132		
2.5	0.04000	25	.8940	.8838	.8540	.8074	.7481	.6103	.4738	.2682		
2.25	0.04938	20.25	.8727	.8610	.8271	.7747	.7089	.5600	.4194	.2227		
2.0	0.06250	16	.8446	.8313	.7930	.7343	.6615	.5021	.3600	.1778		
1.9	0.06925	14.44	.8309	.8169	.7768	.7154	.6399	.4768	.3350	.1603		
1.8	0.07716	12.96	.8155	.8008	.7589	.6949	.6165	.4501	.3094	.1432		
1.7	0.08651	11.56	.7980	.7828	.7390	.6724	.5914	.4221	.2834	.1267		
1.6	0.09766	10.24	.7783	.7624	.7168	.6478	.5643	.3928	.2570	.1108		
1.5	0.11111	9	.7560	.7395	.6923	.6209	.5352	.3623	.2304	.0956		

Table II

GEOMETRY VALUES FOR $\frac{\ell}{a}>1$. S_p VALUES LISTED WHERE $G'_p = G'_o S_p$

$\frac{\ell}{a}$ \ $\frac{z}{a}$	3.0	2.8	2.6	2.4	2.2	2.0	1.8	1.6	1.4	1.2	1.0	0.8	0.6	0.4	0.2	$G'_o = \frac{a^2}{4\ell^2}$	$1/G'_o$
3.0	.9237	.8823	.8380	.7904	.7397	.6857	.6286	.5683	.5049	.4387	.3700	.2989	.2259	.1515	.0760	.027778	36
2.8		.9135	.8723	.8273	.7785	.7252	.6687	.6076	.5425	.4735	.4008	.3249	.2463	.1655	.0831	.031888	31.36
2.6			.9012	.8606	.8155	.7655	.7104	.6500	.5842	.5131	.4369	.3559	.2708	.1825	.0919	.036982	27.04
2.4				.8862	.8471	.8024	.7515	.6941	.6296	.5579	.4790	.3931	.3010	.2038	.1029	.043403	23.04
2.2					.8677	.8312	.7878	.7366	.6767	.6073	.5279	.4382	.3388	.2311	.1172	.051653	19.36
2.0						.8446	.8123	.7717	.7211	.6588	.5831	.4927	.3872	.2676	.1369	.062500	16
1.8							.8155	.7896	.7540	.7057	.6413	.5570	.4497	.3182	.1654	.077160	12.96
1.6								.7782	.7620	.7349	.6920	.6265	.5295	.3921	.2111	.097656	10.24
1.4									.731	.7275	.7131	.6825	.6202	.5026	.2947	.12755	7.84

Set $v = \frac{-1}{2}\frac{z}{a}$ and $u = \left(1 + \frac{z^2}{a^2}\right)^{-1/2}$

Then, from (A-1)

$$\frac{d^n f(z)}{dz^n} = -\frac{1}{2a}\left(z\frac{d^n u}{dz^n} + n\frac{d^{n-1}u}{dz^n}\right) \tag{A-3}$$

Now, the problem remains of evaluating $\frac{d^n u}{dz^n}$. We use the relationship[19]

$$\frac{d^n}{dz^n}(1+\alpha z^2)^{\mu} = \frac{\mu(\mu-1)(\mu-2)\cdots(\mu-n+1)(2\alpha z)^n}{(1+\alpha z^2)^{n-\mu}}\left\{1 + \frac{n(n-1)}{1\cdot(\mu-n+1)}\left(\frac{1+\alpha z^2}{4\alpha z^2}\right)\right.$$

$$+\frac{n(n-1)(n-2)(n-3)}{2!(\mu-n+1)(\mu-n+2)}\left(\frac{1+\alpha z^2}{4\alpha z^2}\right)^2 + \frac{n(n-1)(n-2)(n-3)(n-4)(n-5)}{3!(\mu-n+1)(\mu-n+2)(\mu-n+3)}\left(\frac{1+\alpha z^2}{4\alpha z^2}\right)^3$$

$$\left. + \cdots\cdots\right\}$$

Wherefore,

$$\frac{d^n u}{dz^n} = (-1)^n\frac{1\cdot3\cdot5\cdots(2n-1)az^n}{(z^2+a^2)^{n+1/2}}\left\{1 - \frac{n(n-1)}{(2n-1)}\frac{a^2+z^2}{2z^2}\right. \tag{A-4}$$

$$\left. + \frac{n(n-1)(n-2)(n-3)}{2(2n-1)(2n-3)}\left(\frac{a^2+z^2}{2z^2}\right)^2 + \cdots\right\}$$

$$= (-1)^n\frac{1\cdot3\cdot5\cdots(n-1)}{(z^2+a^2)^{n+1/2}}\frac{a}{2^{n/2}}\left\{[(2n-1)(2n-3)\cdots(n+1)](2z^2)^{n/2}\right.$$

$$-[n(n-1)][(2n-3)(2n-5)\cdots(n+1)][2z^2]^{n/2-1}[a^2+z^2]$$

$$+\frac{1}{2!}[n(n-1)(n-2)(n-3)][(2n-5)(2n-7)\cdots(n+1)][2z^2]^{n/2-2}[a^2+z^2]^2$$

$$+\cdots$$

$$\left.\pm\frac{n!}{\left(\frac{n}{2}\right)!}(a^2+z^2)^{\frac{n}{2}}\right\}$$

---

[19] E. P. Adams, Smithsonian Mathematical Formulae (Smithsonian Institution, 1939), pp. 158, 192.

Substituting (A-4) in (A-3),

$$\frac{d^n}{dz^n} f(z) = \frac{(n+1)!}{2^{n+1}} \frac{z}{(z^2 + a^2)^{n+1/2}} \left\{ - \frac{(2n-1)!}{2^{\frac{n}{2}-1} (n-1)!} \frac{1}{(n+1)!} (2z^2)^{n/2} \right.$$

$$+ [a^2 + z^2] [2z^2]^{\frac{n}{2}-1} \left[\frac{(2n-3)!}{2^{\frac{n}{2}-2} (n-2)!} \right] \frac{1}{(n-1)!}$$

$$- \frac{1}{2!} [a^2 + z^2]^2 [2z^2]^{\frac{n}{2}-2} \left[\frac{(2n-5)!}{2^{\frac{n}{2}-3} (n-3)!} \right] \frac{1}{(n-3)!}$$

$$+ \cdots$$

$$\left. \mp \frac{1}{\left(\frac{n}{2}\right)!} [a^2 + z^2]^{\frac{n}{2}} \frac{n!}{\left(\frac{n}{2}\right)!} \right\}$$

The general term of (8) is then

$$\frac{(-1)^n \rho^{2n}}{2^{2n} (n!)^2} f^{(2n)}(z) = \frac{(-1)^n \rho^{2n} (2n+1)!}{2^{4n+1} (n!)^2} \cdot \frac{z}{(z^2 + a^2)^{2n + 1/2}} \left\{ \quad \right\}$$

where

$$\left\{ \quad \right\} = \left\{ -(2z^2)^n \left[\frac{(4n-1)!}{2^{n-1}(2n-1)!(2n+1)!} \right] \right.$$

$$+ (a^2 + z^2) (2z^2)^{n-1} \left[\frac{(4n-3)!}{2^{n-2}(2n-2)!(2n-1)!} \right]$$

$$- \frac{1}{2!} (a^2 + z^2)^2 (2z^2)^{n-2} \left[\frac{(4n-5)!}{2^{n-3}(2n-3)!(2n-3)!} \right]$$

$$+ \cdots$$

$$\left. \mp \frac{(2n)!}{(n!)^2} (a^2 + z^2)^n \right\}$$

last term = − for n even
+ for n odd

APPENDIX B. GENERAL TERMS FOR (29) AND (30).

The odd Legendre polynomials are expressible in the form:

$$P_{2n-1}(x) = \frac{1}{f_{2n-1}} \left[a_{2n-1}\, x^{2n-1} - b_{2n-1}\, x^{2n-3} + C_{2n-1}\, x^{2n-5} + \cdots\right] \qquad \text{(B-1)}$$

Define

$$T_{2n-2} = \left[\frac{a_{2n-1}}{4n-3} X^{2n-2} - \frac{b_{2n-1}}{4n-5} X^{2n-4} + \frac{C_{2n-1}}{4n-7} X^{2n-6} - \cdots\right] \qquad \text{(B-2)}$$

and

$$U_{2n-2} = -\frac{T_{2n-2}}{1-X^2} \; . \qquad \text{(B-3)}$$

Some values for $\frac{T_{2n-2}}{f_{2n-1}}$ and U_{2n-2} are:

$$\frac{T_2}{f_3} = \frac{1}{2}[X^2-1] \; ; \; \frac{T_4}{f_5} = \frac{1}{8}[7X^4 - 10X^2 + 3] \; ; \; \frac{T_6}{f_7} = \frac{1}{16}[33X^6 - 63X^4 + 35X^2 - 5]$$

$$\frac{T_8}{f_9} = \frac{1}{128}[715X^8 - 1716X^6 + 1386X^4 - 420X^2 + 35] \qquad \text{(B-4a)}$$

$$\frac{T_{10}}{f_{11}} = \frac{1}{256}(4199X^{10} - 12155X^8 + 12870X^6 - 6006X^4 + 1155X^2 - 63)$$

(B-4b)

$$U_2 = 1 \; ; \; U_4 = 7X^2 - 3 \; ; \; U_6 = 33X^4 - 30X^2 + 5 \; ; \; U_8 = 715X^6 - 1001X^4 + 385X^2 - 35$$

$$U_{10} = 4199X^8 - 7956X^6 + 4914X^4 - 1092X^2 + 63$$

The general terms for (29a) and (29b) are:

$$(-1)^n \frac{1.3 \cdots 2n-1}{2.4 \cdots 2n} \frac{2}{f_{2n-1}} Y^{2n-2} X\, T_{2n-2} \; (n \geq 2) \qquad \text{(B-5a)}$$

$$(-1)^{n+1} \frac{1.3 \cdots 2n-1}{2.4 \cdots 2n} \frac{2}{f_{2n-1}} Y^{2n-2} X\, U_{2n-2} \; (n \geq 2) \qquad \text{(B-5b)}$$

The general terms for (30a) and (30b) are:

$$(-1)^n \frac{1.3 \cdots 2n-1}{2.4 \cdots 2n} \frac{2}{f_{2n+3}} W^{2n+1} X\, T_{2n+2} \qquad \text{(B-6a)}$$

$$(-1)^n \frac{1.3 \cdots 2n-1}{2.4 \cdots 2n} \frac{2}{f_{2n+3}} W^{2n+1} X\, U_{2n+2} \qquad \text{(B-6b)}$$

APPENDIX C. SPREAD SOURCE FORMULA IN LEGENDRE POLYNOMIAL FORM

Inserting (14b) into (24b) with $x = \frac{z}{\ell}$ and $\rho\, d\rho = \ell\, d\ell = \frac{-z^2}{x^3}\, dx$, for $\frac{a}{\ell} < 1$,

$$G_S = \frac{z^2}{b^2} \int_X^1 \frac{dx}{x^3} \left(\frac{1}{2} y^2 P_1 - \frac{3}{8} y^4 P_3 + \cdots \right)$$

$$= \frac{z^2}{b^2} \int_X^1 \frac{dx}{x^3} \left[\sum_n (-1)^{n+1} \frac{1.3 \cdots 2n-1}{2.4 \cdots 2n} \left(\frac{a}{z}\right)^{2n} x^{2n} \; P_{2n-1} \right] \qquad \text{(C-1)}$$

$$= \frac{a^2}{b^2} \sum_n (-1)^{n+1} \frac{1.3 \cdots 2n-1}{2.4 \cdots 2n} \left(\frac{a}{z}\right)^{2n-2} \int_X^1 x^{2n-3} \; P_{2n-1} dx$$

Some useful recursion properties of the Legendre polynomials are:[19]

$$(k+1)\; P_{k+1} + kP_{k-1} = (2k+1) x P_k \qquad \text{(C-2a)}$$

$$kP_k = x \frac{dP_k}{dx} - \frac{dP_{k-1}}{dx} \qquad \text{(C-2b)}$$

$$P_k(1) = 1 \qquad \text{(C-2c)}$$

$$(1-x^2) \frac{dP_k}{dx} = k(P_{k-1} - xP_k) \qquad \text{(C-2d)}$$

Setting $2n-2 = k$ in (C-1) and using (C-2a), (C-2b), and (C-2c),

$$\int_X^1 x^{k-1} \; P_{k+1} dx = \int_X^1 dx \left\{ \frac{x^{k-1}}{k+1} \left[(2k+1)\, x\, P_k - kP_{k-1} \right] \right\}$$

$$= \frac{1}{k+1} \int_X^1 dx \left\{ x^{k-1} \left[(k+1)\, xP_k + x \left(x \frac{dP_k}{dx} - \frac{dP_{k-1}}{dx} \right) - kP_{k-1} \right. \right.$$

$$\text{(C-3)}$$

$$= \frac{1}{k+1} \int_X^1 dx \left\{ kx^{k-1} (xP_k - P_{k-1}) + x^k \left(P_k + x \frac{dP_k}{dx} - \frac{dP_{k-1}}{dx} \right) \right\}$$

$$= \frac{1}{k+1} \int_X^1 \frac{d}{dx} \left\{ x^k (xP_k - P_{k-1}) \right\} dx = \frac{1}{k+1} X^k \left\{ P_{k-1} - XP_k \right\}$$

Where $P_k = P_k(X)$. The resulting form of G_S is shown in (31a); the general term in (31b).

Since $\frac{a^2}{b^2} = \frac{a^2}{L^2}\frac{1}{(1-X^2)}$, from (C-2d), the term $\left(P_{2n-3} - XP_{2n-2}\right)$ may be replaced by

$\frac{1}{2n-2}\frac{dP_{2n-2}}{dx}$, resulting in (32a) and (32b).

Inserting (14a) into (24b), with the previous substitutions, for $\frac{\ell}{a}<1$,

$$G_S = \frac{z^2}{b^2}\int_X^1 \frac{dx}{x^3}\left(1-wP_1 + \frac{w^3}{2}P_3 - \cdots\right)$$

$$= \frac{z^2}{2b^2}\left\{\frac{1-X^2}{X^2}\left(1-\frac{z}{a}\right) + 2\int_X^1 \frac{dx}{x^3}\left[\sum_{n=1}^{\infty}(-1)^{n+1}\frac{1.3\cdots 2n-1}{2.4\cdots 2n}\left(\frac{z}{a}\right)^{2n+1}\frac{P_{2n+1}}{x^{2n+1}}\right]\right. \tag{C-4}$$

$$= \frac{L^2}{2b^2}\left\{(1-X^2)\left(1-\frac{z}{a}\right) + 2\Sigma(-1)^{n+1}\frac{1.3\cdots 2n-1}{2.4\cdots 2n}\left(\frac{z}{a}\right)^{2n+1} X^2\int_X^1 \frac{P_{2n+1}}{x^{2n+4}}\,dx\right.$$

Setting $2n+1 = k$, and using (C-2b),

$$\frac{P_k}{x^{k+3}} = -\frac{1}{k+2}\left\{-\frac{k+2}{x^{k+3}}P_k + \frac{k+1}{x^{k+2}}P_{k+1} - \frac{k+1}{x^{k+2}}P_{k+1}\right\}$$

$$= -\frac{1}{k+2}\left\{-\frac{k+2}{x^{k+3}}P_k + \frac{k+2}{x^{k+2}}P_{k+1} - \frac{1}{x^{k+2}}P_{k+1} + \frac{1}{x^{k+2}}\left(\frac{dP_k}{dx} - x\frac{dP_{k+1}}{dx}\right)\right\} \tag{C-5}$$

$$= -\frac{1}{k+2}\left\{-\frac{k+2}{x^{k+3}}\left(P_k - xP_{k+1}\right) + \frac{1}{x^{k+2}}\left(\frac{dP_k}{dx} - x\frac{dP_{k+1}}{dx} - P_{k+1}\right)\right\}$$

$$= -\frac{1}{k+2}\frac{d}{dx}\left\{\frac{1}{x^{k+2}}\left(P_k - xP_{k+1}\right)\right.$$

$$\int_X^1 \frac{P_{2n+1}}{x^{2n+4}}\,dx = \frac{1}{2n+3}\frac{1}{X^{2n+3}}\left[P_{2n+1} - XP_{2n+2}\right] \tag{C-6}$$

with P_k evaluated at X.

Bragg additivity rule Sautter, Zimmerman Phys Rev 140, A 490 (1965)
Phys Rev 131, 1611 (1963)
Pam Schuster

RANGES OF HEAVY IONS IN AMORPHOUS OXIDES*

B. DOMEIJ,† F. BROWN, J. A. DAVIES, AND M. MCCARGO
Research Chemistry Branch, Chalk River Nuclear Laboratories, Chalk River, Ontario
Received May 11, 1964

ABSTRACT

The range distributions of Na^{24}, Ar^{41}, Kr^{85}, and Xe^{125} ions in amorphous Al_2O_3 and WO_3 have been measured in the energy interval 0.5 to 160 keV. The experimental technique consisted of measuring the transmission through oxide layers formed anodically on metal foils. The penetrating tail of distributions measured in crystalline targets is found to be absent in amorphous targets. Comparison with the calculations of Lindhard *et al.* (1963), who assume a random distribution of the target atoms, shows good agreement between theory and experiment.

INTRODUCTION

A large number of range distributions for heavy ions in metals have been measured at this laboratory‡ and elsewhere§ using the electrochemical peeling method (Davies *et al.* 1960*a*). Although comparison with the calculations of Nielsen (1956) and Lindhard *et al.* (1963), based on randomly distributed target atoms, shows rough agreement, the accuracy of the experiments has been good enough to establish that the measured ranges in all cases were significantly greater than the theoretically predicted ones. The effect of the crystallographic structure on the slowing down of an atom, recently postulated theoretically‖ and verified experimentally (Piercy *et al.* 1963), offers an explanation for the discrepancy between polycrystalline range measurements and gas model calculations. On the other hand, this means that only a limited number of data, for example, the measurements of ranges in gases by Lassen *et al.* (1962), are available for comparison with gas-model calculations.

In this work, distributions in *amorphous* Al_2O_3 and WO_3 targets have been measured in order to supply accurate data for comparison with random-model calculations. The results also provide comparison data for single-crystal work (Piercy *et al.* 1964; Kornelsen *et al.* 1964).

EXPERIMENTAL TECHNIQUES

The experimental technique consisted of letting a monoenergetic beam of radioactive ions impinge on a target consisting of a metal foil (Al or W) on the surface of which an oxide layer had been formed anodically. After bombardment the target activity was measured; the oxide layer was then dissolved, and the target activity remeasured. Repeating this experiment for different oxide thicknesses produces a transmission curve as a function of thickness, or an integral range distribution curve.

*Issued as A.E.C.L. No. 1995.
†On leave of absence from the Nobel Institute of Physics, Stockholm 50, Sweden.
‡Davies *et al.* (1960*a*); Davies *et al.* (1960*b*); Davies and Sims (1961); Davies *et al.* (1961); Davies *et al.* (1963*a*); McCargo *et al.* (1963*a*); McCargo *et al.* (1963*b*).
§Davies *et al.* (1963*b*); Bergström *et al.* (1963); Uhler *et al.* (1963).
‖Robinson and Oen (1963); Beeler and Besco (1963); Lehmann and Leibfried (1963).

The technique for producing reproducibly thin oxide layers of known thickness and dissolving them without affecting the metal has been described previously for Al (Davies *et al.* 1960*b*) and for W (McCargo *et al.* 1963*a*). To minimize hydration (and porosity) in the preparation of the Al_2O_3 films, an almost nonaqueous electrolyte was used (50 grams/liter $Na_2B_4O_7 \cdot 10H_2$) in 5% H_2O + 95% $(CH_2OH)_2$ (Vermilyea 1954) and all rinsing was done in alcohol. The WO_3 films were prepared in the manner described earlier.

Anodically formed oxide films are believed to be amorphous (Stirland and Bicknell 1959; Young 1961). This was verified at this laboratory by electron diffraction, which showed that the films contained no crystallites of dimensions larger than 100 Å.

The Chalk River isotope separator was used to produce the beam of radioactive ions. The separator produces ion beams in the energy range 20–70 keV. To obtain lower-energy ions the beam was electrostatically retarded. To obtain higher energies the beam was accelerated, or multiple-charged ions were used. As discussed in an earlier paper from this laboratory (Davies *et al.* 1963*a*), this introduces the complication that the small fraction of the ion beam that becomes neutralized after leaving the magnetic field will hit the target with the wrong energy. With a low enough pressure in the machine this component can, however, be made very small, $\approx 0.1\%$.

The radioactivity in the targets was measured with an end-window flowing-gas proportional counter having a low-energy discriminator to minimize background.

EXPERIMENTAL RESULTS

As discussed by McCargo *et al.* (1963*a*), one factor to be considered in the interpretation of range data is the loss of impinging atoms from the target during bombardment, either by wide-angle scattering or diffusional escape. It therefore became necessary to measure the sticking factor (the fraction of the incoming ions that becomes trapped) in order to establish the significance of the data obtained.

The sticking factors were measured for all ions used both in Al_2O_3 and WO_3 over the whole energy interval employed, using the method described earlier (Brown and Davies 1963). For energies above 5 keV the sticking factor was >0.95 in all cases, which is close enough to unity to make corrections to the range insignificant. Below 5 keV it dropped rather rapidly and the results were very irreproducible, indicating that range measurements in this energy region are of doubtful significance when made by the present technique.

Range distributions were measured for Na^{24}, Ar^{41}, Kr^{85}, and Xe^{125} in Al_2O_3 and WO_3 for energies between 0.5 and 160 keV. Examples of the experimental results for energies above 5 keV are shown in Fig. 1 for Kr^{85} in Al_2O_3 and in Fig. 2 for Na^{24} in WO_3.

Below a fractional transmission of 10^{-3} the measurements became irregular and irreproducible. We believe that this was caused by flaws (pinholes, etc.) in the oxide films due to handling. This explanation is supported by an experiment performed with extra care in which we managed to follow the

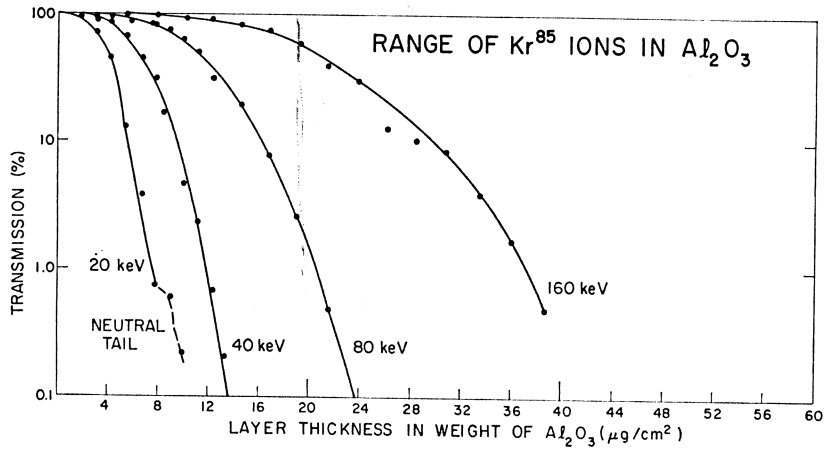

FIG. 1. Integral range distributions of Kr^{85} ions in Al_2O_3.

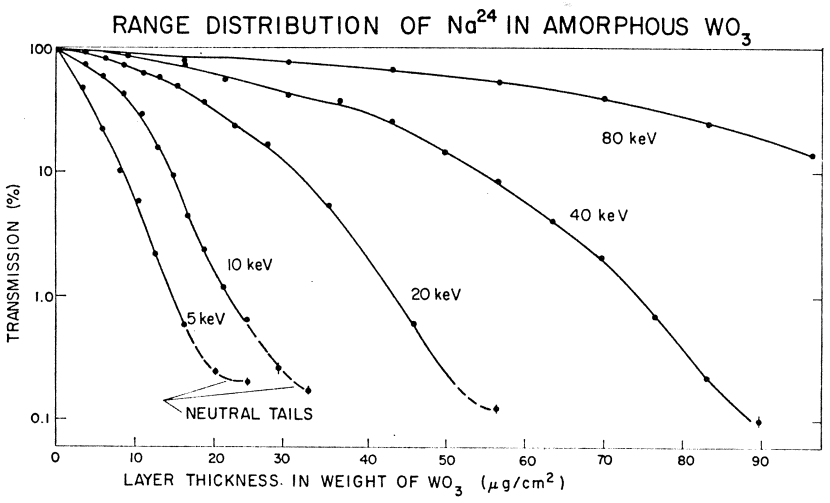

FIG. 2. Integral range distributions of Na^{24} ions in WO_3.

transmission down to 10^{-5}. The portions marked "neutral tails" in the figures are due to the unretarded fraction of the incoming beam, as mentioned above.

Figure 3 shows a comparison of the range distribution of 40-keV Kr^{85} in Al and in Al_2O_3. The most striking feature of the distribution in the oxide is the lack of the penetrating tail observed in polycrystalline and monocrystalline measurements (Piercy *et al.* 1964). This further supports the assumption that this tail is due to crystallographic effects.

Figure 4 shows the range distributions for Xe^{125} in Al_2O_3 for low energies. Only the experimental points and the bounding curves are shown. The points are quite irregular and the variation in median range is at most a factor of 2 for an energy variation of a factor of 10. A possible explanation for this effect,

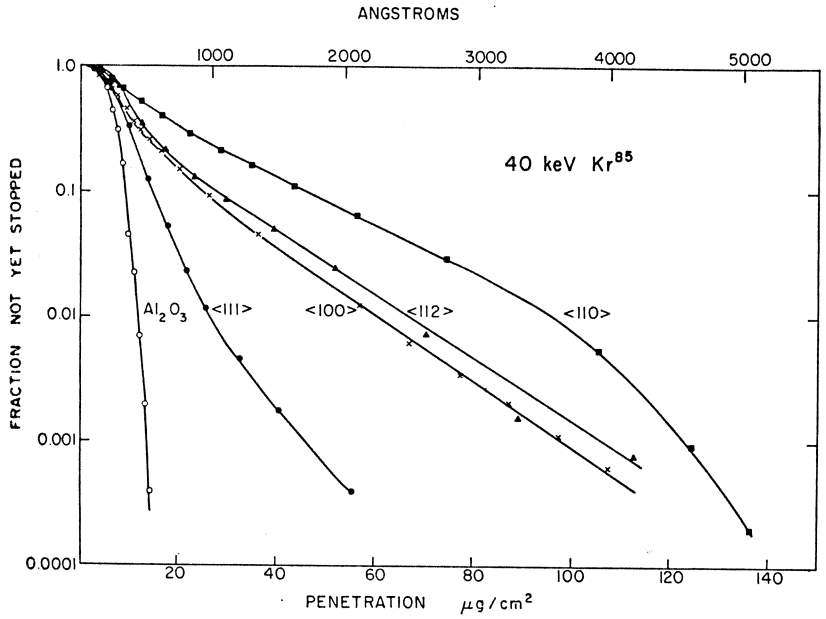

FIG. 3. Comparison of range distributions of 40-keV Kr^{85} in Al_2O_3 and in single crystals of Al.

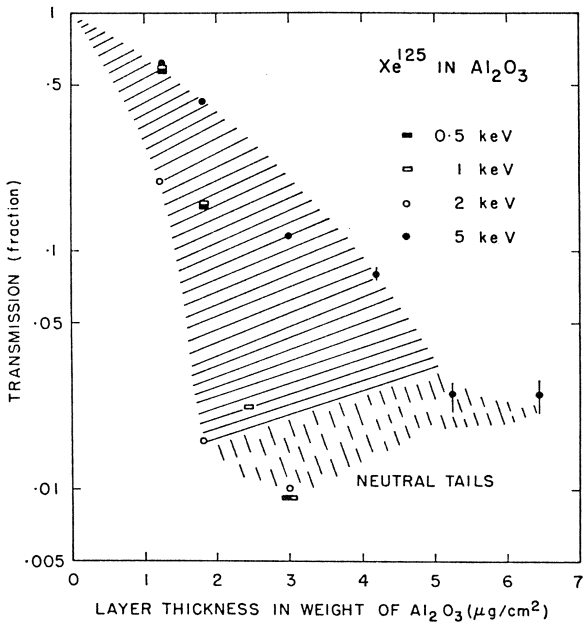

FIG. 4. Integral range distributions of Xe^{125} in Al_2O_3 (low energy). The shaded area indicates the region over which the distributions extend.

as well as the irreproducible sticking factors at these energies, is that the oxides are not truly amorphous but consist of microcrystallites perhaps 50 Å in size. This would not affect the high-energy data, where the range is greater than the size of the crystallites, but the low-energy runs would be influenced considerably.

In Tables I and II the characteristics of the measured range distributions

TABLE I

Characteristics of range distributions in Al_2O_3

Ion	Energy (keV)	R_p (μg/cm^2)	R_m (μg/cm^2)	$\bar{R}$ (μg/cm^2)	W_{rms} (μg/cm^2)
Na^{24}	2	—	(1.2)	—	—
	10	3.5	3.9	4.7	2.6
	20	5.8	6.4	6.7	3.8
	40	11.5	12.4	12.7	6.5
	80	28.5	28.8	29.5	11.3
Ar^{41}	0.5	—	(1.2)	—	—
	1	—	(1.2)	—	—
	2	—	(1.5)	—	—
	5	—	(1.7)	—	—
	10	2.5	2.6	2.5	1.2
	20	6.2	5.5	5.3	2.5
	40	10.4	9.4	9.3	4.5
	80	15.4	16.3	16.6	6.8
	160	32	34.4	35.2	10.9
Kr^{85}	0.5	—	(0.6)	—	—
	1	—	(0.6)	—	—
	2	—	(1.4)	—	—
	5	—	(1.6)	—	—
	10	2.5	2.4	2.4	1.2
	20	4.2	3.8	3.7	1.7
	40	7.2	6.4	6.2	2.5
	80	11.0	11.0	10.7	4.5
	160	19.6	20.1	20.4	6.7
Xe^{125}	0.5	—	(1.3)	—	—
	1	—	(1.3)	—	—
	2	—	(0.8)	—	—
	5	—	(1.5)	—	—
	10	2.5	2.3	2.3	0.96
	20	2.3	2.5	2.6	1.4
	40	5.7	5.3	5.2	1.8
	80	8.5	8.6	8.7	2.9
	160	13.5	14.3	14.7	4.4

are given. The parameters are:

R_p = most probable range,
R_m = median range,
$\bar{R}$ = mean range, and
W_{rms} = root mean square deviation from the mean range.

The unit for penetration depth employed is the total weight of Al_2O_3 (or WO_3) per unit area (μg/cm^2).

For the lower energies only the median range is given. The brackets indicate the uncertainty in these numbers. The errors in the other data are $\pm 6\%$ for R_m and $\bar{R}$, and around $\pm 10\%$ for R_p and W_{rms}. The different ranges (R_p, R_m,

TABLE II

Characteristics of range distributions in WO_3

Ion	Energy (keV)	R_p (μg/cm^2)	R_m (μg/cm^2)	$\bar{R}$ (μg/cm^2)	W_{rms} (μg/cm^2)
Na^{24}	0.5	—	(2.4)	—	—
	1	—	(2.4)	—	—
	2	—	(2.4)	—	—
	5	—	3.2	3.8	3.2
	10	6	7.2	7.6	4.7
	20	14	14.9	16.3	10.2
	40	21	27.0	28.8	17.6
	80	56	58	58	33
Ar^{41}	2	—	(2.9)	—	—
	5	—	(1.5)	—	—
	10	—	3.9	4.4	3.3
	20	5	8.4	9.1	5.9
	40	14	16.6	17.6	10.4
	80	34	33.8	34.9	20
	160	84	71	68	34
Kr^{85}	2	—	(0.8)	—	—
	5	—	(1.0)	—	—
	10	—	2.5	2.9	2.1
	20	6.6	6.7	7.4	4.0
	40	11.7	1.27	13.5	6.2
	80	14.5	19.7	20.5	10.2
	160	38	38.0	41.0	19.5
Xe^{125}	0.5	—	(1.0)	—	—
	1	—	(1.4)	—	—
	2	—	(1.9)	—	—
	5	—	(2.9)	—	—
	10	3.2	3.5	3.5	2.1
	20	5.2	5.7	5.8	3.2
	40	9.9	10.2	10.5	4.5
	80	15.6	16.4	17.0	7.9
	160	30	28.9	28.5	13.4

and $\bar{R}$) are almost identical, in marked contrast to what is observed in crystalline material. W_{rms} is within 20% of the half-width at half-maximum of the differential range distribution.

COMPARISON WITH THEORY

The experimental results will be compared with the theoretical predictions of Nielsen (1956) and of Lindhard *et al.* (1963).

Lindhard *et al.* (1963) assume a Thomas–Fermi potential for calculating the energy lost by elastic collisions. They obtain a universal range–energy curve in terms of dimensionless range and energy parameters given by

$$\rho = RNM_2 4\pi a^2 \frac{M_1}{(M_1 + M_2)^2}, \tag{1}$$

$$\epsilon = E \frac{aM_2}{Z_1 Z_2 e^2 (M_1 + M_2)}, \tag{2}$$

where R is the range,
E is the energy,

N is the number of target atoms per unit volume,
Z_1 and Z_2 are the nuclear charge of the incoming particle and the target atom, respectively,
M_1 and M_2 are the corresponding masses,
e is the electronic charge,
and a is the screening radius given by

$$a = a_0 \cdot 0.8853\ (Z_1^{2/3} + Z_2^{2/3})^{-1/2}, \tag{3}$$

where a_0 is the first Bohr radius in the hydrogen atom.

The contribution of inelastic collisions is included by adding to the elastic stopping power a term that in dimensionless units has the form

$$(\mathrm{d}\epsilon/\mathrm{d}\rho)_{\mathrm{inel}} = k\epsilon^{1/2}, \tag{4}$$

where

$$k = \xi_e \cdot \frac{0.0793 Z_1^{1/2} \cdot Z_2^{1/2} (M_1 + M_2)^{3/2}}{(Z_1^{2/3} + Z_2^{2/3})^{3/4} M_1^{3/2} M_2^{1/2}}, \qquad \xi_e \simeq Z_1^{1/6}. \tag{5}$$

The calculations thus produce a set of curves of ρ versus ϵ, each characterized by the value of k.

The straggling or mean square deviation from the mean is given as curves by plotting the quantity

$$\frac{(M_1 + M_2)^2}{4M_1M_2} \frac{\overline{\Delta R^2}}{\bar{R}^2}$$

as a function of ϵ for different values of k.

A complication in comparing our results with the predictions of Lindhard *et al.* is that the effect of the oxygen in the oxide has to be corrected for. If the stopping cross-sections due to the different atoms in a compound are all proportional to the same power of the energy, simple formulae can be worked out for the range and straggling. In a compound, $\mathrm{C} = \mathrm{A}_x \mathrm{B}_y$, the range R_C is given by

$$\frac{R_\mathrm{C}}{M_\mathrm{C}} = \frac{1}{(xM_\mathrm{A}/R_\mathrm{A}) + (yM_\mathrm{B}/R_\mathrm{B})} \qquad (R \text{ in } \mu\mathrm{g/cm}^2). \tag{6}$$

M_C, M_A, and M_B are the masses of the compound C and the constituent atoms A and B, respectively, and R_A and R_B are the ranges in pure A and B, respectively. (A similar formula is given by Lindhard *et al.*)

Similarly the straggling is given by:

$$\omega_\mathrm{C}^2 = \frac{x(M_\mathrm{A}/R_\mathrm{A})(R_\mathrm{B}/M_\mathrm{B})\omega_\mathrm{A}^2 + y\omega_\mathrm{B}^2}{x(M_\mathrm{A}/R_\mathrm{A})(R_\mathrm{B}/M_\mathrm{B}) + y} \qquad (R \text{ in } \mu\mathrm{g/cm}^2), \tag{7}$$

where ω_i^2 is the relative straggling $(\overline{\Delta R_i^2}/\bar{R}_i^2)$.

To get the range in Al from equation (6) and the measured range in $\mathrm{Al_2O_3}$ we need to know the ratio between the range in Al and that in O. We assume that this ratio is given accurately enough by the calculations of Lindhard

et al. (1963). The justification for this assumption is that even the uncorrected range in Al_2O_3 agrees fairly well with the theory. This ratio and the measured range are used to calculate the range in Al and in O from equation (6). The experimental range in WO_3 and the range in O obtained above are then used to calculate the range in W.

To obtain the straggling, an assumption has again to be made about the ratio between the values in Al and in O. According to Lindhard, the quantity

$$\frac{(M_1 + M_2)^2}{4M_1M_2} \frac{\overline{\Delta R^2}}{\bar{R}^2}$$

varies very slowly with M_1, M_2, and ϵ. Assuming it to be constant, we get a ratio between the straggling in Al and the straggling in O. Equation (7) then gives the straggling in Al. For reasons outlined below, no comparison with theory was attempted for the WO_3 straggling data.

The data still have to be corrected for the fact that the theory involves the range distribution along the path of the particle, whereas our measurements give the range distribution projected onto the direction of the incoming beam. Lindhard *et al.* give this path-length correction for the range as a function of energy and the parameter k for mass ratios μ ($\mu = M_2/M_1$) up to 2. For larger mass ratios (Na and Ar in WO_3), their approximate formula was used.

The path-length correction to the straggling is more difficult to assign. Lindhard quotes a 30% correction to the relative straggling ($\overline{\Delta R^2}/\bar{R}^2$) in the case where $\mu = 1$. We have applied this value to the case of Na^{24} in Al_2O_3 and assumed the correction to vary linearly with μ up to $\mu = 1$. No attempt was made to compare the WO_3 straggling data with theory because of the difficulty of finding a suitable path-length correction for the large mass ratios.

Figures 5 and 6 show the *mean* ranges in Al_2O_3 and WO_3 compared with the theory of Lindhard *et al.* Figure 7 shows the straggling in Al_2O_3 compared with theory.

The accuracy of the range analysis described above depends on the difference between the constituents of the oxide. For Al_2O_3, it is thought that the analysis does not contribute any error, and the $\pm 6\%$ error of the experimental ranges has been used in the figure. For WO_3 the assumption that the stopping cross-sections of W and O are proportional to the same power of the energy is not a good one, since this is strictly true only if the ϵ value is the same in both W and O (cf. Lindhard *et al.* 1963, Fig. 2), which is obviously not the case. A tentative error of $\pm 15\%$ has therefore been assigned to the points in Fig. 6. Owing to the uncertainty in estimating the path-length correction, no errors are shown for the Na^{24} and Ar^{41} data.

For the straggling data in Fig. 7, the error is largely due to the uncertain path-length correction. An error of $\pm 30\%$ has been assigned to these data.

From Fig. 5 it can be seen that the agreement between theory and experiment for mean ranges in Al_2O_3 is excellent. Only 4 points out of 19 do not agree with theory within the assigned error. For the WO_3 range data in Fig. 6 the agreement is not so good. This can be attributed, at least partly, to inaccuracy in the analysis.

$\frac{M_s}{M_p}$ $\frac{M_2}{M_1}$

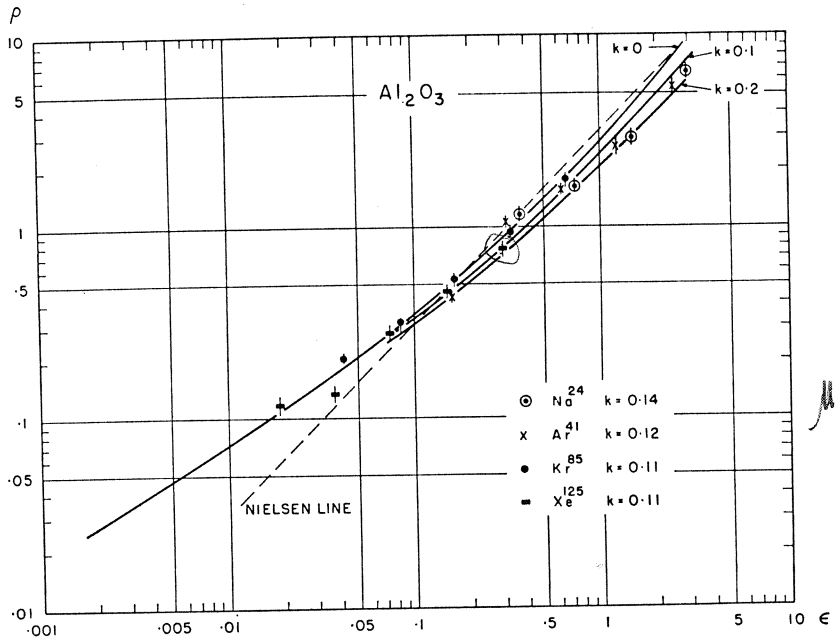

FIG. 5. Comparison of the experimental mean ranges in Al_2O_3 with the theoretical curves of Lindhard *et al.* The appropriate k value for each projectile has been calculated from equation (5).

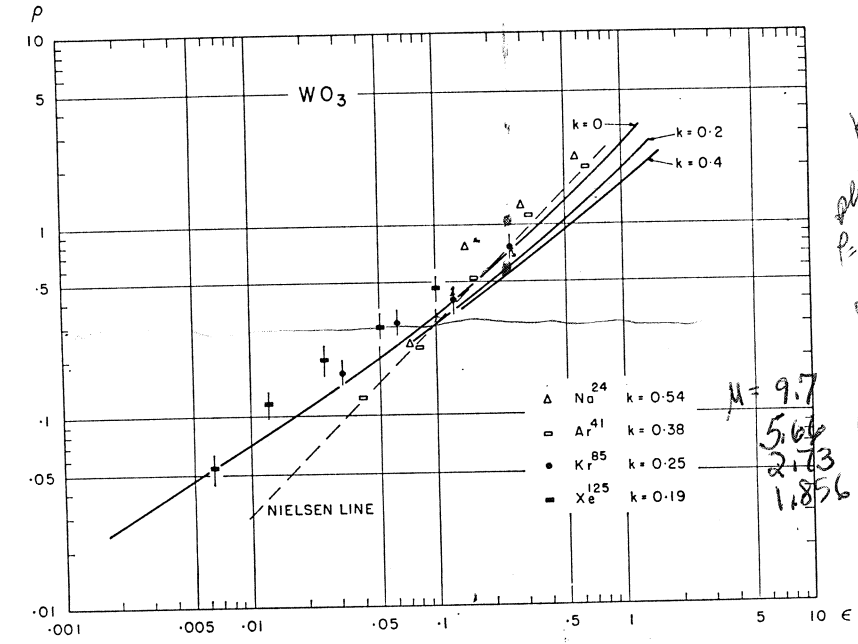

FIG. 6. Comparison of the experimental mean ranges in WO_3 with the theoretical curves of Lindhard *et al.* The appropriate k value for each projectile has been calculated from equation (5).

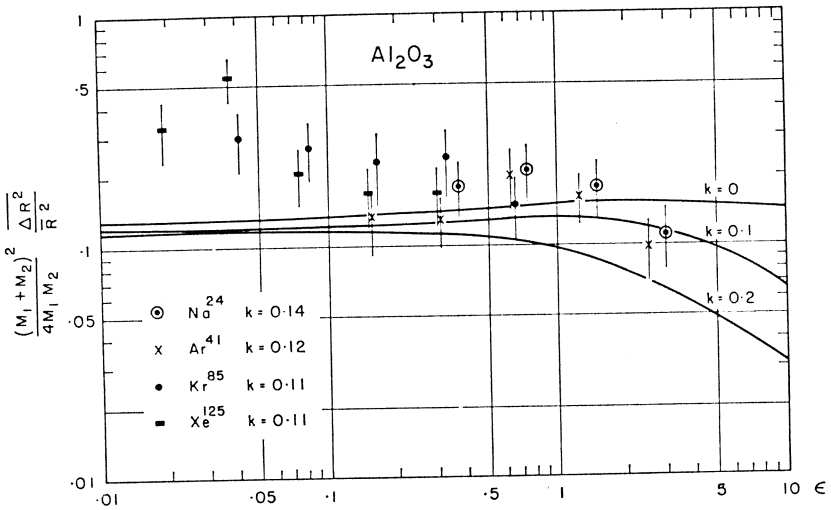

FIG. 7. Comparison of the experimental relative straggling in Al_2O_3 with the theoretical curves of Lindhard *et al.* The appropriate k value for each projectile has been calculated from equation (5).

The straggling data in Fig. 7 agree fairly well with theory, although the experimental data are slightly higher. This may be due to the mathematical approximations used by Lindhard *et al.* (1963) which, according to their paper, tend to give too small values to the relative straggling.

Oen and Robinson (1964) have calculated the range in a target consisting of randomly distributed atoms using a Monte Carlo approach. A detailed comparison is not possible, since the calculations deal with targets containing only one type of atom. However, the results suggest that, if calculations were made specifically for WO_3 and Al_2O_3, good agreement with experiment would be obtained. A detailed discussion is given by Oen and Robinson (1964).

CONCLUSIONS

Range distributions in amorphous solids lack the penetrating tails observed in crystalline materials, further confirming the assumption that these are due to crystallographic effects. The most probable, median, and mean ranges are very close, indicating a rather symmetrical distribution. Comparison with the theory of Lindhard *et al.* over the energy interval 10 to 160 keV shows that this theory predicts satisfactorily the range and straggling in amorphous solids.

ACKNOWLEDGMENTS

The authors are indebted to J. L. Whitton for making the electron diffraction studies of the anodic oxide films. R. L. Cushing and J. C. Tole assisted by operating the mass separator and G. A. Sims assisted with the anodizing and counting procedures.

change in ~~stand~~ constant :

$$\bar{S} - \bar{S}^{\circ} = -R \ln\left(\frac{P_{(atm)}}{T_{atm}}\right)$$

REFERENCES

BEELER, J. R. and BESCO, D. G. 1963. J. Appl. Phys. **34**, 2873.
BERGSTRÖM, I., DAVIES, J. A., DOMEIJ, B., and UHLER, J. 1963. Arkiv Fysik, **24**, 389.
BROWN, F. and DAVIES, J. A. 1963. Can. J. Phys. **41**, 844.
DAVIES, J. A., BROWN, F., and MCCARGO, M. 1963*a*. Can. J. Phys. **41**, 829.
DAVIES, J. A., DOMEIJ, B., and UHLER, J. 1963*b*. Arkiv Fysik, **24**, 377.
DAVIES, J. A., FRIESEN, J., and MCINTYRE, J. D. 1960*a*. Can. J. Chem. **38**, 1526.
DAVIES, J. A., MCINTYRE, J. D., CUSHING, R. L., and LOUNSBURY, M. 1960*b*. Can. J. Chem. **38**, 1535.
DAVIES, J. A., MCINTYRE, J. D., and SIMS, G. A. 1961. Can. J. Chem. **39**, 611.
DAVIES, J. A. and SIMS, G. A. 1961. Can. J. Chem. **39**, 601.
KORNELSEN, E. V., BROWN, F., DAVIES, J. A., DOMEIJ, B., and PIERCY, G. R. 1964. To be published.
LASSEN, N. O., POULSEN, N. O. R., SIDENIUS, G., and VISTISEN, L. 1962. Paper presented at the Conference on the Physics of the Electromagnetic Separation Method, Paris.
LEHMANN, C. and LEIBFRIED, G. 1963. J. Appl. Phys. **34**, 2821.
LINDHARD, J., SCHARFF, M., and SCHIØTT, H. E. 1963. Kgl. Danske Videnskab. Selskab, Mat.-Fys. Medd. **33**, No. 14, 1.
MCCARGO, M., BROWN, F., and DAVIES, J. A. 1963*b*. Can. J. Chem. **41**, 2309.
MCCARGO, M., DAVIES, J. A., and BROWN, F. 1963*a*. Can. J. Phys. **41**, 1231.
NIELSEN, K. O. 1956. Electromagnetically enriched isotopes and mass spectrometry (Academic Press, New York), p. 68.
OEN, O. S. and ROBINSON, M. T. 1964. J. Appl. Phys. (in press).
PIERCY, G. R., BROWN, F., DAVIES, J. A., and MCCARGO, M. 1963. Phys. Rev. Letters, **10**, 399.
PIERCY, G. R., MCCARGO, M., BROWN, F., and DAVIES, J. A. 1964. To be published.
ROBINSON, M. T. and OEN, O. S. 1963. Appl. Phys. Letters, **2**, 30.
STIRLAND, D. J. and BICKNELL, R. W. 1959. J. Electrochem. Soc. **106**, 481.
UHLER, J., DOMEIJ, B., and BORG, S. 1963. Arkiv Fysik, **24**, 413.
VERMILYEA, D. A. 1954. Acta Met. **2**, 482.
YOUNG, L. 1961. Anodic oxide films (Academic Press, London).

$$E_{CN} = E_b \cdot \frac{A_b A_R}{(A_b + A_T)^2}$$

$U + p$ 100 $\frac{1 \times 235}{(236)^2} = .423$

$U + \alpha$ 140 $\frac{4 \times 235}{(239)^2} = 2.304$

lev/particle = 23 kcal/mole ~ 3.82×10^{-23} cal/particle

a $2.07 \times 10^{17} \frac{\text{particles}}{cm^2}$ x beam size

Fluorine - Uranium bond strength = F^- 1.33

ΔH_f of gas from elements in their standard states

kcal/mole at 25°C

F_2 (g) 18.5

U (c) 117

bond lengths Å

U-U 2.77

3.058 (b.c.c.)

Th-Th α (25°) 3.595 (fcc)

β (1450°) 3.56 (bcc)

Th ~ bp ~ 4800°C — 1845°C melt 1132°C

U bp 3818°C

UF_4 melts 960°C

ThF_4 melts > 900°C

crystal atomic radii

U +4 .97

+6 .80

Th +4 1.02

F_2 $S^\circ = 48.6$ $\Delta H^\circ = \Delta F^\circ = 0$

ThF_4 (c) $\Delta H_f^\circ = -477$

Th $S^\circ = 13.6$

	ΔH_f°	ΔF_f°	
UF_4 (c)	−443	−421	$S^\circ = 36.1$
(III c) U			$S^\circ = 12.03$

73.6×10^{-23} kcal/atom

NUCLEAR INSTRUMENTS AND METHODS 78 (1970) 277–284; © NORTH-HOLLAND PUBLISHING CO.

STRAGGLING AND PARTICLE IDENTIFICATION IN SILICON DETECTORS*

H. BICHSEL†

Lawrence Radiation Laboratory, University of California, Berkeley, California

Received 25 August 1969

The distribution functions for the straggling of charged particles in silicon detectors are given in a comprehensive graphical form. Approximate quantum mechanical corrections have been applied to the Vavilov functions.

A simple identification procedure for use with a digital computer is described.

1. Introduction

A system frequently used for the identification of charged particles of kinetic energy T consists of one or more thin silicon detectors ("ΔT counters") in which the particles experience energy losses Δ, and a final detector ("T counter") thick enough to absorb the total residual energy of the incident particles[1]). The resolution of this system is limited by straggling, dominated by the effect in the ΔT counter. If different particles of the same incident kinetic energy T have overlapping straggling curves in the thin detector, it will not be possible to identify particles having energy losses in the region of overlap (figs. 1–3).

It is often assumed that, for large absorber thicknesses t, the straggling curve is Gaussian[2]). This is only an approximation (see figs. 5–7). A better approximation is given by the Vavilov theory[3]), which has been shown to be fairly accurate for the description of the energy loss of charged particles in silicon[4-6]).

The observation of pulse heights in a thin detector is described by the probability density function $f(\Delta, t)$, but the determination of the overlap of the energy loss functions requires a knowledge of the distribution function $\Phi(\Delta, t) = \int_0^{\Delta} f(\Delta', t)\, d\Delta'$. Notice that physicists frequently use the expression "distribution function" to describe $f(\Delta, t)$. If the mean energy losses of particles A and B are called $\bar{\Delta}_A$ and $\bar{\Delta}_B$ respectively, it will be found for an energy loss Δ_1 defined by

* Work supported in part by the U.S. Atomic Energy Commission and Public Health Service Research Grant No. CA-08150 from the National Cancer Institute.

† Now at the Department of Radiology, University of Washington, Seattle, Washington 98105, U.S.A.

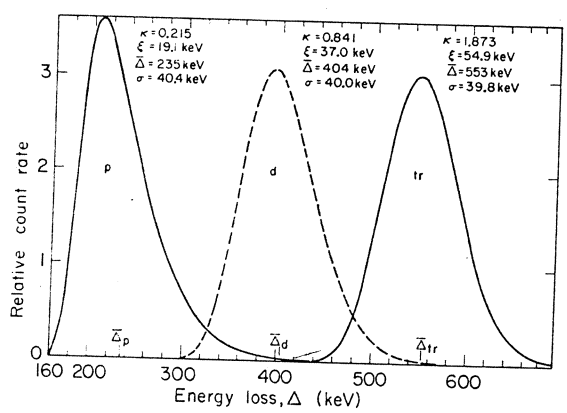

Fig. 1. Calculated energy losses of 40-MeV protons, deuterons, and tritons in a silicon detector of thickness t = 20 mg/cm². The same numbers of particles of each kind are incident. The mean energy loss $\bar{\Delta}$ is quite different from the most probable energy loss, especially for the protons. If the cross-over point of the curves is selected for the separation of protons and deuterons (Δ = 327 keV), about 2.7% of the protons will be identified as deuterons, while about 1.5% of the deuterons will appear as protons. Similarly, for Δ = 480 keV, about 3.6% of the deuterons will appear as tritons and 2.6% of the tritons will appear as deuterons. It should be noted that, with the assumed system, it is not possible to distinguish between protons and deuterons in the overlapping region (approximately 300 to 420 keV).

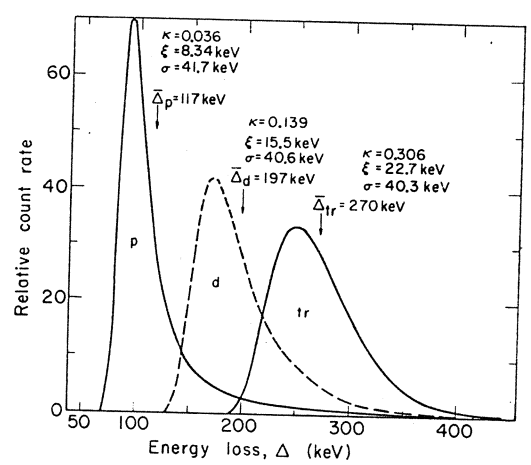

Fig. 2. Energy loss of 100-MeV p, d, tr in a silicon detector with thickness 20 mg/cm². For protons, with $\bar{\Delta}$ = 117 keV, the most probable energy loss is about 93 keV. About 14% of the protons will lose energies in excess of 145 keV, about 7% of deuterons will have smaller energy losses. About 5% of the protons suffer energy losses exceeding 200 keV; 23% of the deuterons exceed energy losses of 218 keV (intercept of d and tr curves), and 7.5% of the tritons fall below this point. A detector this thin would obviously not be practical for particle identification at this energy.

$\bar{\Delta}_A \leqslant \Delta_1 \leqslant \bar{\Delta}_B$ that a fraction

$$P_A = 1 - \Phi_A(\Delta_1, t) \qquad (1)$$

of all particles A will exceed the energy loss Δ_1, while a fraction

$$P_B = \Phi_B(\Delta_1, t) \qquad (2)$$

of all particles B will have energy losses smaller than Δ_1.

The distribution functions are given and discussed in this paper. Also, some comments are made about the use of on-line computers in particle identification.

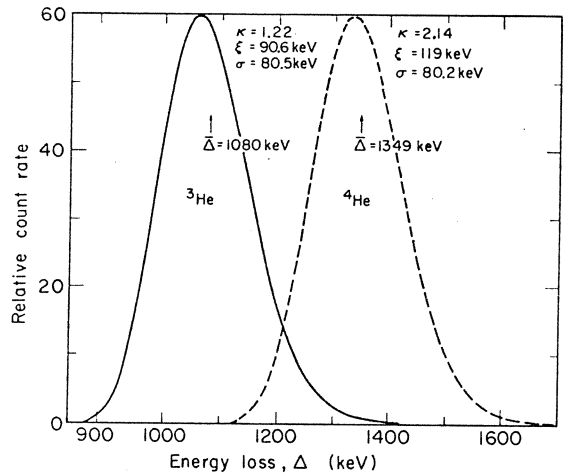

Fig. 3. Energy-loss distribution for 100-MeV ^{3}He and ^{4}He ions; 7.2% of the ^{3}He will experience energy losses larger than 1213 keV (crossover point of the curves), and 4.3% of the ^{4}He ions will be found below this point.

2. The distribution functions

The probability that charged particles will experience energy losses between Δ and $\Delta + d\Delta$ in traversing an absorber of thickness t is given by the probability density function $f(\Delta, t)$, which also depends on the charge ze and the velocity $v = \beta c$ of the incident particle. The discussion in this paper is based on the Vavilov theory[3]), with some corrections brought about by the use of quantum mechanical collision cross sections[7,8]) instead of the $1/E^2$ cross section used by Vavilov. An extensive discussion has been given by Seltzer and Berger[9]). Their nomenclature is used for this discussion. It has recently been found[10]) that, in the stopping power, there is a charge dependence over and above the z^2 term usually assumed. It presumably would appear in the theory with the use of

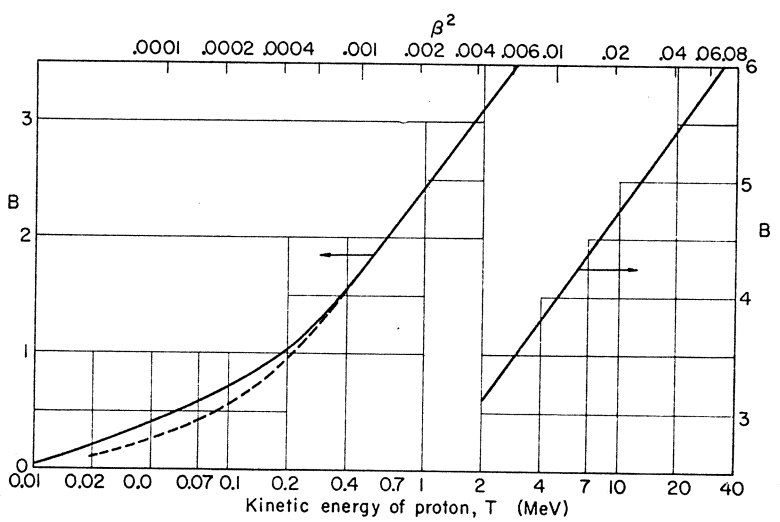

Fig. 4. The reduced stopping number B for protons in silicon, $\beta^2 \approx 2\,T/Mc^2$. The stopping power is given by

$$S = 0.1531\, z^2\, B/\beta^2 \qquad (\text{MeV cm}^2/\text{g}),$$

the mean energy loss by

$$\bar{\Delta} = 153.1\, z^2\, t\, B/\beta^2 \qquad (\text{keV}).$$

The curve is semi-empirical, and applies approximately for other particles. For $\beta^2 \geqslant 0.04$,

$$B = \ln[5891\,\beta^2/(1-\beta^2)] - \beta^2 - 0.0019/\beta^2.$$

For $\beta \leqslant 0.024\, z^{\frac{2}{3}}$ the nuclear charge is partly shielded by atomic electrons, and z has to be replaced by z^*, given approximately by

$$z^* = z\,[1 - \exp(-1.316x + 0.1112\,x^2 - 0.065\,x^3)],$$

where $x = 100\,\beta/z^{\frac{2}{3}}$ and $z \geqslant 2$. For $x \leqslant 0.27$, the theory does not apply. For the solid curve, a charge state correction is applied for all particles. The dashed curve is B corrected for the charge state of the proton.

higher Born approximations, and would influence the straggling somewhat at low energies. No correction for this effect is included here.

The distribution functions required for the determination of the overlap of the straggling functions of different particles in a given ΔT counter are defined in terms of the modified Vavilov functions[7,8]):

$$\Phi(\Delta, t) \equiv \int_0^{\Delta} f(\Delta', t)\,\mathrm{d}\Delta', \tag{3}$$

with

$$\Phi(\infty, t) \equiv \int_0^{\infty} f(\Delta', t)\,\mathrm{d}\Delta' = 1.$$

The parameters z and β are implicitly included in eq. (3). The accuracy of $f(\Delta,t)$ is limited due to uncertainties in the quantum mechanical corrections (including the deviations from the z^2 behavior); the numerical integration in eq. (3) is accurate only to about 0.2%. The overall accuracy of Φ is estimated to be about 0.01 for $\Phi \geqslant 0.3$, and about 0.005 for $\Phi < 0.3$. For the present application to silicon absorbers, the following reduced variables have to be calculated:

$$\sigma^2 = 78.22 \times tz^2(1-\tfrac{1}{2}\beta^2)(1+q)Q'/(1-\beta^2) \quad (\mathrm{keV}^2), \tag{4}$$

$$\xi = 0.076\,54 \times tz^2/\beta^2 \quad (\mathrm{keV}), \tag{5}$$

$$\varkappa = 7.490 \times 10^{-5} \times tz^2(1-\beta^2)/\beta^4, \tag{6}$$

where particles of charge ze, rest mass M, and initial velocity $v = \beta c$ are incident on a silicon detector of thickness t (in mg/cm^2); q is the quantum mechanical correction, given approximately by

$$q = 0.001\,86\,\beta^{-2} \ln(102\beta^2 + 0.746) \quad \text{for } 0.0005 < \beta^2 < 0.0075, \tag{7}$$

$$q = 0.0009\,\beta^{-2} \ln(306\beta^2) \quad \text{for } 0.0075 < \beta^2; \tag{7'}$$

Q' is a factor caused by the increase in straggling due to the spread in energy of the particle beam[11]); with $T_1 = T - \overline{\Delta}$,

$$Q' = (T/T_1)^{\frac{1}{3}} \text{ for } T_1/T > 0.4, \quad B \approx 2.3,$$

$$Q' = 0.99\,(T/T_1)^{\frac{1}{2}} \quad T_1/T > 0.4, \quad B \approx 3.5, \tag{8}$$

$$Q' = 0.985\,(T/T_1)^{\frac{2}{3}} \quad T_1/T > 0.6, \quad B \approx 6.9,$$

where B is the stopping number (fig. 4).

Here σ is the standard deviation of the straggling function, and ξ and $\varkappa$ are the parameters of the Vavilov theory[9]). Furthermore, the mean energy loss has to be calculated:

$$\overline{\Delta} = \int_0^{\infty} f(\Delta, t)\,\Delta\,\mathrm{d}\Delta = tS = 2\xi B\,(\mathrm{keV}), \tag{9}$$

where S in (keV cm^2/mg) is the stopping power[12-14]) and B the stopping number (see fig. 4). The velocity should be calculated with

$$\beta^2 = \tau(\tau+2)/(\tau+1)^2, \text{ with } \tau = T/Mc^2. \tag{10}$$

Notice that $\sigma^2 = \xi^2(1-\frac{1}{2}\beta^2)/\varkappa$ except for the corrections given by q and Q'. The probability densities $f(\Delta, t)$ are given in ref. [9]) in terms of the parameters $\varkappa$ and β^2 and as a function of the dimensionless energy-loss variable

$$\lambda = \hat{\lambda} + (\Delta - \overline{\Delta})/\xi, \tag{11}$$

where

$$\hat{\lambda} = 0.577\,216 - 1 - \beta^2 - \ln \varkappa.$$

For present purposes, another dimensionless energy-loss variable is more suitable:

$$p = (\Delta - \overline{\Delta})/\sigma. \tag{12}$$

The parameters $\varkappa$ and β^2 are kept unchanged.

Eq. (3) can be rewritten in terms of these parameters as

$$\Phi(p, \varkappa, \beta) = \int_0^{p} f(p', \varkappa, \beta)\,dp'. \tag{13}$$

Distribution functions have been calculated by numerical integration of $f(p', \varkappa, \beta)$, and are given in figs. 5-7 for three values of β^2. The dependence on β^2 is quite small, and it will not be necessary to use interpolation for β^2.

The functions presented here do not include corrections for effects connected with the operation of silicon detectors, e.g., electronic noise, inhomogeneity of detector thickness, counting statistics, and channeling.

Since the function Φ does not change very much for $\varkappa > 6$, the exact choice of $\varkappa$ for $T_1/T < 0.8$ is not very critical. It is seen, though, that even for $\varkappa = 10$ there is a difference between the straggling function and a Gaussian curve (see fig. 6).

Note that the "skewness parameter" γ_3 in fig. 4 of ref. [11]) is related to $\varkappa$ in a simple way: $\varkappa \approx 1/(4\gamma_3^2)$. For $\beta^2 = 0$, the expression is exact.

A Fortran program VPLOT, giving graphs similar

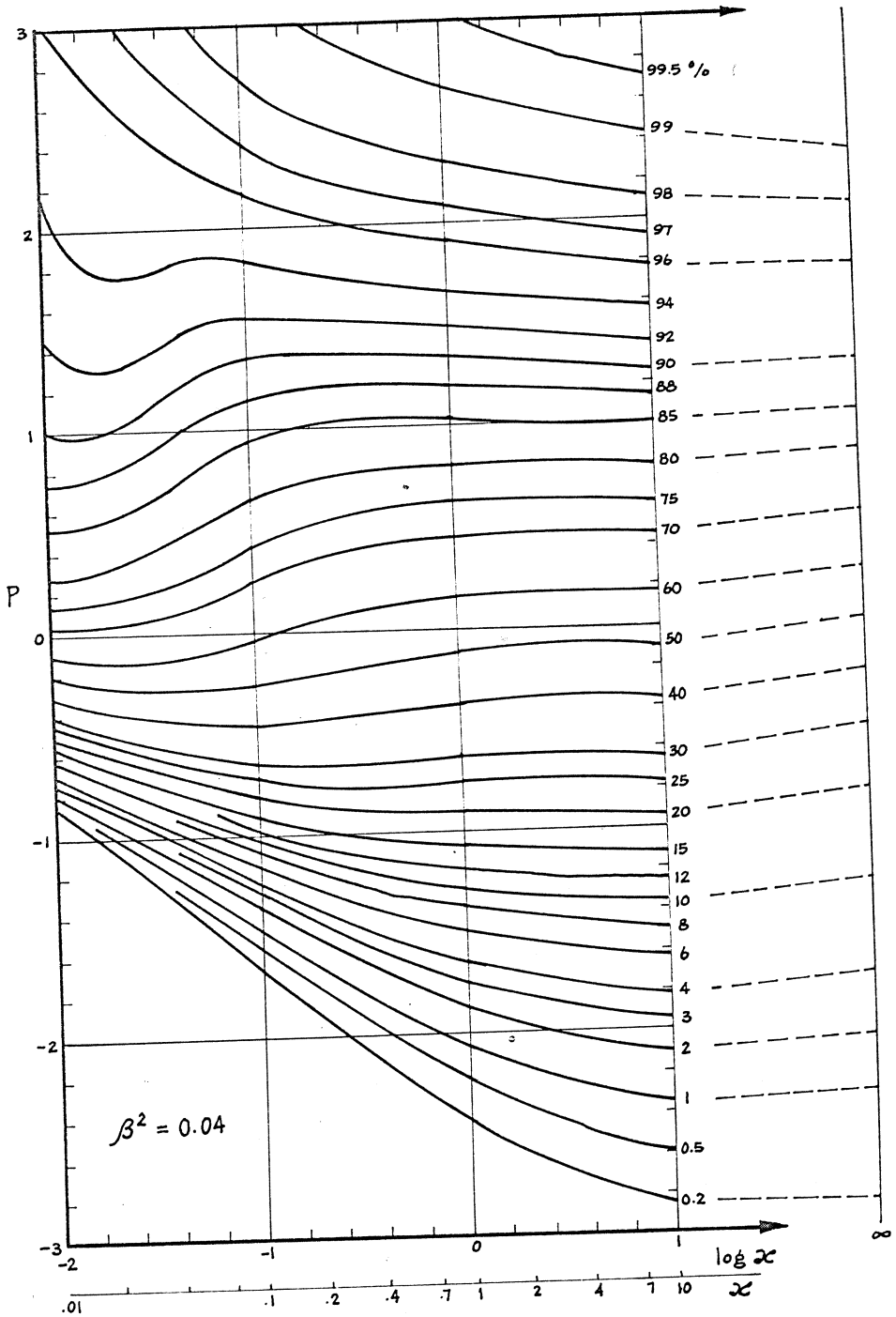

Fig. 5. Contour lines for straggling curves, modified for quantum mechanical corrections, for $\beta^2 = 0.04$ (protons of about 20 MeV). The ratio $p(\Phi, \varkappa) = (\Delta_q - \overline{\Delta})/\tau$ is plotted for different values of Φ, as a function of $\varkappa$. Φ is the fraction of particles experiencing energy losses less than Δ_q, eq. (1). The accuracy of the numbers is about 3%. The location of the mean is given by $p = 0$.

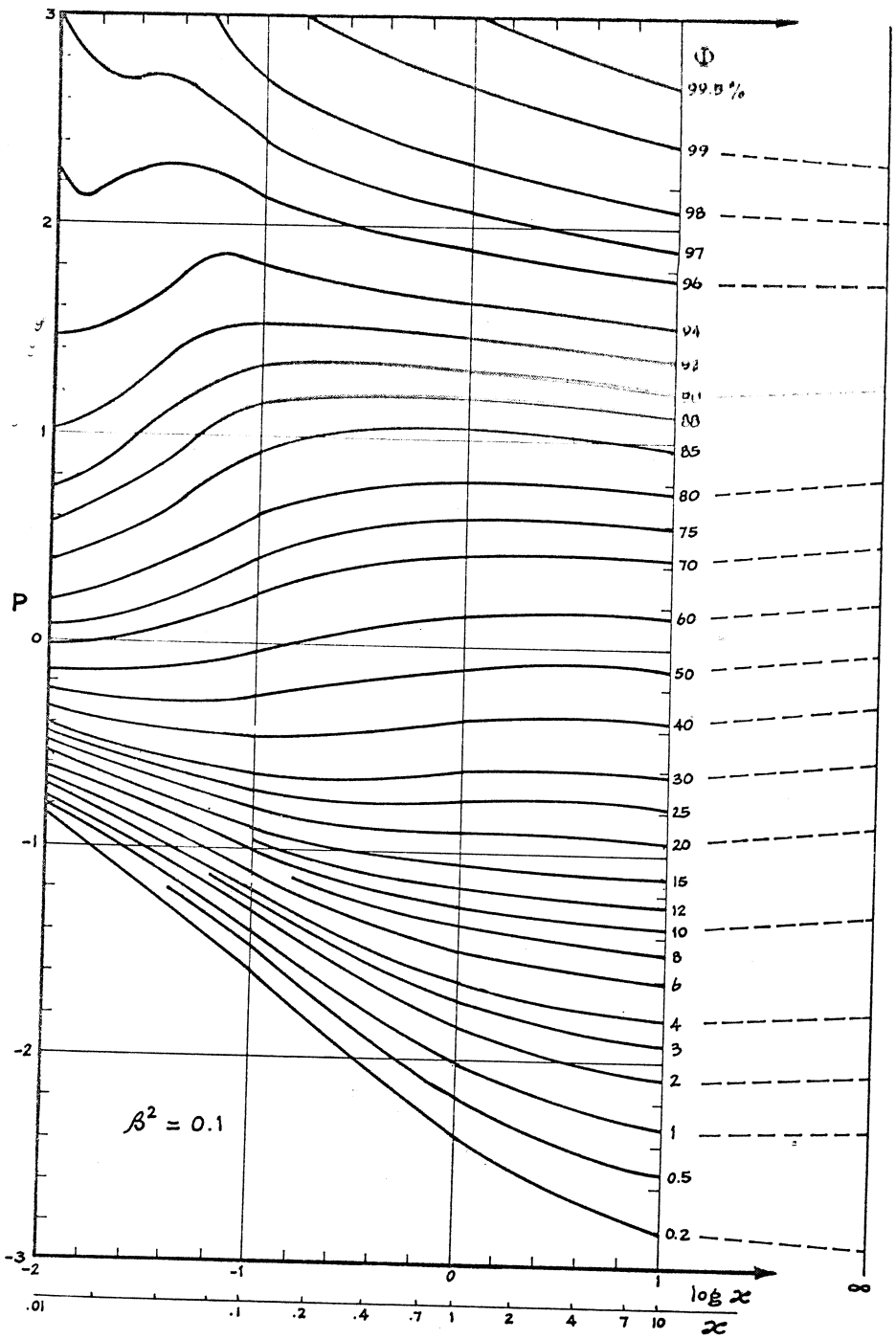

Fig. 6. Contour lines for $\beta^2 = 0.1$ (protons of about 50 MeV), $\varkappa = \infty$ is a Gaussian.

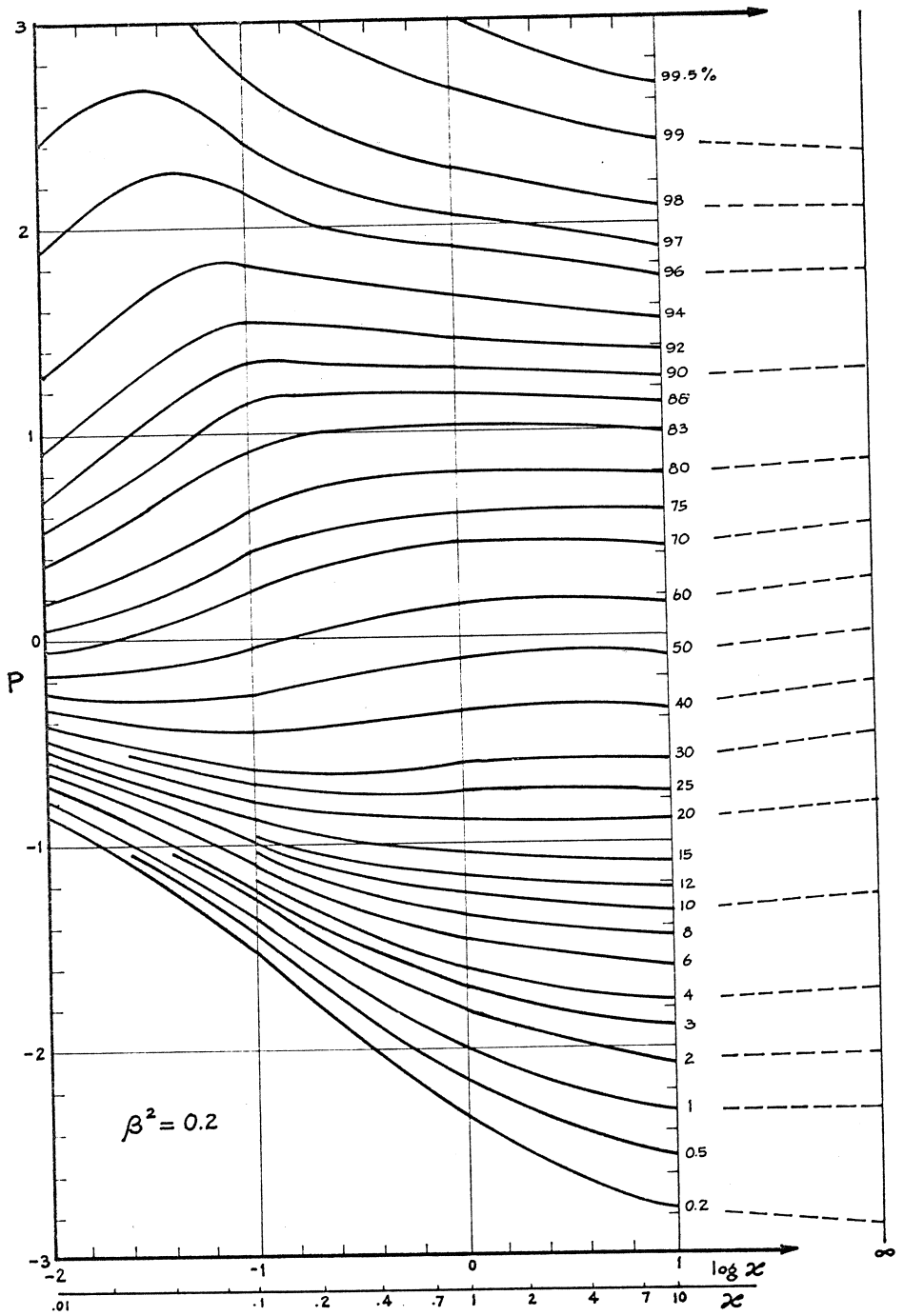

Fig. 7. Contour lines for $\beta^2 = 0.2$ (protons of about 110 MeV).

to figs. 1–3 and both $f(\Delta, t)$ and $\Phi(\Delta, t)$, is available from the author.

It should be noted that it may frequently be easier to calculate the moments of an experimental straggling function and compare them with the theoretical moments[12]) than to calculate a Vavilov function.

3. Approximate expressions and examples

For estimates at low and moderate energies, the following simplified expressions can be used for the parameters:

$$\sigma = 9\, z \sqrt{t}\ (\text{keV}),$$
$$\xi = 36\, z^2\, tA/T\ (\text{keV}),$$
$$\varkappa = 16.3\, z^2\, tA^2/T^2,$$
$$\beta^2 = 0.002\,14\, T/A,$$

where T in (MeV) is the kinetic energy, and A the atomic number of the *incident* ion. If the energy loss $\bar{\Delta} = (T - T_1)$ in the ΔT counter amounts to more than 10% of T, σ should be multiplied by $\sqrt{Q'}$ from eq. (8).

Examples

1. In fig. 1, to determine the fraction Φ_{300} of protons exceeding an energy loss $\Delta = 300$ keV, calculate p, using σ from the figure: $p = (300–235)/40.4 = 1.61$. From fig. 6, for $\varkappa = 0.215$, we obtain $\Phi \approx 93\%$, showing that 7% of the protons suffer energy losses of more than 300 keV.
2. Consider deuterons and tritons of 40 MeV. To calculate the fraction of particles appearing beyond the energy loss $\Delta_m = \frac{1}{2}(\bar{\Delta}_d + \bar{\Delta}_{tr})$ as a function of detector thickness t(mg/cm^2), we have, from ref. [14]), $S_d = 20.2$ keV cm^2/mg, $S_{tr} = 27.7$ keV cm^2/mg, from ref. [12]), $\beta_d^2 = 0.0414$, $\beta_{tr}^2 = 0.0279$, $\varkappa_d = 0.0419\, t$, $\varkappa_{tr} = 0.0934\, t$, $p_{tr} = -p_d$. We get

	t (in mg/cm^2)			
	3	10	30	100
$\bar{\Delta}_d$(keV)	60.6	202	606	2020
$\bar{\Delta}_{tr}$(keV)	83.1	277	831	2770
Δ_m(keV)	71.8	239.5	718	2395
σ(keV)	15.9	29.0	50.0	89.5
p_d	0.71	1.29	2.24	4.2
$\varkappa_d$	0.126	0.419	1.26	4.2
$\varkappa_{tr}$	0.28	0.934	2.80	9.3
Φ_d(%)	82	89	97.7	99.5+
$1-\Phi_{tr}$(%)	28	9	1.9	0.2−

4. The use of on-line computers in particle identification

Different approaches have been used for the identification of charged particles using the ΔT-T system described in the introduction[15–19]) [see, e.g., ref. [2]) for a review].

The following method seems to be the simplest and also the most accurate for use with digital computers, if a few hundred words of fast memory are available to store range-energy tables for the different particles to be identified. Basically, the method consists of a table look-up of the ranges associated with the energies T and $T_1 = T - \Delta$. The range difference $r_M = R_M(T) - R_M(T_1)$ for an arbitrarily chosen particle of mass M is compared with the detector thickness t. If

$$(t - t_l) \leqslant r_M \leqslant (t + t_u)$$

the mass M of the detected particle is as assumed. For $r_M < (t - t_l)$ or $r_M \geqslant (t + t_u)$ the range table for another particle has to be used. The determination of appropriate values of t_l and t_u is described later. A suitable sequencing of the table look-up has to be chosen. To achieve the fastest operation, it is necessary to use as table entries the ranges associated with the energies corresponding to the center of each channel of the pulse-height analyzer. If the analyzing systems for the two counters have different calibration constants, the pulse height in one of them has to be converted into the equivalent pulse height in the other. It is then possible to use the pulse heights directly as the index for the range tables.

Sample program

The pulse height from the T counter is called JT, from the ΔT counter, JD. The ratio of the calibration constants C_T (in keV/channel) of T and C_D of ΔT is CA $= C_T/C_D$. The range table RA has been calculated previously for three different particles in such a way that one has RA(JEA) = R [T(JEA)], where T(JEA) $= C_D \cdot$ JEA, and RA(JEA+1) = R[T(JEA)+C_D]. In other words; the range tables are listed for energies equal to the channel width multiplied by an integer. The lower and upper limits, $t - t_l$ = PIL and $t + t_u$ = PIU, for each particle have to be determined either from diagrams corresponding to figs. 1–3 or from the curves in fig. 5 of ref. [14]). If the detector thickness t is not known accurately, it can be determined experimentally in preliminary test runs.

```
      SUBROUTINE XIDENT (JD, JT, ID)
      COMMON/RD/RA(3,450), PIL(3), PIU(3), CA
1     JEA = INT(CA* FLOAT(JT))
      JEF = JEA+JD
      DO 5 M = 1,3
```

```
2 TA = RA(M, JEF) - RA(M, JEA)
  IF (TA - PIL(M)) 7,3,3
3 ID = M
  IF (TA - PIU(M)) 9,9,5
5 CONTINUE
7 ID = 99
9 RETURN
  END
```

This program is especially simple for $C_D = C_T$: statement 1 can be eliminated, and in each test for a mass, three subtractions are necessary, and two comparisons.

In a program using the relation

$$R_M(T_M) = (M/z^2)\, R_p(m_r \times T_M),$$

where R_p is the proton range and $m_r = 938.259\,(\mathrm{MeV})/Mc^2$, the two products $m_r T_M$ and $m_r(T_M - \Delta)$, and also $(M/z^2)\,(R_T - R_{T_1})$, have to be calculated before the comparison can be made. Notice that a considerable simplification can be introduced if $R_p = CT^\alpha$, with a constant α for a certain energy range. Then

$$R_M(T_M) = (M/z^2)\, C m_r^\alpha T^\alpha,$$

and

$$\langle r \rangle = \langle R_M(T_M) - R_M(T_M - \Delta) \rangle$$
$$= (M/z^2)\, C\, \langle m_r^\alpha\, [T_M^\alpha - (T_M - \Delta)^\alpha] \rangle .$$

Since $\langle r \rangle = t$, the experimental coefficient

$$\langle [T_M^\alpha - (T_M - \Delta)^\alpha] \rangle / t = z^2 / (M\, \langle m_r^\alpha \rangle)$$

can be used to determine the identity of the particle[2]). The method breaks down if α is not constant [see fig. 3 of ref. [14])]. Since T_M^α can of course also be obtained in a table look-up, this method is simpler if α can be considered to be constant.

I am grateful for the hospitality of the Lawrence Radiation Laboratory and the use of the CDC 6600 computers.

References

1) F. S. Goulding, D. A. Landis, J. Cerny and R. H. Pehl, Nucl. Instr. and Meth. **31** (1964) 1.
2) D. D. Armstrong, J. G. Berry, E. R. Flynn, W. S. Hall, P. W. Keaton, Jr. and M. P. Kellog, Nucl. Instr. and Meth. **70** (1969) 69.
3) P. V. Vavilov, Soviet Phys. JETP **5** (1957) 749.
4) H. D. Maccabee, M. R. Raju and C. A. Tobias, Phys. Rev. **165** (1968) 469.
5) J. J. Kolata, T. M. Amos and H. Bichsel, Phys. Rev. **176** (1968) 484.
6) D. W. Aitken, W. L. Lakin and H. R. Zulliger, Phys. Rev. **179** (1969) 393.
7) H. Bichsel, University of Southern California Report USC-136-147 (Jan. 1969).
8) P. Shulek, B. M. Golovin, L. A. Kulyukina, S. V. Medved' and P. Pavlovich, Soviet J. Nucl. Phys. **4** (1967) 400.
9) S. M. Seltzer and M. J. Berger, Publication 1133, 2nd ed. (Nat. Acad. Sci. Nat. Res. Council, 1967) sec. 9.
10) H. H. Andersen, H. Simonsen and H. Sørensen, Nucl. Phys. **A125** (1969) 171.
11) C. Tschalär, Nucl. Instr. and Meth. **61** (1968) 141; and **64** (1968) 237.
12) H. Bichsel, *American Institute of Physics Handbook*, 3rd ed. (McGraw-Hill, New York) to be published; also USC-136-150 (July 1969).
13) D. J. Skyrme, Nucl. Instr. and Meth. **57** (1967) 61.
14) H. Bichsel and C. Tschalär, Nuclear Data **A3** (1967) 343; also UCRL-17663 Rev. (1969).
15) R. H. Stokes, J. A. Northrop and K. Boyer, Rev. Sci. Instr. **29** (1958) 61.
16) L. Wåhlin, Nucl. Instr. and Meth. **14** (1961) 281.
17) F. S. Goulding, D. A. Landis, J. Cerny and R. H. Pehl, IEEE Trans. **NS-13**, no. 3 (1966) 514.
18) P. R. Alderson and K. Bearpark, Nucl. Instr. and Meth. **62** (1968) 217.
19) B. Hird and R. W. Ollerhead, Nucl. Instr. and Meth. **71** (1969) 231.

Pam Schiøtt

Matematisk-fysiske Meddelelser
udgivet af
Det Kongelige Danske Videnskabernes Selskab
Bind 33, nr. 14

Mat. Fys. Medd. Dan. Vid. Selsk. 33, no. 14 (1963)

Proc. Int. Conf. Nuc
orth-Holland Publis
ibid. p. 258.
BROMLEY: ibid. p.
c. Sec. Conf. Reac
C-4, p. 151 and pa
450, 1962.
Mat. Fys. Med
1955, p. 421.

RANGE CONCEPTS AND HEAVY ION RANGES

(NOTES ON ATOMIC COLLISIONS, II)

BY

J. LINDHARD, M. SCHARFF(†) AND H. E. SCHIØTT

København 1963
i kommission hos Ejnar Munksgaard

CONTENTS

Synopsis

A theoretical discussion is given of the range of heavy ions with moderate velocity. The treatment is based on the theory of quasi-elastic collisions given elsewhere. The region where electronic and nuclear stopping compete is of particular interest. Use is made of a simple velocity proportional Thomas-Fermi type formula for electronic stopping, and a universal approximate differential cross section for scattering. Simplified models of nuclear scattering assuming power law scattering are also included. They turn out to be useful for exploratory computations of various range quantities.

The straightforward theory of ranges is studied in § 2. Range curves are computed for any atomic numbers of particle Z_1, and substance Z_2. It is found that when nuclear stopping is dominating, a $\varrho - \varepsilon$ plot gives a universal range energy description.

Probability distribution in total range and various averages are studied (§ 3), in order to assess corrections to measurements when necessary. Similarly, corrections to measurements of projected ranges are obtained (§ 4). The range correction due to nuclear stopping is obtained for ions of high initial energy.

In § 5 a survey is given of numerous recent measurements of range. They are found to be in fair accord with theoretical results, for energies between 100 MeV (fission fragments) and ~ 1 keV.

Printed in Denmark
Bianco Lunos Bogtrykkeri A/S

S

ange of heavy ions with moderate
ry of quasi-elastic collisions given
uclear stopping compete is of par-
ty p ortional Thomas-Fermi type
rsa. proximate differential cross
nuclear scattering assuming power
t to be useful for exploratory com-

studied in § 2. Range curves are
Z_1, and substance Z_2. It is found
ε plot gives a universal range energy

and various averages are studied
rements when necessary. Similarly,
nges are obtained (§ 4). The range
d for ions of high initial energy.
ecent measurements of range. They
al results, for energies between 100

nmark
trykkeri A/S

§ 1. Introduction

The present paper is a theoretical study of ranges of heavy ions of low velocity, and their connection to the basic problem of quasi-elastic collisions between ions and atoms. Three characteristic features give rise to complications. First, both electronic and nuclear stopping must be studied thoroughly, because they are similar in magnitude. Second, because of the frequent large deflections of the ions one must distinguish carefully between various range concepts. Third, the variety of choice of atomic number of both ion and substance gives an additional difficulty. We shall try to show that our present knowledge of quasi-elastic collisions, in spite of the above complications, can give us a simple and fairly accurate range theory. In point of fact, in the following we use a much simplified description of quasi-elastic collisions, which could be improved upon without difficulty. Aspects of quasi-elastic collisions are studied also in three associated papers: Notes on Atomic Collisions I, III, and IV. The aim is to exploit similarity properties of Thomas-Fermi type in collisions between heavy ions and atoms. In fact, similarity enables us to treat in a comprehensive way both slowing-down and damage effects by heavy ions.

The total range of a swift particle may be observed in track detectors like photographic emulsions. The observation of many tracks can then give the probability distribution in total range. In measurements of this kind the observed range depends on energy losses only, and not on scattering of the particle. For energetic heavy particles this separation of energy loss from scattering is especially valuable, since the two are due to unconnected processes, i. e. respectively electron excitation and Coulomb scattering by the atomic nuclei.

However, in nearly all other cases one observes somewhat different and less well-defined types of ranges. It is then customary to make corrections for multiple scattering in order to obtain the total range, but since these corrections are not insignificant—even in cases like high energy protons where deflections are small—it would seem appropriate to introduce explicitly these other types of ranges.

The scattering of a particle—in contrast to its energy loss—is always dominated by nuclear collisions, i. e. deflections in the screened electric field of the atom. In the case of electrons, large scattering angles are quite common during slowing-down. For heavy particles of high energy (e. g. protons with MeV-energies), scattering effects are relatively small, but since a high precision is desirable here, the distinction between different types of ranges again becomes important. Although the description in the following could be applied to electrons and to fast heavy particles, we shall aim at the case mentioned in the beginning of the introduction. In fact, for heavy ions of low velocity, e. g. $v \sim v_0 = e^2/\hbar$, scattering effects are large and the scattering can not be completely separated from energy loss, simply because the nuclear collisions here begin to dominate the energy loss too. This somewhat complicated case will be used as a basic example in our general discussion of range concepts.

The following discussion does not at all pretend to give an exhaustive treatment of range concepts. Thus, we are throughout concerned with stopping by a random system of atoms, i. e. uncorrelated atoms and separated collisions. This might never seem to include stopping of a relatively slow heavy ion in a solid, where the interatomic distance is short and atoms are arranged in a periodic lattice. Still, the effects are only sometimes large; they are not well understood and appear to be dependent on the structure of the lattice (cf. § 5).

Before turning to the various—and often complicated—range concepts and range distributions, we may take a more straightforward point of view. In § 2 we proceed as if the energy loss along the path was a nearly continuous process. This is not at all a poor first approximation. It both enables us to get a clearer picture of the essential points and permits comparisons with experiments (cf. § 5).

§ 2. Simple Unified Range Theory

Suppose that the range along the path is a well-defined quantity, so that we need not distinguish between e. g. average range, most probable range, and median range. We may introduce first the simple concept of specific energy loss, (dE/dR),—or average energy loss per unit path length—defined by

$$\frac{dE}{dR} = N \cdot S = N \int d\sigma\, T, \tag{2.1}$$

where N is the number of scattering centres (e. g. atoms) per unit volume and S the stopping cross section per scattering centre. Further, $d\sigma$ is the differential cross section for an energy transfer T to atoms and atomic electrons.

The basic range concept is then obtained simply by integration of (dE/dR),

$$R(E) = \int_0^E \frac{dE'}{(dE'/dR)} = \frac{1}{N}\int_0^E \frac{dE'}{S(E')}. \tag{2.2}$$

The formulations (2.1) and (2.2) give a simple connection between range, specific energy loss, and differential cross section. We do not at present distinguish between different types of ranges. A better understanding of the connection between (2.2) and e. g. the average range is obtained in the detailed discussions in § 3.

In an analogous way we may introduce the range straggling (cf. Bohr (1948)). Similarly to (2.1) the average square fluctuation in energy loss becomes

$$\overline{(\Delta E)^2} = N\Omega^2\, dR = N dR \int d\sigma\, T^2, \tag{2.3}$$

if the individual events have average occurrence $N dR d\sigma$, and are uncorrelated. We may next derive the average square fluctuation in range, $(\Delta R)^2$, using the present assumption that fluctuations are small,

$$(\Delta R)^2 = \int_0^E \frac{dE' N\Omega^2(E')}{(dE'/dR)^3} = \frac{1}{N^2}\int_0^E \frac{dE' \cdot \Omega^2(E')}{S^3(E')}. \tag{2.4}$$

If we were precise, we would say that the interpretation of (2.4) as the average square fluctuation in range is not quite correct. For the present purposes, however, we have by means of (2.2) and (2.4) defined the range, R, and its fluctuation, ΔR, and the results are sufficiently accurate for most purposes. We now use (2.2) and (2.4) in a first study of the ranges of slow heavy ions.

Quite apart from using at first simple expressions like (2.2) and (2.4), it seems important—at the present stage of accuracy of theory and experiments—to be able to give a comprehensive description of slowing-down. It would for instance be futile to aim at an individual stopping curve for every one out of $\sim 10^4$ possibilities for the set of atomic numbers (Z_1, Z_2), where the suffixes 1 and 2 denote the penetrating particle and the atoms of the medium, respectively. If we are concerned with very high velocities, where the Bethe-Bloch stopping formula applies, the question of

dependence on Z_1 drops out because the stopping is simply proportional to Z_1^2. In that case the dependence on Z_2 is not far from being given by a Thomas-Fermi description, i. e. Bloch's relation $I = Z_2 \cdot I_0$, and only when high accuracy is demanded need we introduce deviations from the Thomas-Fermi results. Considering again the present case of comparatively low velocities, where the stopping is not proportional to Z_1^2, it is very important that descriptions of a Thomas-Fermi-like character are introduced, even though the resulting accuracy might not be high.

In point of fact, we hope to show in this section, and in § 5, that a Thomas-Fermi-like treatment of the dependence on both Z_1 and Z_2 has a quite satisfactory accuracy at the present stage of experimental precision. Our treatment should be based on a self-contained theory of the quasi-elastic collisions between ions and atoms. This theory will not be derived here; it is studied in two associated papers (Notes on Atomic Collisions, I and IV, unpublished). We shall merely summarize a few results of interest to us in the present connection (cf. also LINDHARD and SCHARFF, (1961)).

Electronic stopping

It is well known that for penetrating charged particles of high velocity, the energy loss to atomic electrons is completely dominating. The corresponding stopping cross section per atom is denoted by S_e, so that the specific energy loss is $N \cdot S_e$, where N is the number of atoms per unit volume. At high velocities S_e increases with decreasing particle velocity and has a maximum for a velocity of order of $v_1 = v_0 \cdot Z_1^{2/3}$. However, we shall consider low velocities only and in fact assume that $0 < v < v_1$. In the whole of this velocity region simple theoretical considerations lead to velocity proportional stopping, and a Thomas-Fermi picture shows that (Notes on Atomic Collisions, IV; see also LINDHARD and SCHARFF (1961))

$$S_e = \xi_e \cdot 8\,\pi e^2 a_0 \cdot \frac{Z_1 Z_2}{Z} \cdot \frac{v}{v_0}, \quad v < v_1 = v_0 \cdot Z_1^{2/3}, \tag{2.5}$$

where the constant ξ_e is of order of $Z_1^{1/6}$, and $Z^{2/3} = Z_1^{2/3} + Z_2^{2/3}$. It is interesting that the approximate formula (2.5) holds down to extremely low velocities, i. e. also for $v << v_0$, in contrast to previous theoretical descriptions, where S_e was assumed to vanish for $v \lesssim v_0$ (cf. BOHR (1948), SEITZ (1949)).

It should be emphasized that (2.5) is approximate in more than one sense. The constant in (2.5) is based on Thomas-Fermi arguments, and it is to be expected that fluctuations around this constant can occur, especially for $Z_1 \lesssim 10$*. Moreover, a precise proportionality to v will not be correct over the whole of the velocity region $v < v_1$. However, in the present context we shall not analyse electronic stopping in detail. As to stopping near the maximum $v \sim v_1$, cf. NORTHCLIFFE (1963).

* The presence of such ionic shell effects is confirmed in the systematic measurements by ORMROD and DUCKWORTH (1963), WIJNGAARDEN and DUCKWORTH (1962).

ping is simply proportional
ot far from being given by a
n $I = Z_2 \cdot I_0$, and only when
deviations from the Thomas-
case of comparatively low
al to Z_1^2, it is very important
racter are introduced, even
igh.
n, and in § 5, that a Thomas-
oth Z_1 and Z_2 has a quite
experimental precision. Our
l theory of the quasi-elastic
y will not be derived here;
on Atomic Collisions, I and
a few results of interest
D and SCHARFF, (1961)).

pa les of high velocity, th
ns e corresponding stoppin
e specific energy loss is $N \cdot S_e$.
At high velocities S_e increases
um for a velocity of order o
s only and in fact assume th
heoretical considerations lead
l picture shows that (Notes o
ARFF (1961))

$= v_0 \cdot Z_1^{2/3}$, (2.5

$Z_1^{2/3} + Z_2^{2/3}$. It is interesting th
ely low velocities, i. e. also
ions, where S_e was assumed

e in more than one sense. T
ents, and it is to be expect
ecially for $Z_1 \lesssim 10$*. Moreov
ver the whole of the veloci
not analyse electronic stoppi
I. NORTHCLIFFE (1963).

n the systematic measurements
KWORTH (1962).

140
2/28

Another important circumstance may be mentioned. The energy loss to electrons is actually correlated to the nuclear collisions, and in close collisions considerable ionization will take place. Although the correlations are fairly well known, we disregard them in first approximation and consider electronic stopping as a continuous process. The correlation may be of some importance especially in straggling or higher order moments of the range.

Nuclear stopping and scattering cross section

A basic quantity is the nuclear stopping cross section, S_n. However, since the energy transfer in individual collisions can be quite large, the slowing-down by nuclear collisions cannot always be considered as a nearly continuous process. It is therefore important to know the differential cross section too. We shall here consider various approximations, of which the first one lends itself to a particularly simple mathematical treatment.

Suppose that there is a potential $V(r)$ between the ion and the atom, such that $V(r) = (Z_1 Z_2 e^2 a_s^{s-1}/s\, r^s)$, with $a_s \approx a = 0.8853\ a_0 Z^{-1/3}$ (the number $0.8853 = (9\pi^2)^{1/3} 2^{-7/3}$ is a familiar Thomas-Fermi constant). It is interesting that then the classical differential scattering cross section may be obtained approximately from an extrapolated perturbation procedure (Notes on Atomic Collisions I), leading to the simple result

a heat capacity is analogous to C_n?

$$d\sigma_n = \frac{C_n}{T_m^{1-1/s}} \frac{dT}{T^{1+1/s}}, \quad s \geq 1, \tag{2.6}$$

for an energy transfer T from the ion of energy E to an atom at rest. Here $T \leq T_m = \gamma E = 4 M_1 M_2 (M_1 + M_2)^{-2} E$, T_m being the maximum energy transfer in the collisions. Furthermore, the constant C_n is connected to the stopping cross section S_n, and is approximately given by

$$C_n = \frac{\pi}{s} \left(b^2 \cdot a_s^{2s-2} \cdot \frac{3s-1}{8s^2} \right)^{1/s} \cdot T_m = \left(1 - \frac{1}{s}\right) S_n, \tag{2.7}$$

where the collision diameter b is equal to $2 Z_1 Z_2 e^2 / M_0 v^2$, $M_0 = M_1 M_2 / (M_1 + M_2)$. In the particular case of $s = 1$, i. e. simple Coulomb interaction, equation (2.6) also gives the correct Rutherford scattering, but in this case S_n in (2.7) does not represent the stopping cross section, the convergence of which is a result of adiabaticity in distant collisions.

Is this valid or should actual conditions be isothermal-like - since beam is always on?

As we shall demonstrate below, formulas of type of (2.6) are valuable for explorative purposes, interesting values of s being 1, 3/2, 2, 3 and 4. The cross sections (2.6) are furthermore in accord with the Thomas-Fermi scaling of units. Corresponding to the case of $s = 2$, we shall sometimes approximate S_n by constant standard stopping cross section S_n^0 (similar to that quoted by BOHR (1948)),

$$S_n^0 = (\pi^2 / 2.7183)\, e^2 a_0 Z_1 Z_2 M_1 \cdot Z^{-1/3} (M_1 + M_2)^{-1}. \tag{2.7'}$$

Beside the simple power potential we study the case provided by a screened potential, $U(r) = (Z_1 Z_2 e^2/r) \cdot \varphi_0(r/a)$, where φ_0 is the Fermi function, and further

Z = medium

$a = a_0 \cdot 0.8853\,(Z_1^{2/3} + Z_2^{2/3})^{-1/2}$, which is a fair approximation to the ion-atom force. Bohr (1948) has employed a similar potential, with $\exp(-r/a_B)$ in place of $\varphi_0(r/a)$; however, an exponential function falls off too rapidly at large distances.

A screened Coulomb potential, involving only one screening parameter, a, leads for dimensional reasons to a natural measure of range and energy, for an ion colliding with atoms at rest. In fact, we may introduce, respectively,

$$\varrho = RNM_2 \cdot 4\,\pi\,a^2 \frac{M_1}{(M_1 + M_2)^2} \quad \text{and} \quad \varepsilon = E \frac{a M_2}{Z_1 Z_2 e^2 (M_1 + M_2)} \tag{2.8}$$

as dimensionless measures of range and energy. Note that ε^{-1} is essentially the parameter ζ used by Bohr (1948). The scattering in the screened potential, $U(r)$, is obtained by means of the extrapolated perturbation method for classical scattering used in deriving (2.6), and one obtains a universal differential cross section

$$d\sigma = \pi a^2 \frac{dt}{2\,t^{3/2}} f(t^{1/2}), \tag{2.9}$$

where $t^{1/2} = \varepsilon \cdot \sin(\vartheta/2)$ and ϑ is the deflection in centre of gravity system. When elastic collisions are assumed, we find $\sin^2(\vartheta/2) = (T/T_m)$, where T and T_m are the energy transfer and its maximum value, respectively, in a collision with an atom at rest. The function $f(t^{1/2})$ is shown in Fig. 1. At high values of t it approaches the Rutherford scattering. In Fig. 1 is also shown (2.6) for the case of $s = 2$.

It may be noted that the power law (2.6) leads to $f = f_s$, where

$$f_s(t^{1/2}) = \lambda_s \cdot t^{\frac{1}{2} - \frac{1}{s}}, \quad 0.3 \lesssim \lambda_s \lesssim 1. \tag{2.6'}$$

In the above, we have at first considered approximate potentials representing the ion-atom interaction and next, in an approximative way, derived the scattering from the potentials. However, we shall in the following take a simpler and more direct point of view. We consider (2.6) and (2.9) directly as approximations to the true scattering cross section and disregard the connection to a corresponding potential. This is the more justified, since the scattering is only quasi-elastic and cannot in detail be described by a potential between two heavy centres.

From (2.9) and Fig. 1 may be derived the nuclear stopping cross section, by means of the formula $(d\varepsilon/d\varrho)_n = \int_0^{\varepsilon} dx\, f(x)\, \varepsilon^{-1}$. The result is shown in Fig. 2, together with the stopping from (2.6) for $s = 2$. Also the electronic stopping may be expressed in $\varrho - \varepsilon$ units, and is then $(d\varepsilon/d\varrho)_e = k \cdot \varepsilon^{1/2}$, where the constant k varies only slowly with Z_1 and Z_2, and according to (2.5) is given by

$$k = \xi_e \cdot \frac{0.0793\, Z_1^{1/2} Z_2^{1/2} (A_1 + A_2)^{3/2}}{(Z_1^{2/3} + Z_2^{2/3})^{3/4} A_1^{3/2} A_2^{1/2}}, \quad \xi_e \simeq Z_1^{1/6}. \tag{2.10}$$

Thus, k is normally of order of 0.1 to 0.2, and only in the exceptional case of $Z_1 << Z_2$ can k become larger than unity. If $Z_1 = Z_2$, $A_1 = A_2$, the constant k is given by the simple expression $k = 0.133\, Z_2^{2/3} A_2^{-1/2}$. A representative case of electronic stop-

$2^{1/6} \times 2^{3/6}$

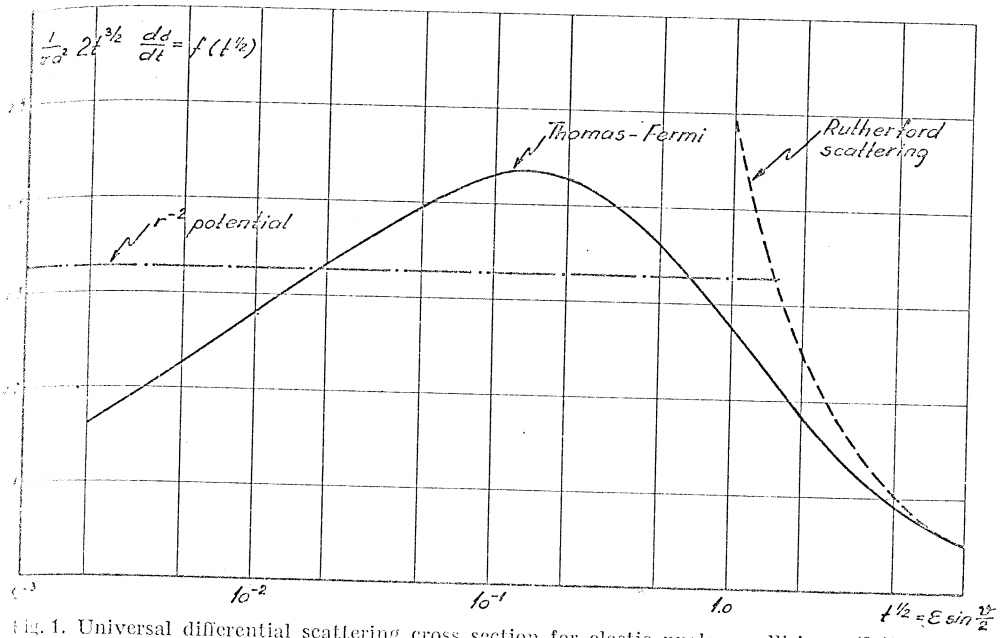

Fig. 1. Universal differential scattering cross section for elastic nuclear collisions, (2.9), based on a Thomas-Fermi type potential. At high values of $t^{1/2}$ it joins smoothly the Rutherford scattering. The cross section corresponding to power law scattering (2.6), or (2.6′), with $s = 2$ is also shown.

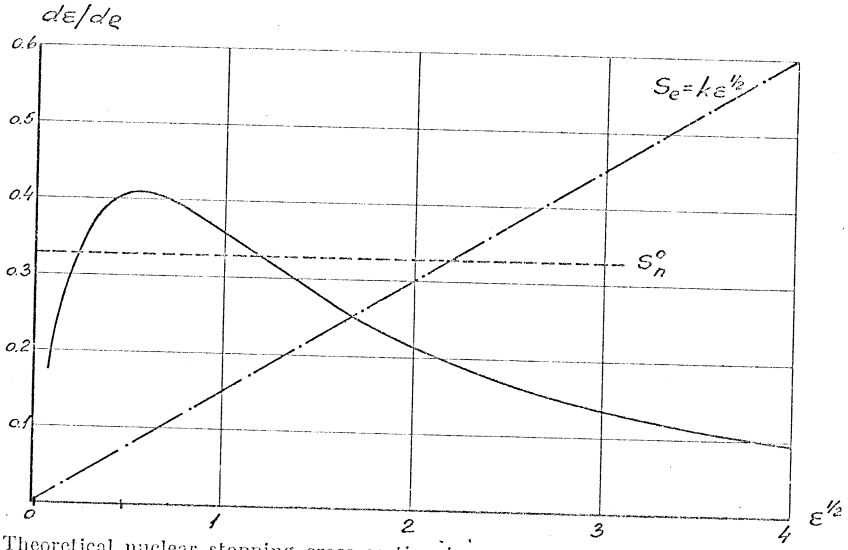

Fig. 2. Theoretical nuclear stopping cross section in $\varrho - \varepsilon$ variables. The abscissa is $\varepsilon^{1/2}$, i.e. proportional to v. The full-drawn curve is $(d\varepsilon/d\varrho)_n$, computed from Fig. 1. The horizontal dashed line indicates (2.7′). The dot-and-dash line is the electronic stopping cross section, $k\varepsilon^{1/2}$, for $k = 0.15$.

Nr. 14

o to the ion-atom force
r/a_B) in place of $\varphi_0(r/a)$
arge distances.
ning parameter, a, lead
energy, for an ion col
ectively,

$$\frac{aM_2}{e^2(M_1 + M_2)} \qquad (2.8)$$

t ε^{-1} is essentially the
reened potential, $U(r)$,
d for classical scatterin
tial cross section

(2.9)

gravity system. When
here T and T_m are the
collision with an atom
ues of t it approaches
the case of $s = 2$.
$_s$, where

(2.6′)

nti representing the
de d the scattering
e a simpler and more
approximations to the
o a corresponding po
only quasi-elastic and
avy centres.
ping cross section, by

own in Fig. 2, together

stopping may be ex
the constant k varies
by

/6. (2.10)

ional case of $Z_1 << Z$
onstant k is given by
ase of electronic stop

00693

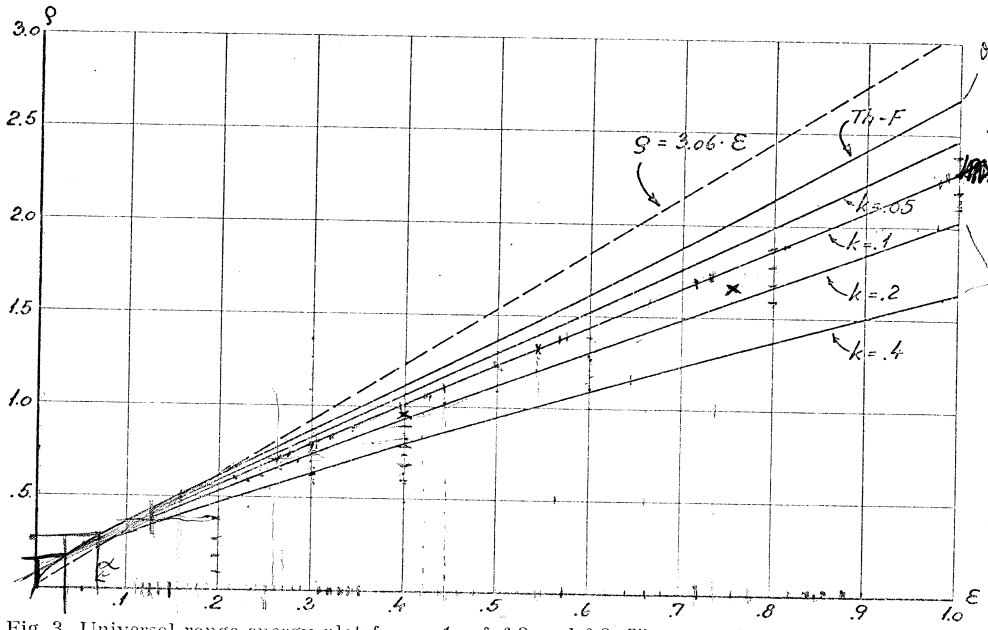

Fig. 3. Universal range-energy plot for $\varepsilon < 1$, cf. § 2 and § 3. The curve Th.–F. gives $\overline{\varrho}_1(\varepsilon)$, i. e. (2.2), as a function of ε with neglect of electronic stopping. Curves for various values of the constant k in electronic stopping are also shown. Dotted straight line is the standard range, $\varrho = 3.06\,\varepsilon$.

ping, $k = 0.15$, is shown in Fig. 2. Formula (2.10) applies for $v < v_1$, or approximately $\varepsilon < 10^3$. In the above we have for simplicity distinguished between electronic excitation and elastic nuclear collisions. This is not quite justified, since in close collisions there is a strong coupling between the two, i. e. the nuclear collisions are not elastic. In first approximation this need hardly be taken into account; the reader is referred to Notes on Atomic Collisions IV for a more detailed treatment of quasi-elastic collisions.

The nuclear scattering cross section is expected to be fairly accurate, but while shell effects should be of little importance, a systematic overestimate may occur, due to neglect of inelastic effects. A more thorough discussion is given in Notes on Atomic Collisions I. At low energies nuclear stopping dominates over electronic stopping (2.5). It must be emphasized though, that at extremely low ε-values, $\varepsilon \lesssim 10^{-2}$, the nuclear scattering and stopping becomes somewhat uncertain, because the Thomas-Fermi treatment is a crude approximation when the ion and the atom do not come close to each other.

Range-energy relations

By means of the simple formula (2.2), and the above stopping cross sections, we are now able to estimate total ion ranges. Now, if we consider nuclear stopping only, and one screening length a in the scattering, the

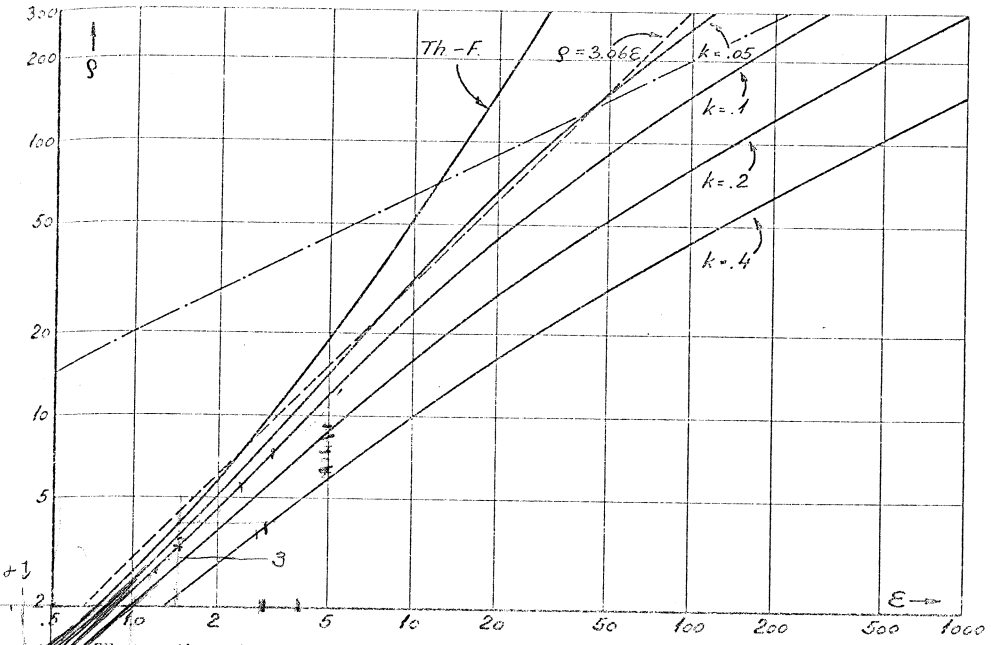

Fig. 4. The continuation at higher ε-values of the ranges $\bar{\varrho}_1(\varepsilon)$ in Fig. 3, for various values of constant k in electronic stopping. Straight dot-and-dash line is hypothetical range without nuclear stopping and $k = 0.1$.

dimensional arguments leading to (2.8) apply, and in these units the range in (2.2), ϱ, must be a function of ε only, i. e.

$$\varrho = \varrho(\varepsilon)$$

for all ions and atoms. This formula holds both when (2.7) and when (2.9) is introduced in (2.2). The resulting range, based on (2.9) and $f(t^{1/2})$ from Fig. 1 is shown by the solid curve in Fig. 3, for relatively small values of ε. The particular approximation of $s = 2$, i. e. the constant standard stopping cross section in (2.7′) and Fig. 2 leads to the straight line $\varrho = 3.06\ \varepsilon$ in Fig. 3. This standard range is closely similar to the range formula used by Bohr (1948) and also by Nielsen (1956). For small ε-values the numerical curve remains above the straight line and has a downward curvature, corresponding to the effective power of the potential being higher than 2, in fact of order of 3. The detailed behaviour of the range curve can be easily understood from the stopping curves in Fig. 2. If we use the straight line as a standard in Fig. 3, i. e. the horizontal line as a standard in Fig. 2, the range must at first be higher than the standard straight line in Fig. 3. Next, since the actual stopping rises above the horizontal line, the range

must drop considerably relative to the straight line, and actually fall below it. Finally, since the nuclear stopping becomes small in the high energy region with Rutherford scattering, the range must again increase above the straight line as may be seen in Fig. 4.

In this description we have so far omitted electronic stopping. This omission is justified at low energies because S_e/S_n tends to zero for small velocities, but at higher energies it becomes less and less adequate until the range finally is dominated by the electronic stopping, as may be judged from the stopping cross section in Fig. 2. Let us therefore take electronic stopping into account and write

$$\frac{d\varepsilon}{d\varrho} = \left(\frac{d\varepsilon}{d\varrho}\right)_n + k \cdot \varepsilon^{1/2}, \tag{2.11}$$

where $(d\varepsilon/d\varrho)_n$ is shown in Fig. 2, and the electronic stopping is assumed to be proportional to $\varepsilon^{1/2}$, i. e. we are concerned with moderate velocities, $v < v_1$. We choose a number of representative values of the constant k, $k = 0.05$, 0.1, 0.2 and 0.4. Values of k between 0.1 and 0.2 are quite common, according to (2.5). In Figs. 3 and 4 are shown the range curves for the above four values of k. The most conspicuous effects of electronic stopping are, first, that it leads to appreciable range corrections even at quite low ε-values. Second, for ε large compared to unity, the reduction in range always dominates, so that the range never increases above the straight line $\varrho = 3.06\,\varepsilon$, in contrast to the range with neglect of electronic stopping. In Fig. 4 is also shown the hypothetical range $\varrho = (2/k)\,\varepsilon^{1/2}$, which would result if there were no nuclear stopping, in the case of $k = 0.1$.

By means of curves like those in Figs. 3 and 4 we are able to compare or estimate ranges for all ions in all substances. But only for ε-values below, say, $\varepsilon = 10$ are curves for the various k-values fairly close together and easy to compare. For light ions in heavy substances deviations start at even smaller ε-values, because k becomes quite large. Moreover, only for these low values are we able to check in a direct manner the nuclear stopping, which here remains dominating.

Although we may well use Fig. 4 for estimates of ranges when $\varepsilon >> 10$, we can in this case introduce a more critical comparison between theory and experiments. In fact, it is apparent from Fig. 2 that for high values of ε the range is mainly determined by the electronic stopping, and only a minor range correction is due to nuclear stopping which dominates at low values of ε. Since nuclear stopping drops off quickly while electronic stopping increases, the nuclear stopping correction to the range remains fairly con-

Another circumstance may be noted in this connection. Since Δ tends to a constant at high ε-values, we may moreover use (2.12), together with Fig. 5, for comparisons with measurements at high ε-values, i. e. $v >> v_1$, where electronic stopping no longer increases proportionally to v, but instead decreases approximately as v to a power between -1 and -2.

In the present paragraph we do not make comparisons with actual range measurements, one of the reasons being that measured ranges require corrections of the kind discussed in § 4. Instead, we have presented these comparisons in § 5, where recent measurements are compiled. We do not discuss critically the accuracy of the measurements; this is perhaps unsatisfactory, because several new experimental methods have been applied. We merely make approximate and obvious range corrections, corresponding to the results in § 4. One result emerging from § 5 is that the theoretical nuclear stopping, as leading to the range curves in Figs. 3 and 4, for moderate ε-values appears to be in good agreement with observations, perhaps within $\sim$20 percent. It should be noted that the theory is somewhat uncertain at quite low ε-values, i. e. $\varepsilon \lesssim 10^{-2}$.

Beside the general experimental checking of the present range-energy relations there are several other ways of comparison. An immediate possibility is to measure directly stopping powers, which has been done in a few cases, but mostly when electronic stopping dominates. We shall not enter more critically into these questions, since the theory of electronic stopping is not the topic of the present paper. Nor will we attempt a detailed discussion of individual inelastic collisions between energetic ions and atoms at rest. But it may be mentioned that more subtle comparisons of ranges may be made. For instance, isotope effects are quite informative, and can elucidate both electronic and nuclear stopping, cf. § 5.

Range straggling

The simple description used here, with a range along the particle path based on (2.2), may now be extended to include an average square fluctuation in range, given by (2.4). This description contains the assumption that range fluctuations are relatively small. We may suppose that the fluctuations around the average correspond nearly to a Gaussian. In fact, if this were not so, the distribution in range would have a sizable skewness. Then we would have to distinguish between e. g. the most probable and the average range, and the simple relation (2.2) would have to be revised. Still, even in such cases the results in the present paragraph may be useful. We can in fact consider the present ranges, i. e. (2.2) as an approximation to the

region electronic stopping has become quite dominating, and the absolute value of the square straggling, $(\Delta\varrho)^2$, does not increase much beyond this point. For high ε-values it is then convenient to consider the absolute value of the range straggling. The corresponding curves are given in Fig. 7, for various values of k. We therefore conclude that accurate measurements of straggling in range at high energies, where the electronic stopping does not at all correspond to (2.5), may give information about the predicted values of k, as given by (2.10).

The above treatment of simple ranges and range straggling is intended to be fairly comprehensive, and from the accompanying curves it is easy to obtain reasonable estimates of these quantities for any value of Z_1, A_1, Z_2, A_2 and v. However, we have disregarded completely those cases where the substance contains several atomic elements, $Z_2^{(1)}$, $Z_2^{(2)}$, etc., in given ratios. In all such cases, the nuclear stopping contribution from each element may be derived from the solid curve in Fig. 2, with a rescaling of units. The electronic stopping contributions are obtained from (2.5) or (2.10). The resulting ranges can be derived by numerical integration. However, considerable simplification occurs in an energy region where, e. g. the stopping cross section $S^{(i)}$, due to any atomic component i, is proportional to the same power of E, because in this case straightforward computations of averages may be made. For two components, a and b, we have $R = R_a R_b (R_b x_a + R_a (1 - x_a))^{-1}$, where R_a and R_b are the ranges in a and b, and x_a and $1 - x_a$ are the relative abundances of a and b. Similar procedures may be used in the case of straggling in range.

§ 3. Distribution in Range Measured Along the Path

In the present chapter we shall try to go one step beyond the treatment in § 2, where only a simple range straggling was considered, and where it was tacitly assumed that straggling effects were small. We wish to check the validity of this picture and also to extend it. A basic reason for the extended treatment are the large fluctuations, known to result from encounters between slow heavy ions and atoms. We therefore attempt to study the probability distribution in range measured along the path. Although this distribution is much simpler than the distribution in space of the endpoint of the path, it is not easily obtained. One might perhaps employ Monte Carlo methods* for the solution of representative cases, but we shall limit the treatment to typical and simple approximations, and in particular consider the power law scattering cross sections given by (2.6).

Consider again a particle (Z_1, A_1) with energy E, in a medium (Z_2, A_2).

* Monte Carlo methods were applied by e. g. Robinson, Holmes and Oen (1962) to various models of nuclear scattering, but with neglect of electronic stopping, cf. also Holmes (1962).

We denote by R the range measured along the particle path, i. e. the total distance traversed by the particle. Let $p(R, E)\,dR$ represent the probability that the particle has a range between R and $R+dR$, so that

$$\int_0^\infty p(E, R)\,dR = 1 \quad \text{and} \quad \langle R^m \rangle = \int_0^\infty p(E, R)\,R^m\,dR\,.$$

An integral equation for $p(E, R)$ may be derived as follows. Suppose that the particle with energy E moves a path length δR in a medium containing N atoms per unit volume. There is then a probability $N\delta R d\sigma_{n,e}$ for a collision specified by energy transfer $\sum_i T_{ei}$ to electrons (electrons labelled by suffix i) and by an energy transfer T_n to translational motion of the struck atom. The particle will thus have an energy $E - T_n - \sum_i T_{ei}$. If the collision takes place, the particle has a probability $p(R-\delta R,\ E - T_n - \sum_i T_{ei})$ of obtaining the total range R. Multiplying by the probability of collision, $N\delta R d\sigma_{n,e}$, we get the contribution from this specified collision to the total probability for range R. We next sum over all collisions. There is left a probability $1 - N\delta R\int d\sigma_{n,e}$ that no collision occurs. In this event we clearly get a contribution $(1 - N\delta R\int d\sigma_{n,e})\cdot p(R-\delta R, E)$ to the total probability for the range R.

Collecting the above contributions we have an alternative expression for $p(R, E)$,

$$p(R, E) = N\delta R\int d\sigma_{n,e}\, p(R-\delta R, E - T_n - \sum_i T_{ei})$$
$$+ (1 - N\delta R\int d\sigma_{n,e})\cdot p(R-\delta R, E),$$

and in the limit of $\delta R \to 0$,

$$\frac{\partial p(R, E)}{\partial R} = N\int d\sigma_{n,e}\left\{p(R, E - T_n - \sum_i T_{ei}) - p(R, E)\right\}, \tag{3.1}$$

which expression constitutes the basic integral equation governing the probability distribution in range along the path. In the remainder of this chapter we study the integral equation (3.1) and its consequences, using a number of approximations. We shall not further elaborate on the derivation of (3.1), but it may be noted that the formal limit of $\delta R \to 0$ corresponds to separability between consecutive collisions. If there is no separability, the equation still holds, or may be easily amended, as long as collisions with moderate or large T-values remain separable.

$p(R-\delta R, E) - (N\delta R\int d\sigma_{n,e})\cdot p(R-\delta R, E)$

Besides separability we have assumed that successive collisions are not correlated. This holds if the atoms in the substance are in fact randomly distributed, or if e. g. impact parameters corresponding to sizable deflections are extremely small compared to interatomic distances, giving effectively uncorrelated events. A system where collisions are separated and uncorrelated may be termed a random system of atoms. The derivation of (3.1) is based on a random system, and we limit our treatment to this case. A solid with periodic lattice is for many purposes a random system, but at low ion energies deviations from (3.1) can occur. These deviations contain directional effects and are sensitive to lattice structure, cf. p. 32.

On the assumption that energy losses to electrons are small and separated from nuclear collisions, we obtain

$$\left.\begin{aligned}\frac{\partial p(R,E)}{\partial R} &= N\int d\sigma_n \left\{p(R,E-T_n)-p(R,E)\right\}\\ &\quad - NS_e(E)\frac{\partial}{\partial E}p(R,E),\end{aligned}\right\} \tag{3.2}$$

which formula is somewhat less general, but applicable to our previous cross sections for scattering.

We may rewrite (3.2) on the assumption that the Thomas-Fermi-like scattering formula (2.9) applies (note that this also includes (2.6) and (2.6′)), and then introduce the variables ϱ and ε. We readily obtain

$$\left.\begin{aligned}\frac{\partial}{\partial\varrho}\Pi(\varrho,\varepsilon) &= \frac{1}{\gamma}\int_0^{\varepsilon^2}\frac{dt}{2\,t^{3/2}}f(t^{1/2})\left\{\Pi\left(\varrho,\varepsilon-\frac{\gamma t}{\varepsilon}\right)-\Pi(\varrho,\varepsilon)\right\}\\ &\quad -\left(\frac{d\varepsilon}{d\varrho}\right)_e\frac{\partial}{\partial\varepsilon}\Pi(\varrho,\varepsilon),\end{aligned}\right\} \tag{3.3}$$

where $\Pi(\varrho,\varepsilon)\,d\varrho$ is the probability that a particle with energy parameter ε has a range between ϱ and $\varrho+d\varrho$, and where $\gamma = 4M_1M_2/(M_1+M_2)^2$. We have seen that in a wide region ($v<v_1$, i. e. roughly $\varepsilon<10^3$), one may write $(d\varepsilon/d\varrho)_e = k\cdot\varepsilon^{1/2}$. In equation (3.3) we then have two parameters, k and γ.

A simple approach to the study of the integral equations (3.1), (3.2) or (3.3) is to obtain from these equations the moments $<R^m>$, whereby—at least in principle—the probability distribution itself may be determined too.

From (3.1) we obtain directly, when multiplying by R^m and integrating by parts

$$\left.\begin{aligned}&m<R^{m-1}(E)>=\\ &N\int d\sigma_{n,e}\left\{<R^m(E)>-<R^m(E-T_n-\sum_i T_{ei})>\right\}.\end{aligned}\right\} \tag{3.4}$$

Similarly, if (3.3) holds we arrive at a somewhat simpler relation

$$\left.\begin{aligned} m<\varrho^{m-1}(\varepsilon)> = \frac{1}{\gamma}\int_0^{\varepsilon^2}\frac{dt}{2\,t^{3/2}}f(t^{1/2})\left\{<\varrho^m(\varepsilon)> - <\varrho^m\left(\varepsilon-\frac{\gamma t}{\varepsilon}\right)>\right\} \\ +\left(\frac{d\varepsilon}{d\varrho}\right)_e\cdot\frac{d}{d\varepsilon}<\varrho^m(\varepsilon)>. \end{aligned}\right\} \tag{3.5}$$

By means of equations (3.4) or (3.5) we may successively derive the first, second, etc., moments of the range. In the resulting formulas the equations (3.4) are applied, because they have a wider applicability. In actual evaluations, however, we turn to (3.5), and to the analogous reformulations of (3.6) to (3.13) in $\varrho-\varepsilon$ variables, although the reformulations are not explicitly stated. Let us ask for the average range $\bar{R}(E) = <R(E)>$. According to (3.4)

$$1 = N\int d\sigma_{n,e}\left\{\bar{R}(E)-\bar{R}(E-T_n-\sum_i T_{ei})\right\}. \tag{3.6}$$

An obvious procedure in solving (3.6) is to make a series development in powers of $T = T_n+\sum_i T_{ei}$. This approximation might seem poor when $M_1\sim M_2$, because $E-T$ can then take on any value between E and 0. However, we can profit from the circumstance that the energy transfer to electrons, $\sum_i T_{ei}$, is normally quite small, and that the nuclear scattering cross sections (2.9) are strongly forward peaked, since $f(t^{1/2})t^{-3/2}$ decreases approximately as t to a power between -1 and -2. We shall presently look into the accuracy of the various approximations.

Take at first only the first order terms in the brackets and denote the corresponding approximation to average range by $\bar{R}_1(E)$. We obtain from (3.6)

$$\frac{dR_1(E)}{dE} = \frac{1}{NS(E)},\quad \bar{R}_1(E) = \int_0^E\frac{dE'}{NS(E')}, \tag{3.7}$$

where $S(E) = S_n(E)+S_e(E)$ is the total stopping cross section. The formula (3.7) is exactly the straightforward equation (2.2) used in § 2.

Similarly, we can include higher order terms from (3.6),

$$1 = NS(E)\frac{d}{dE}\bar{R}(E)-\frac{1}{2}N\Omega^2(E)\frac{d^2}{dE^2}\bar{R}(E)+\ldots, \tag{3.8}$$

where the quantity $\Omega^2(E) = \int d\sigma_{n,e}T^2$ is related to the straggling. If we include only the second order term we obtain a second order differential

equation which may be solved directly. Still, since the second order term may be considered small, we may express the second derivative by means of $\bar{R}_1$. This leads to $\bar{R}_2(E)$, the second approximation to average range

$$\bar{R}_2(E) = \int_0^E \frac{dE'}{NS(E')} \left\{ 1 + \frac{\Omega^2(E')}{2} \frac{d}{dE'} \left(\frac{1}{S(E')} \right) \right\}. \tag{3.9}$$

The average square fluctuation in range, $\overline{\Delta R^2}(E) = \overline{R^2}(E) - \bar{R}^2(E)$, is obtained from the second moment in (3.4), if we multiply (3.6) by $2\bar{R}(E)$ and subtract

$$\left.\begin{aligned} &\int d\sigma_{n,e} \left\{ \overline{\Delta R^2}(E) - \overline{\Delta R^2}(E - T_n - \sum_i T_{ei}) \right\} = \\ &\int d\sigma_{n,e} \left\{ \bar{R}(E) - \bar{R}(E - T_n - \sum_i T_{ei}) \right\}^2. \end{aligned}\right\} \tag{3.10}$$

In this equation the right hand side is a known source term. If we take the same successive steps as in the computation of $\bar{\varrho}$, we make a series development in (3.10), in powers of T. The first terms on both sides of the equation lead to the approximation $(\overline{\Delta R^2})_1$,

$$S(E) \frac{d}{dE} (\overline{\Delta R^2})_1 = \Omega^2(E) \left(\frac{d}{dE} \bar{R}(E) \right)^2, \tag{3.11}$$

where for $\bar{R}(E)$ we should use the first approximation, $\bar{R}_1(E)$. Therefore, (3.11) brings us back exactly to our previous assumptions in § 2, in case to (2.4).

Including terms in (3.10) up to second order, we get

$$\left.\begin{aligned} &S(E) \frac{d}{dE} (\overline{\Delta R^2}) - \frac{\Omega^2(E)}{2} \frac{d^2}{dE^2} (\overline{\Delta R^2}) = \\ &\left(\frac{d}{dE} \bar{R} \right)^2 \Omega^2 - \frac{K(E)}{2} \frac{d}{dE} \left(\frac{d}{dE} \bar{R} \right)^2, \end{aligned}\right\} \tag{3.12}$$

where $K(E) = \int d\sigma_{n,e} T^3$. When assuming the new terms in (3.12) to be small, we obtain the second approximation to $(\overline{\Delta R^2})$,

$$\frac{d}{dE} (\overline{\Delta R^2})_2 = \frac{\Omega^2(E)}{S^3(E) N^2} \left\{ 1 + \left(\frac{K}{\Omega^2 S} - \frac{5\,\Omega^2}{2\,S^2} \right) \frac{dS}{dE} + \frac{1}{2\,S} \frac{d\Omega^2}{dE} \right\}. \tag{3.13}$$

In terms of the expression (3.13) we are able to estimate the accuracy of the straightforward formulas (3.11) and (2.4). It is important to notice that

TABLE 1

Comparison of first and second approximation of expansion in γ, for power law scattering. Results for average range and range straggling.

s	$\bar{R}_2/\bar{R}_1$	$\overline{(\Delta R^2)_2}/\overline{(\Delta R^2)_1}$
3/2	$1+\gamma/24$	$1+\gamma\cdot 0.10$
2	1	$1+\gamma/6$
3	$1-\gamma/15$	$1+\gamma\cdot 0.14$

the successive approximations made above are simply series expansions of average range and straggling to successive powers of $\gamma = T_m/E$.

It is of interest to compare the above approximations. For simplicity let us consider low energies and disregard electronic stopping. Since electronic stopping here tends to diminish fluctuation effects, we obtain in this way slightly exaggerated differences between successive range approximations. Moreover, we use power law scattering cross sections (2.6) or (2.6′). This permits exact computation of $\bar{R}(E)$. Note that according to (2.6) the ranges are proportional to $E^{2/s}$, while the square straggling in range behaves as $E^{4/s}$. We may compare $\bar{R}_1$, $\bar{R}_2$ and $\bar{R}$, and similarly $\overline{(\Delta R^2)_1}$, $\overline{(\Delta R^2)_2}$ and $\overline{\Delta R^2}$. The results depend on γ, i. e. on the mass ratio. For small values of γ, a series development in powers of γ is accurate. Since γ is often close to its maximum value, $\gamma = 1$, we also compare the approximations in this case. The results are listed in Table 1 ($\gamma << 1$) and Table 2 ($\gamma = 1$), in the cases $s = 3/2$, 2 and 3. Notice that at low energies values of s between 2 and 3 are of particular interest.

In the approximation used in Table 1 the range $\bar{R}_2$ and its fluctuation $\overline{(\Delta R^2)_2}$ are equal to the exact average values $\bar{R}$ and $\overline{\Delta R^2}$, respectively. From Tables 1 and 2 it is apparent that $\bar{R}_2(E)$ is always a very good approximation to $\bar{R}(E)$, and one need not distinguish between the two. The range $\bar{R}_1(E)$ is somewhat less accurate, but deviates from $\bar{R}(E)$ by no more than 10 percent in the least favourable case ($\gamma = 1$). In actual range observations the deviation is reduced by electronic stopping and by the change in effective s with particle energy. There remains a difference between $\bar{R}_1$ and $\bar{R}$ only at the lowest values of ε. For our present purposes where all range curves (e. g. Figs. 3 and 4) are stated in terms of $\bar{R}_1(E)$ we need hardly distinguish between $\bar{R}_1(E)$ and $\bar{R}(E)$, because of obvious uncertainties in theory and experiment. Still, one might ask why the range curves are computed for $\bar{R}_1$ in place of $\bar{R}_2$. This is simply because a universal range curve would not result when $\bar{R}_2$ is used.

TABLE 2

Comparison of first and second approximation with exact formula when $\gamma = 1$. Average ranges and range straggling for power law scattering.

s	$\bar{R}/\bar{R}_1$	$\bar{R}/\bar{R}_2$	$(\overline{\Delta R^2})/(\overline{\Delta R^2})_1$	$(\overline{\Delta R^2})/(\overline{\Delta R^2})_2$
2	1.053	1.01	1.03	0.94
2	1	1	1.20	1.03
3	0.904	0.97	1.26	1.10

The straggling approximations $(\overline{\Delta R^2})_1$ and $(\overline{\Delta R^2})_2$ are, as a rule, a little smaller than $\overline{\Delta R^2}$ when $\gamma = 1$. This deviation becomes quite pronounced if instead we consider the relative straggling in range. Thus, in the extreme cases of $s = 3$ and $\gamma = 1$ we have $(\overline{\Delta R^2})_1/\bar{R}_1^2 = 0.133$ according to (2.13), while $\overline{\Delta R^2}/\bar{R}^2 \cong 0.20$ for $\gamma = 1$ and $2 < s < 3$. At quite low values of ε, and $\gamma \sim 1$, the straggling in Fig. 6 is therefore somewhat lower than the straggling in average range; still it is noteworthy that the electronic stopping has a considerable influence on straggling also for quite low values of ε. We infer moreover that the absolute values of range straggling in Fig. 7 are expected to represent $\overline{\Delta R^2}$ quite accurately, i. e. they are superior to the relative straggling values in Fig. 6. Note that the deviations are only important when $\gamma \sim 1$. The outcome of the discussion in the present chapter is therefore that the simple quantities $\bar{R}_1$ and $(\overline{\Delta R^2})_1$, introduced already in § 2, are satisfactory estimates of average range and average square fluctuation in range.

Results for power law scattering

In the interesting case of power law scattering, (2.6′), the formula (3.3) takes a particularly simple form if electronic stopping is neglected. In fact, we then obtain

$$\frac{\partial}{\partial r} P(r,\varepsilon) = \int_0^1 \frac{dy}{y^{1+1/s}} \left\{ (1-\gamma y)^{-2/s} P(r \cdot [1-\gamma y]^{-2/s},\ \varepsilon \cdot [1-\gamma y]) - P(r,\varepsilon) \right\}, \quad (3.13)$$

where $r = \lambda_s \varrho \cdot (2\gamma\varepsilon^{2/s})^{-1}$ and $\int_0^\infty P(r,\varepsilon)\,dr = 1$. If the power law holds down to zero energy, equation (3.13) permits us to choose $P(r,\varepsilon)$ independent of ε, and an extremely simple recursion formula is obtained for the moments of the distribution,

$$m < r^{m-1} > = < r^m > \cdot I(\gamma, m, s), \qquad I(\gamma, m, s) = \int_0^1 \left\{ 1 - (1-\gamma y)^{2m/s} \right\} \frac{dy}{y^{1+1/s}}. \quad (3.14)$$

The moments therefore only depend on one parameter, γ, for any given power law scattering.

This result, where virtually the whole range distribution is determined immediately for any energy when merely the power s is stated (and γ is known), is

clearly a direct consequence of universal cross sections, $f(t^{1/2})$. In a more qualitative sense, it is apparent that if at one particle energy a cross section is given as a function of $T/T_m = \sin^2\vartheta/2$, this cross section leads to a certain ion-atom potential from which the scattering at all lower energies may be derived. This circumstance is expressed in an approximate way by the unified cross section, (2.9), and the results happen to be analytically simple for a power law cross section.

The integral $I(\gamma, m, s)$ may be expressed by means of the incomplete beta function (cf. ERDÉLYI et al. (1953)),

$$I(\gamma, m, s) = -s\left\{1-(1-\gamma)^{2m/s}\right\} + 2m\gamma^{1/s} B_\gamma\left(1-\frac{1}{s}, \frac{2m}{s}\right), \tag{3.15}$$

and is particularly simple when $\gamma << 1$, in which case a power series in γ converges rapidly,

$$\left.\begin{aligned} I(\gamma, m, s) = \frac{2m\gamma}{s-1}\Bigg\{1 - \frac{\gamma}{2s}\,\frac{s-1}{2s-1}(2m-s) \\ + \frac{\gamma^2}{3s^2}\,\frac{s-1}{3s-1}(2m-s)(m-s) + \ldots\ldots\Bigg\},\ \gamma << 1. \end{aligned}\right\} \tag{3.16}$$

An interesting case is also $\gamma = 1$, where the incomplete beta function in (3.15) becomes the usual beta function $B_1(p, q) = \Gamma(p)\Gamma(q)/\Gamma(p+q)$.

The results in (3.14), (3.15) and (3.16) were used in Tables 1 and 2 for the computation of the first and second moments in various approximations. It is easy to derive also higher moments.

§ 4. Projected Ranges and Associated Quantities

Average projected range

An interesting quantity appears to be the projection of the range on the initial direction of the particle path. This quantity is often observed directly. Thus, one might be concerned with a collimated beam of particles passing through a number of foils perpendicular to the direction of the beam; the number of particles collected in each foil gives just the distribution in range projected on the initial direction of the beam. We may, in fact, define the concept of projected range as follows. A particle starts inside an infinite homogeneous medium from the origin in the direction of the x-axis; the value of x for the end point of the path is the projected range, R_p. The distribution in x is the distribution in projected range. Quantities of particular interest here are the average projected range, $\bar{R}_p = \bar{R}_p(E)$, and the average straggling in projected range, $\overline{\Delta R_p^2} = \overline{R_p^2} - \bar{R}_p^2$.

An integral equation for the average projected range may be obtained in analogy to the derivation of (3.1). We find readily

$$1 = N\int d\sigma_{n,e}\{\bar{R}_p(E) - \bar{R}_p(E-T)\cos\varphi\}, \tag{4.1}$$

where $T = T_n + \sum_i T_{ei}$, and φ is the deflection of the ion in the laboratory system. There is a close similarity to the integral equation (3.6) for the average range, the only difference being the factor $\cos\varphi$ in (4.1).

Let us consider some approximations which can be useful in solving (4.1). If always $T << E$, i. e. $\gamma << 1$, or if $\bar{R}_p$ is nearly proportional to E, we may write

$$1 = \bar{R}_{p1}(E)\, N\int d\sigma_{n,e}(1-\cos\varphi) + \frac{d\bar{R}_{p1}(E)}{dE} N\int d\sigma_{n,e}\cdot T\cdot\cos\varphi. \tag{4.2}$$

This approximation is similar to the one for $\bar{R}_1$ in (3.7) and (2.2), and we therefore use the notation $\bar{R}_{p1}$ for the projected range in (4.2). Actually, if the deflection φ may be neglected, we obtain $(d\bar{R}_{p1}/dE) = N\cdot S$, i. e. $\bar{R}_{p1}$ becomes equal to $\bar{R}_1$.

When solving (4.2) we can introduce the familiar transport mean free path, λ_{tr}, and a transport stopping cross section, S_{tr},

$$\frac{1}{\lambda_{tr}} = N\int d\sigma_{n,e}(1-\cos\varphi),\quad S_{tr} = \int d\sigma_{n,e}\, T\cos\varphi. \tag{4.3}$$

With this notation, equ. (4.2) becomes

$$1 = \frac{\bar{R}_{p1}(E)}{\lambda_{tr}(E)} + \frac{d\bar{R}_{p1}(E)}{dE}\cdot NS_{tr}(E), \tag{4.4}$$

which equation (4.4) has the solution

$$\bar{R}_{p1}(E) = \int_0^E \frac{dE'}{NS_{tr}(E')}\exp\left\{\int_E^{E'}\frac{dE''}{\lambda_{tr}(E'')\,N\cdot S_{tr}(E'')}\right\}, \tag{4.5}$$

and this result should be a good approximation to $\bar{R}_p(E)$ if γ is small, or if R_p is nearly proportional to energy. We may solve the equation for $\bar{R}_p$ in the lowest approximation. This corresponds to taking the leading term in a series development in $\mu = M_2/M_1$, assuming μ to be small. The approximation is similar to that in § 3, for $\gamma << 1$. In the limit of small μ, the angle φ is always small and we need only include φ^2-terms in (4.3). Using

if $M_p >> M_s$

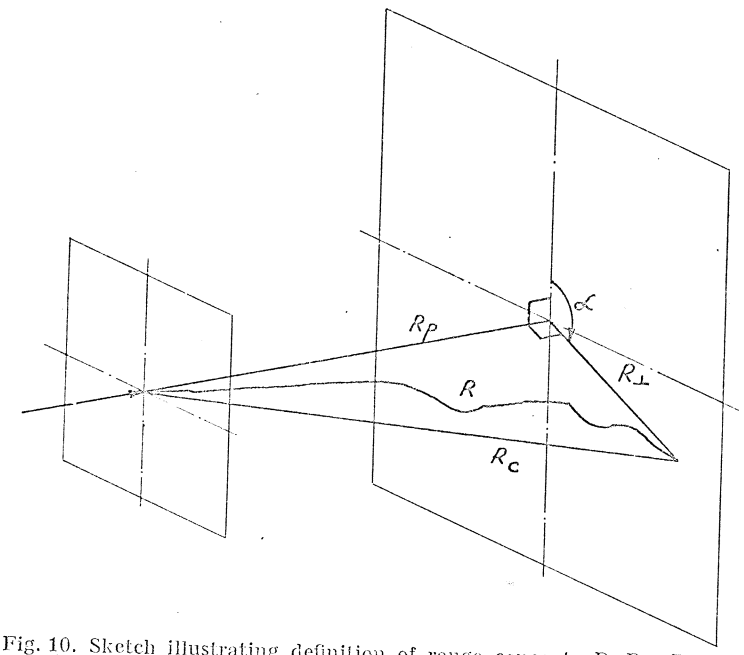

Fig. 10. Sketch illustrating definition of range concepts R, R_p, R_c and $R_\perp$.

The integral equations for $\overline{R_p^2}$ are derived in a similar way as (3.1). The following two equations are obtained, after rearrangement of terms,

$$2\,\bar{R}_p(E) = N\int d\sigma_{n,e}\left\{\overline{R_c^2}(E) - \overline{R_c^2}(E-T)\right\}, \tag{4.8}$$

$$2\,\bar{R}_p(E) = N\int d\sigma_{n,e}\left\{\overline{R_r^2}(E) - \left(1-\frac{3}{2}\sin^2\varphi\right)\overline{R_r^2}(E-T)\right\}, \tag{4.9}$$

where

$$\overline{R_c^2} = \overline{R_p^2} + \overline{R_\perp^2} \text{ and } \overline{R_r^2} = \overline{R_p^2} - \frac{1}{2}\overline{R_\perp^2}\,. \tag{4.10}$$

The two equations (4.8) and (4.9) may be solved separately, and then $\overline{R_p^2}$ is found from (4.10).

First order solutions of (4.8) and (4.9), for $\mu << 1$, can be obtained in a direct manner. However, we shall merely consider the case of power law scattering, with neglect of electronic stopping. The exact solutions may then be expressed as beta functions. In Table 3 we quote the results for $\mu = 1$ and various values of s. It is seen that in these cases $\overline{\Delta R_p^2}$ is of order of $\overline{\Delta R^2}$.

TABLE 3

Straggling in projected range for power law scattering and $\mu = 1$.

s	3/2	2	3
$\sqrt{\overline{\Delta R^2}}/\sqrt{\overline{R_p^2}}$	1.25	1.33	1.38
$\sqrt{\overline{\Delta R^2}}/R_p$	0.204	0.275	0.341

§ 5. Comparison with Experiments

As an illustration of the connection to experiments, we present a brief survey of recent experimental results, interpreted on the lines of the theory of this paper. Before that, it may be worth-while to summarize briefly and comment on the salient features of this theory.

A primary result is that a simple-minded theory of ranges and their fluctuations, as described in § 2, is quite accurate and that corrections of various kinds for projected ranges, etc., may be made without much difficulty, if necessary. A second result, somewhat independently of the details of the theory of collisions, is that a $\varrho - \varepsilon$ plot is useful for a study of ranges of particles with $\varepsilon < 1000$, and particularly for $\varepsilon \lesssim 10$. A third result is that for any ion of high energy a range correction, Δ, for the effect of nuclear stopping has been obtained, which permits a more accurate study of electronic stopping. Fourth, e. g. various isotope effects can serve to check several details of the theory, as may also observations of range straggling.

A theoretical result of special interest is that for $Z_1 = Z_2$ the electronic stopping constant is $k \sim 0.15$, except when $Z_1 = 1$. Therefore, the range energy curve for $Z_1 = Z_2$ should be closely a single curve in a $\varrho - \varepsilon$ plot. However, the corrections for e. g. projected ranges are not negligible in this case.

The numerical results computed here are based on a much simplified model of collisions. It is certainly possible to introduce a more detailed description of the collisions (cf. Notes on Atomic Collisions I and IV), and thereby improve on the present theoretical results. However, it may be more important to remove uncertainties and to correct misconceptions in the theory by measurements of range and stopping.

Another important circumstance is that direct comparisons with measured ranges may be made preferably in gases, where successive collisions are uncorrelated. In several respects stopping in solids may also answer the purpose, but experiments at low ion energies clearly seem to indicate the

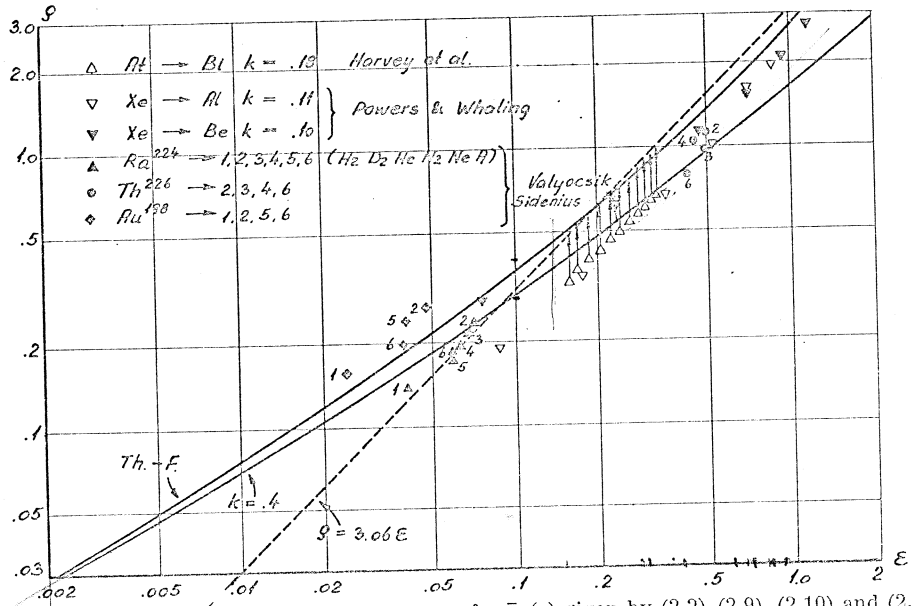

Fig. 11. Comparison between theoretical curves for $\bar{\varrho}_1(\varepsilon)$ given by (2.2), (2.9), (2.10) and (2.11), and measurements for $\varepsilon < 2$. As indicated on the figure, numbers 1, 2, 3, 4, 5 and 6 refer to stopping gases H_2, D_2, He, N_2, Ne and A, respectively. For further comments cf. text.

kind of correlation of collisions described as tunnelling (cf. PIERCY et al. (1963)), with strong directional effects and range lengthening in certain crystal structures. Although these range effects are in themselves highly interesting, their special character make them less suited in a general first comparison between range theory and experiments. In e. g. amorphous solids the effect appears to be absent, as was to be expected.

It should be appreciated that in the following we have merely made a compilation of measurements; not all of them are plotted in the figures. We are not in a position to make any critical examination of the experiments, some of which are in mutual disagreement or obviously inaccurate. We have included primarily the more recent measurements. A review of previous observations is given by HARVEY (1960). We are mainly interested in experiments where nuclear stopping is dominating, and do not discuss electronic stopping. NORTHCLIFFE (1963) has given a valuable survey of measurements on stopping in the energy region just above the one considered here, i. e. when electronic stopping dominates and goes through a maximum.

In plotting the results we have made approximate corrections for projected ranges, etc. Normally, the range measurements are plotted directly

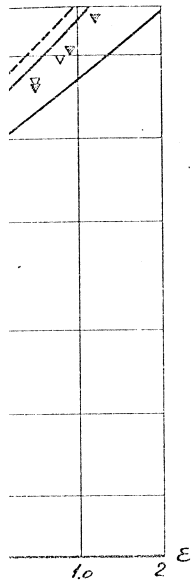

2.9), (2.10) and (2.11), and 6 refer to stopping ments cf. text.

(cf. Piercy et al. heating in certain themselves highly in a general first e. g. amorphous ted.

re merely made a ed in the figures. of the experiments, ly inaccurate. We review of previous interested in ex- not discuss electro- urvey of measure- e considered here, h a maximum. orrections for pro- re plotted directly

on the figures, and range corrections are indicated by arrows. In some cases our knowledge of the measurements was too scanty to permit a range correction. As a general rule, we have corrected for projected ranges, etc., only if the correction exceeds ~10 percent.

Fig. 11 shows the theoretical range curve for values of ε smaller than 2, where nuclear stopping is quite dominating. The ranges for pure nuclear stopping are given by the upper solid curve, denoted as Th.-F. on the figure. A curve for exceptionally large electronic stopping, i. e. $k = 0.4$, is also shown. The actual k-values are quite small, and thus the expected ranges should be close to the Th.-F. curve. Further, note the dashed straight line corresponding to range proportional to energy, $\varrho = 3.06\varepsilon$. It should be emphasized that for extremely low energies, $\varepsilon \lesssim 10^{-2}$, the theoretical curve is not too well-defined.

Harvey, Wade and Donovan (1960) observed projected ranges for At^{205} and At^{207} ions in bismuth. The At recoil ions were produced by α-bombardment of a bismuth foil, leading to an (α, xn) process. This resulted in At ions with various energies between 400 and 900 keV; the energies were not sharply defined. Approximate corrections for projected range are shown by arrows in Fig. 11. The observations of Harvey, Wade and Donovan are in satisfactory accord with the predicted ranges.

Powers and Whaling (1962) studied projected ranges of monoenergetic ions of nitrogen and inert gases in several solids. The depth of penetration of the ions was obtained from a subsequent analysis of the distribution in angle and energy loss of protons scattered from the ions imbedded in the target. The ranges of Powers and Whaling are generally in good agreement with the theoretical curves. In the figure, we have included only their range measurements for Xe in Be and in Al. The corrections for projected ranges are quite small and are omitted. The ranges in Al may be compared with those of Davies et al. in Fig. 12. These two range observations for Xe in Al give quite different results and are placed on either side of the theoretical curve.

Valyocsik (1959) made accurate observations of ranges of Ra^{224} and Th^{226} recoil atoms with, respectively, 97 and 725 keV energies. Ranges are measured in gases using the electrostatic collection technique of Ghiorso and Sikkeland. Ranges and range stragglings were observed in deuterium, helium, nitrogen and argon, and in hydrogen and neon (only for Ra ions). The observations are shown in Fig. 11. They are in good agreement with theory (between 0 and 20 percent below theoretical ranges), and correspond to $k = 0.12$, except in hydrogen where $k = 0.16$.

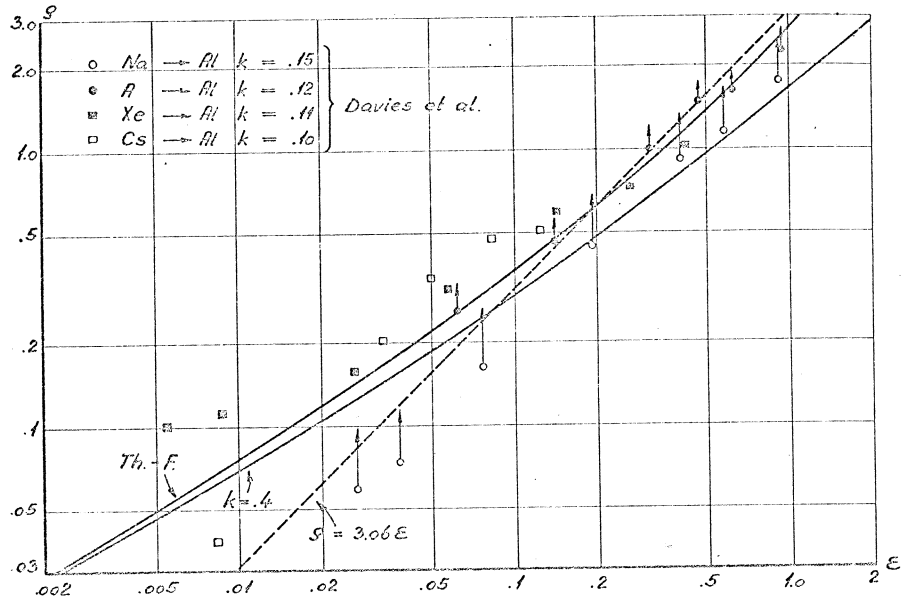

Fig. 12. As Fig. 11; measurements of median ranges by DAVIES et al. in Al. Ranges at low energies exceed theoretical curves, probably as an effect of tunnelling in crystal lattice.

A few measurements by the Copenhagen group (SIDENIUS, private communication) are also included in Fig. 11. The projected range of Au^{198} ions of energy 50 keV is measured by electrostatic collection. The correction for projected range is negligible. The ranges are slightly above theoretical curves. The k-values are as in VALYOCSIK's measurements.

DAVIES et al. (1960, 1961 and private communication) have observed projected ranges in Al, for the following ions: Na^{24}, A^{41}, K^{42}, Rb^{86}, Xe^{133} and Cs^{137}. Monoenergetic radioactive ions of energies between 1 keV and 2 MeV enter a polished Al surface. Thin layers of Al are removed successively by electro-chemical means and the residual activity is measured. In this way the distribution in projected range is obtained. The range values of DAVIES et al. in Fig. 12 are median ranges. At the higher energies there is good agreement with theoretical curves.

The measurements by DAVIES et al. were made with polycrystalline Al. It has turned out that the structure of Al is such that tunnelling of the ions may occur, whereby the average range becomes considerably larger than for a random system, and the range distribution has an exponential tail (PIERCY et al. (1963)). The results of PIERCY et al. for Kr^{85} in Al and Al_2O_3 at 40 keV are compared with theoretical estimates in Table 4. There is

TABLE 4

Ranges (in $\mu g/cm^2$) of 40 keV Kr^{85} in Al and Al_2O_3, and average square straggling in range. Experimental results by PIERCY et al. Computed results (columns 3 and 5) are for random system, as indicated.

	R^{med}_{exp}	$\bar{R}_{exp}$	$\bar{R}_{rand}$	$\overline{(\Delta R)^2_{exp}}$	$\overline{(\Delta R)^2_{rand}}$
Al.....	9.0	11.5	7.1	91	4.6
Al_2O_3.....	7.7	7.7	6.5	7.8	3.5

satisfactory agreement in the amorphous substance Al_2O_3, both as regards ranges and straggling. It appears also from Table 4 that the experimental median range in Fig. 12 is probably somewhat larger than the average ranges of a random system of Al atoms. We therefore infer that the results of DAVIES et al. in Fig. 12 are not in contradiction to the theoretical ranges of a random system. Note the very large experimental range straggling in Table 4 for Al, characteristic of an exponential distribution, where $\overline{\Delta R^2} = \bar{R}^2$.

There are several other measurements in the regions of energy corresponding to Figs. 11 and 12. Thus, BAULCH and DUNCAN (1957) obtain ranges of α-recoils ($\varepsilon \lesssim 0.1$) from 0 to 10 percent below theoretical curves. The results of VAN LINT et al. (1961) are at the higher energies at least about a factor of 2 above theoretical expectations, while at lower energies ($\varepsilon \sim 0.04$) agreement is fair. However, these measurements show a very considerable scatter. GUSEVA, INOPIN and TSYTKO (1959) measured ranges of monoenergetic Si^{30} ions in Ta and Cu backings, at energies between 10 and 25 keV. The depth of penetration was estimated from proton energies necessary for a (p, γ) process, together with knowledge of proton stopping. Their results are about a factor of 2 above the theoretical curves.

Fig. 13 shows some observations for $1 < \varepsilon < 100$, and corresponds to Fig. 4 in § 2. We are here in a region where the electronic stopping begins to take over. It is then important to know the value of the constant k. Some of the projected ranges observed by POWERS and WHALING (1962) are shown in Fig. 13, including one where the ratio $\mu = (M_2/M_1) \sim 2$, i. e. the corrections for projected range are large. The agreement with theoretical curves is good.

WINSBERG and ALEXANDER (1961) and ALEXANDER and SISSON (1962) measured projected ranges for Tb^{149} ions in aluminium, at energies between 4 and 30 MeV, and for At and Po ions in aluminium and gold, at energies between 3.5 and 13 MeV. The projected ranges and the range stragglings were obtained from the activities in stacks of catcher foils. In Fig. 13 we have included results for At and Po in gold and for Tb^{149} in

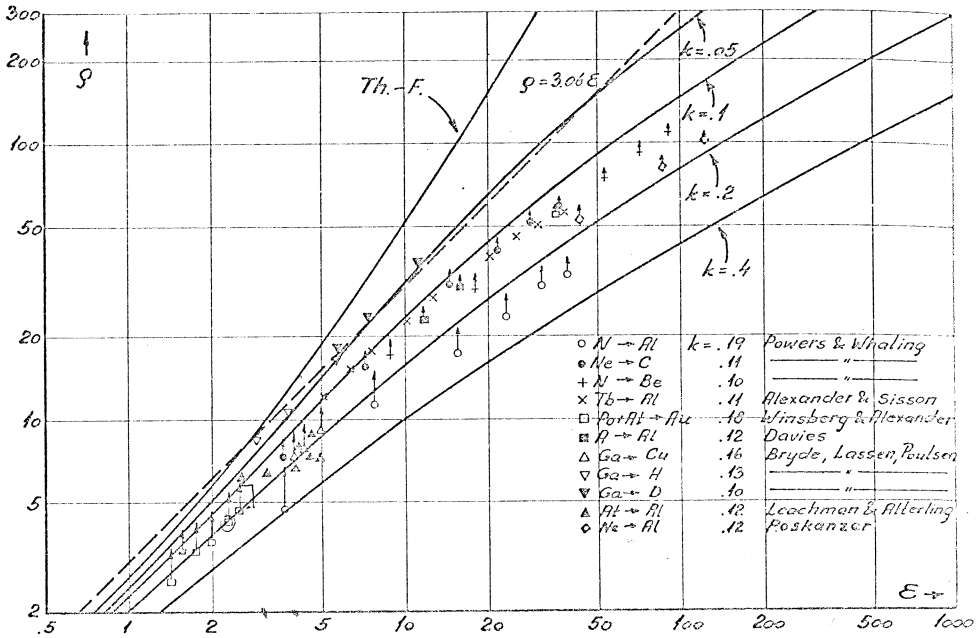

Fig. 13. Comparison with range measurements in the region $1 < \varepsilon < 100$, where electronic stopping becomes important. Theoretical k-values are given, indicating the theoretical curve with which to compare the observations.

aluminium. There is good agreement with the theoretical curves. It may be noted that the ions were formed in a nuclear reaction with subsequent neutron evaporation.

In the case of A^{41} in aluminium, Davies et al. (private communication) performed measurements at energies so high that electronic stopping is important. The ranges are in good agreement with the theoretical curves in Fig. 13.

Bryde, Lassen and Poulsen (1962) measured projected ranges for radioactive Ga^{66} recoil ions in gases using electrostatic collection. As typical representatives of their observations we have in Fig. 13 included ranges in hydrogen and deuterium. These ranges are about 40 percent above theoretical ranges. Bryde, Lassen and Poulsen also observed projected ranges for Ga^{66} in copper; the latter ranges are in good agreement with the theoretical curve. Also included in Fig. 13 are three measurements by Poskanzer (1963) of 1–3 MeV Ne^{22} ions in aluminium; these ranges are smaller than theoretical ranges. Finally, in Fig. 13 is shown the early measurements of ranges by Leachman and Atterling (1957), where recoil ions of At^{203}

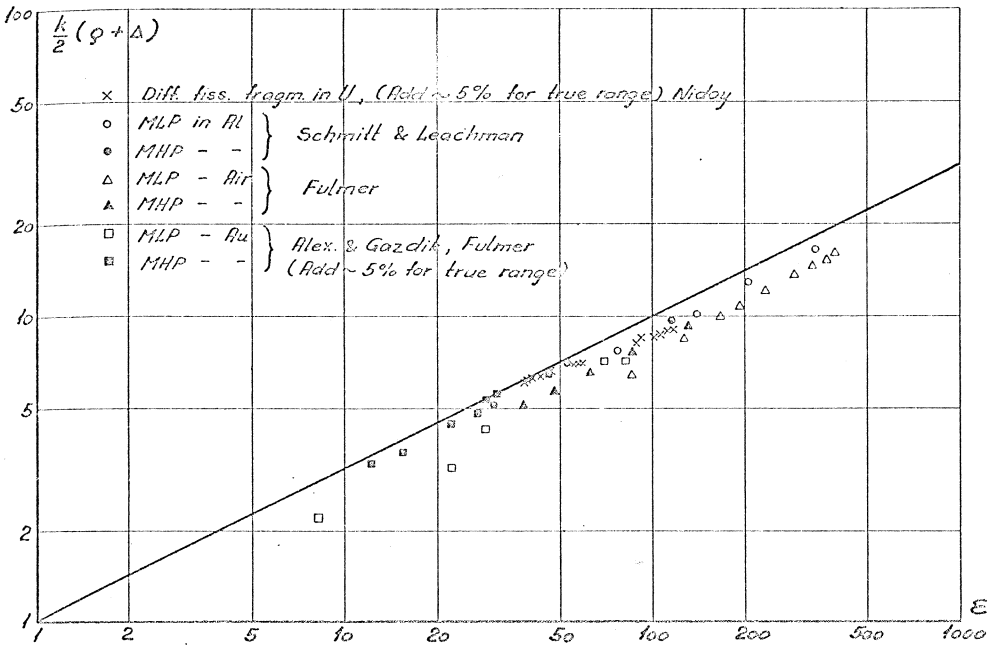

Fig. 14. Comparison between theoretical curve and range measurements for fission fragments, nuclear stopping being eliminated. For large values of ε the representation shown here is superior to that in Fig. 13.

and At^{205} penetrated a stack of aluminium foils, and projected ranges were measured. There is fair agreement, but apparently some fluctuations between individual measurements.

As mentioned previously, in the present paper we do not attempt a systematic study of electronic stopping as obtained from measurements at high values of ε. We may merely show two sets of representative measurements, where the nuclear stopping is eliminated, so that the extrapolated electronic range is obtained. For $v<v_1$ the theoretical extrapolated electronic range is $\varrho_e = 2\varepsilon^{1/2}/k$. Using theoretical range corrections for nuclear stopping, $\Delta(k, \varepsilon)$, as indicated in Fig. 5, we have plotted in Figs. 14 and 15 values of $(k/2)\left\{\varrho+\Delta(k, \varepsilon)\right\}$ obtained from measurements of ϱ. The theoretical curve is the straight line $k\varrho_e/2 = \varepsilon^{1/2}$. Fig. 14 contains only measurements of ranges of fission fragments. In Fig. 14 is shown measurements by Niday (1961) of fission fragment ranges in uranium. Niday used a thick uranium foil packed in aluminium catcher foils. Fission fragments resulted from thermal neutrons. The fragments ending up in aluminium were separated by radiochemical means. In this way an estimate of the ranges along the

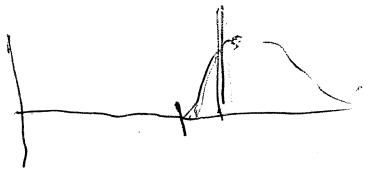

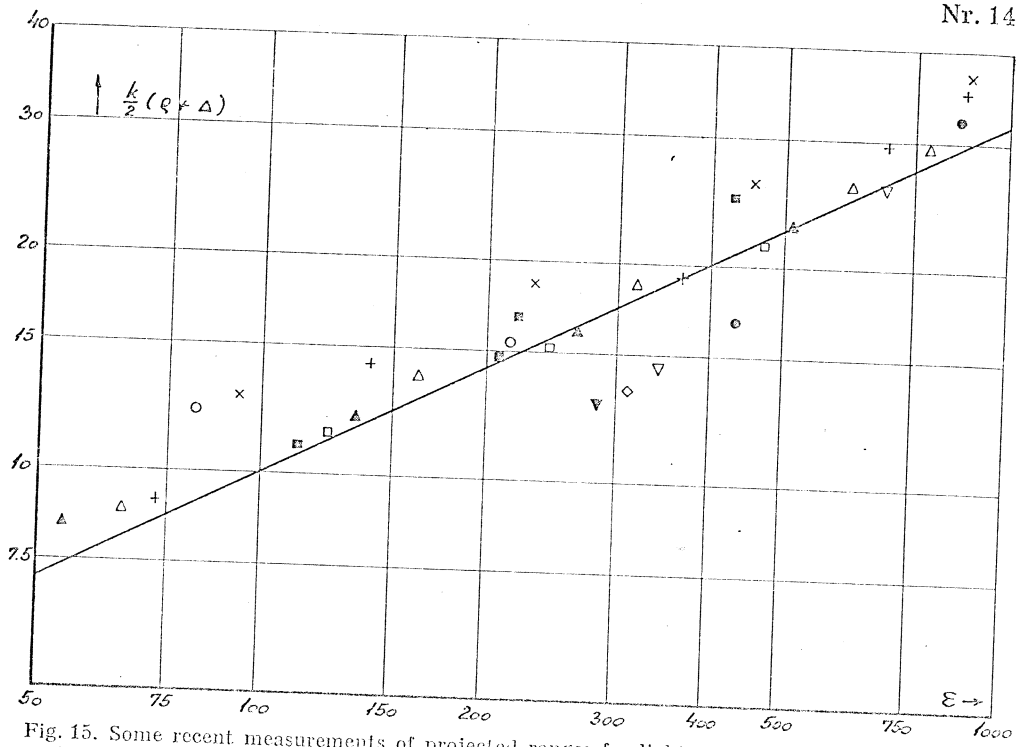

Fig. 15. Some recent measurements of projected ranges for light atoms in gases, corrected for nuclear stopping only, like in Fig. 14. Full-drawn curve is theoretical range $\varepsilon^{1/2}$. Points stand for following ions in air: × Li, + B, △ C, ▲ O, □ F, ⊞ Ne, ○ Na, and following ions in argon: ⊙ Li, ▽ B, ▼ N (measurements by TEPLOVA et al.). Further, ◇ indicates F in nitrogen, measured by BRYDE, LASSEN and POULSEN.

chord was obtained. The ranges of NIDAY should be corrected by approximately +5 percent in order to obtain true ranges. The agreement with the theoretical range is good.

In Fig. 14 is also included observations on fission fragment ranges by ALEXANDER and GAZDIK (1960), FULMER (1957) and LEACHMAN and SCHMITT (1954). In the case of gold, about 5 percent should be added in order to obtain true ranges. There is agreement within ~10 percent.

A number of other authors have measured ranges of fission fragments (SMITH and FRANK (1959), KATCOFF, MISKEL and STANLEY (1948), GOOD and WOLLAN (1956), BØGGILD, ARRØE and SIGURGEIRSSON (1947), DOUTHETT and TEMPLETON (1954), SUZOR (1949), PORILE and SUGARMAN (1957), cf. also the review article by HARVEY (1960)). Some of the earlier measurements may be less accurate than those shown in Fig. 14, but generally there is approximate agreement with theory.

As an example of light ions with substantial energies we have taken measurements of projected ranges by TEPLOVA et al. (1962). A number of ions, from Li to Na, with energies in the interval 1–10 MeV, were slowed down in air, argon and hydrogen. Many of these measurements are shown in Fig. 15. On the figure is also shown a range value for F^{18} in nitrogen gas, measured by BRYDE, LASSEN and POULSEN (1962). We have not indicated corrections for projected ranges on Fig. 15, since the largest correction would be $\sim +8$ percent (for Li in argon gas).

In connection with electronic stopping it should be noted that at low atomic numbers, and particularly at low values of Z_1, there may be deviations from the theoretical k-value based on a Thomas-Fermi treatment. At low atomic numbers one may expect variations in the measured k-values due to shell effects. As an extreme example from a Thomas-Fermi point of view, in the case of Li ions in hydrogen, deuterium and helium, it appears from measurements of stopping (ALLISON and LITTLEJOHN (1957)) and of ranges (CLERC, WÄFFLER and BERTHOLD (1961)) that the electronic stopping may be as much as 2–3 times less than given by (2.5). Measurements by ORMROD and DUCKWORTH (1963) of electronic stopping in carbon for all ions with $Z_1 \lesssim 11$ indicate minor shell variations around the value in (2.5).

Range straggling

As to straggling in range (cf. p. 14) we have not attempted any closer analysis. High accuracy is difficult to obtain in range straggling, and at low ε-values ($\varepsilon < 0.5$) the rule-of-thumb $(\Delta\varrho/\varrho)^2 = \gamma/6 = M_1 M_2 (M_1 + M_2)^{-2} \cdot (2/3)$ is often sufficient. In many experiments a considerable fluctuation was present in the initial ion beam, e. g. because the ion resulted from a compound nucleus after neutron evaporation. The experimental range stragglings are often considerably above the curves. The measurements by VALYOCSIK on 97 keV α-recoils (cf. HARVEY (1960)) correspond to rather well-defined conditions. For 97 keV Ra the straggling in nitrogen, neon and argon is comparable with the theoretical one (cf. Fig. 6), but in the light gases, hydrogen, deuterium and helium, the straggling is much in excess of theoretical estimates. When subtracting a common constant of order of 0.016 from the experimental straggling $(\Delta\varrho)^2_{exp}$, one obtains a relative straggling $\gamma^{-1}(\Delta\varrho/\varrho)^2 \cong 0.14$–$0.18$, in excellent agreement with theory (since $\varepsilon \approx 0.03$–0.07, and $k \cong 0.12$). For 725 keV Th ions, where $\varepsilon \approx 0.4$–0.5, the experimental relative straggling is much too large in deuterium and helium. A reduction of $(\Delta\varrho)^2_{exp}$ by ≈ 0.04 in all gases would give a reasonable order of magnitude of the straggling. As a further example, many measurements by the Copen-

hagen group show rather large straggling effects, but some results (e. g. ranges of 50 keV Ga^{66} in hydrogen, helium, nitrogen and argon, shown in Fig. 11) with $\varepsilon \approx 0.3$–0.5, have a straggling $(\Delta\varrho/\varrho)^2 \gamma^{-1} \approx 0.15$–$0.25$. Even in the difficult case of the lightest gases, where the theoretical straggling is extremely small, there is reasonable accord with theory.

Isotope effects

It is of interest to study isotope effects in range measurements. We shall treat the question of different isotopes used as stopping medium*. Although electronic stopping may dominate in the value of the range itself, isotope effects can still give direct information about the nuclear stopping. An instructive example is provided by the measurements of Bryde, Lassen and Poulsen (1962, and private communication). They observed ranges of Ga^{66} in hydrogen and deuterium; at high energies R_D is slightly larger than R_H, while at low energies R_H exceeds R_D. Now, if there was only electronic stopping, the two ranges would be equal, so that differences are due to nuclear stopping. It is seen from (2.7) that the nuclear stopping behaves as $S_n \propto M_2^{1-2/s}$, when $M_1 >> M_2$. At quite low energies, where the ion cannot penetrate deeply into the atom, the effective power of the potential is of order of $s = 3$, and thus $S_{nD} > S_{nH}$. At high energies, where the screening is weak, the effective power approaches $s = 1$, and therefore $S_{nH} > S_{nD}$ (Lindhard and Scharff (1961)). According to Fig. 2, the change-over in stopping occurs at an ε-value smaller than 0.5. Correspondingly, in Fig. 4 the change-over in slope—from lower to higher than that of the straight dashed line—occurs at $\varepsilon \sim 1$ for the Th.-F. curve.

Instead of this qualitative explanation of experimental results we may directly compare experimental range differences with theoretical ones deduced from Figs. 3 and 4. The results are shown in Table 5. Agreement between theoretical and experimental range differences is quite good,

Table 5

Differences between ranges in D_2 and H_2 for Ga^{66} ions. Ranges are in mm at 300° K, 760 mm Hg.

Energy (keV)	1190	790	610	50
$(R_D - R_H)_{th}$	0.9	0.7	0.6	−0.05
$(R_D - R_H)_{exp}$	1.5	0.8	0.5	−0.05

* A measurement, where different isotopes are chosen for the incoming particle, is discussed by Lindhard and Scharff (1961).

especially at the lower energies. This result is obtained in spite of the fact that at the three higher energies the absolute ranges of BRYDE, LASSEN and POULSEN are as much as ~40 percent higher than theoretical ranges (Fig. 13).

In further measurements by the Copenhagen group (SIDENIUS, private communication), other examples of isotope effects were obtained for 50 keV ions. Thus, for Na^{24} in hydrogen and deuterium ($\varepsilon = 2.4$ and 4.65) one found $(R_D - R_H)_{exp} = +0.157$ mm, while $(R_D - R_H)_{th} = +0.104$ mm, the ranges themselves being of order of 0.9–1.0 mm, and ~50 percent larger than theoretical ranges. For Au^{198} ions in hydrogen and deuterium, ε is so small ($\varepsilon = 0.024$ and 0.047) that the effective power has shifted to $s > 2$, and $(R_D - R_H)_{exp} = -0.061$ mm, while $(R_D - R_H)_{th} = -0.087$ mm; experimental ranges are ~ 0.4 mm, i. e. about 30 percent larger than theoretical ranges. Finally, for Ga^{66} in helium isotope gases ($\varepsilon \sim 0.4$) one found $(R_{He^4} - R_{He^3})_{exp} = -0.016$ mm, to be compared with $(R_{He^4} - R_{He^3})_{th} = -0.006$ mm; experimental ranges are ~0.4 mm, or 20 percent above theoretical ranges. All ranges quoted here are in mm at 300° K, 760 mm Hg. The agreement with theoretical isotope shifts of ranges is thus fairly good, and it is interesting that normally the change from larger to shorter range in the heavier isotope occurs at $\varepsilon \sim 1$.

Acknowledgments

A few of the above results were obtained seven years ago, following discussions with Dr. R. B. LEACHMAN on his observations of range distributions. They have been referred to various times in the literature. A brief summary of the present work (LINDHARD and SCHARFF (1961)) was published at the time of MORTEN SCHARFF's death.

We are much indebted to Drs. R. B. LEACHMANN, J. M. ALEXANDER, B. G. HARVEY, N. O. LASSEN, N. O. ROY POULSEN, W. WHALING, J. A. DAVIES, H. E. DUCKWORTH, Mr. G. SIDENIUS and many others for discussions and communication of experimental results prior to publication.

We wish to express our gratitude to all who have encouraged us and assisted in this work, in particular to P. V. THOMSEN, M. Sc.

We are much indebted to Miss S. TOLDI and Mrs. A. GRANDJEAN for assistance in the preparation of the paper.

Institute of Physics,
University of Aarhus.

References

J. M. Alexander & M. F. Gazdik (1960). Recoil Properties of Fission Products. Phys. Rev. **120**, 874.

J. M. Alexander & D. H. Sisson (1962). Recoil Range Evidence for the Compound-Nucleus Mechanism in Reaction between Complex Nuclei. UCRL-10098.

S. K. Allison & C. S. Littlejohn (1957). Stopping Power of Various Gases for Li Ions of 100–450 keV Kinetic Energy. Phys. Rev. **104**, 959.

D. L. Baulch & J. F. Duncan (1957). The Range-Energy-Relation for α-Recoil Atoms. Austral. J. Chem. **10**, 112.

N. Bohr (1948). Penetration of Atomic Particles through Matter. Mat. Fys. Medd. Dan. Vid. Selsk. **18**, no. 8.

L. Bryde, N. O. Lassen & N. O. Roy Poulsen (1962). Ranges of Recoil Ions from α-Reactions. Mat. Fys. Medd. Dan. Vid. Selsk. **33**, no. 8.

J. K. Bøggild, O. H. Arroe & T. Sigurgeirsson (1947). Cloud-Chamber Studies of Electronic and Nuclear Stopping of Fission Fragments in Different Gases. Phys. Rev. **71**, 281.

H. G. Clerc, H. Wäffler & F. Berthold (1961). Reichweite von Li^8-Ionen der Energie 40–450 keV in H_2, D_2 und He. Zeitsch. f. Naturf. **16a**, 149.

J. A. Davies, J. D. McIntyre, R. L. Cushing & M. Lounsbury (1960). The Range of Alkali Metal Ions of Kiloelectron Volt Energies in Al. Can. J. Chem. **38**, 1535.

J. A. Davies & G. A. Sims (1961). The Range of Na^{24} Ions of Kiloelectron Volt Energies in Al. Can. J. Chem. **39**, 601.

J. A. Davies, J. D. McIntyre & G. A. Sims (1961). Isotope Effects in Heavy Ion Range Studies. Can. J. Chem. **39**, 611.

B. Domeij, I. Bergström, J. A. Davies & J. Uhler (1963). A Method of Determining Heavy Ion Ranges by Analysis of α-Line Shapes. To appear in Arkiv f. Fysik.

E. M. Douthett & D. H. Templeton (1954). The Ranges of Fragments from High Energy Fission of Uranium. Phys. Rev. **94**, 128.

A. Erdélyi, W. Magnus, F. Oberhettinger & F. G. Tricomi (1953). Higher Transcendental Functions, I. McGraw-Hill.

U. Fano (1953). Degradation and Range Straggling of High Energy Radiations. Phys. Rev. **92**, 328.

C. B. Fulmer (1957). Scintillation Response of CsI(Tl) Crystals to Fission Fragments and Energy vs. Range in Various Materials for Light and Heavy Fission Fragments. Phys. Rev. **108**, 1113.

W. M. Good & E. O. Wollan (1956). Range and Range Dispersion of Specific Fission Fragments. Phys. Rev. **101**, 249.

M. I. Guseva, E. V. Inopin & S. P. Tsytko (1959). Depth of Penetration and Character of Distribution of Atoms Injected into Si^{30} Isotope Targets. Sovj. Phys. JETP 9, 1.

B. G. Harvey (1960). Recoil Techniques in Nuclear Reaction and Fission Studies. Ann. Rev. of Nucl. Sci. 10, 235.

B. G. Harvey, P. F. Donovan, J. R. Morton & E. W. Valyocsik (1959). Range Energy Relation for Heavy Atoms. UCRL-8618.

B. G. Harvey, W. H. Wade & P. F. Donovan (1960). Recoil Studies of Heavy Element Nuclear Reactions, II. Phys. Rev. 119, 225.

D. K. Holmes & G. Leibfried (1960). Radiation Induced Primary Knock-Ons in the Hard Core Approximation. J. Appl. Phys. 31, 1046.

D. K. Holmes (1962). The Range of Energetic Atoms in Solids. "Radiation Damage in Solids", vol. I, IAEA, Vienna.

F. Joliot (1934). Ranges of α-Recoils in Cloud Chamber. J. Phys. Rad. (7), 5, 219.

S. Katcoff, J. A. Miskel & C. W. Stanley (1948). Ranges in Air and Mass Identification of Plutonium Fission Fragments. Phys. Rev. 74, 631.

R. B. Leachman & H. W. Schmitt (1954). Fine Structure in the Velocity Distribution of Slowed Fission Fragments. Phys. Rev. 96, 1366.

R. B. Leachman & H. Atterling (1957). Nuclear Collision Stopping of Astatine Atoms. Arkiv f. Fysik 13, 101.

J. Lindhard & M. Scharff (1961). Energy Dissipation by Ions in the keV Region. Phys. Rev. 124, 128.

J. Lindhard, V. Nielsen, M. Scharff & P. V. Thomsen (1963). Integral Equations Governing Radiation Effects. Notes on Atomic Collisions, III. Mat. Fys. Medd. Dan. Vid. Selsk. 33, no. 10.

V. A. J. van Lint, R. A. Schmitt & C. S. Suffredini (1961). Range of 2–60 keV Recoil Atoms in Cu, Ag, Au. Phys. Rev. 21, 14517.

J. B. Niday (1961). Radiochemical Study of the Ranges in Metallic Uranium of the Fragments from Thermal Neutron Fission. Phys. Rev. 121, 1471.

K. O. Nielsen (1956). The Range of Atomic Particles with Energies about 50 keV. "Electro-Magnetically Enriched Isotopes and Mass Spectrometry". Proc. 1955. Harwell Isotope Conf.

L. C. Northcliffe (1963). Passage of Heavy Ions through Matter. To appear in Ann. Rev. Nucl. Sci.

J. H. Ormrod & H. E. Duckworth (1963). Stopping Cross-Sections in Carbon for Low Energy Atoms with $Z \leq 12$. To appear in Canad. J. Phys.

G. R. Piercy, F. Brown, J. A. Davies & M. McCargo (1963). An Experimental Study of a Crystalline Structure on the Ranges of Heavy Ions. Phys. Rev. Letters 10, 399.

N. T. Porile & N. Sugarman (1957). Recoil Studies of High-Energy Fission of Bi and Ta. Phys. Rev. 107, 1410.

A. M. Poskanzer (1963). Range of 1–3 MeV Ne^{22} Ions in Al and the Analysis of Some Na^{24} Recoil Data. Phys. Rev. 129, 385.

D. Powers & W. Whaling (1962). Range of Heavy Ions in Solids. Phys. Rev. 126, 61.

M. T. Robinson, D. K. Holmes & O. S. Oen (1961). Monte Carlo Calculation of the Ranges of Energetic Atoms in Solids. ORNL-3212.

R. A. Schmitt & R. A. Sharp (1958). Measurement of the Range of Recoil Atoms. Phys. Rev. Letters 1, 12.

F. Seitz (1949). On the Disordering of Solids by Action of Fast Massive Particles. Disc. Far. Soc. 5, 271.

E. R. Smith & P. W. Frank (1959). Recoil Range of Fission Fragments in Zirconium. WAPD-TM-198.

F. Suzor (1949). Tracks in Various Materials of Uranium Fission Fragments. Ann. Phys. 4, 269.

Ya. A. Teplova, V. S. Nikolaev, I. S. Dmitriev and L. N. Fateeva (1962). Slowing Down of Multicharged Ions in Solids and Gases. Sovj. Phys. JETP 15, 31.

E. W. Valyocsik (1959). Range and Range Straggling of Heavy Recoil Atoms. UCRL-8855.

W. Whaling (1958). The Energy Loss of Charged Particles in Matter. Hdb. d. Phys. vol. 34, 193.

A. van Wijngaarden & H. E. Duckworth (1962). Energy Loss in Condensed Matter of H^1 and He^4 in the Energy Range 4 to 30 keV. Can. J. Phys. 40, 1749.

L. Winsberg & J. M. Alexander (1961). Ranges and Range Straggling of Tb^{149}, At and Po. Phys. Rev. 121, 518.

Indleveret til Selskabet den 24. april 1963.
Færdig fra trykkeriet den 17. oktober 1963.

Appendix 1 Recoil ranges and catcher efficiencies

This appendix contains a discussion of range concepts for the recoil ion energies where nuclear stopping dominates the energy loss process. The theory of Lindhard, Sharff and Schiøtt (LSS-) is discussed and applied to the recoil ion systems of this work

Continued →

A. Characteristics of the range; terms used

Path length

The range of a (moving) recoiling ion in some stopping material is the total distance the ion travels as it slows down from various energy loss processes. The range is the sum of the collision lengths along the path of the ion; it is not the vector distance between the starting and ending points (figure i)

figure i

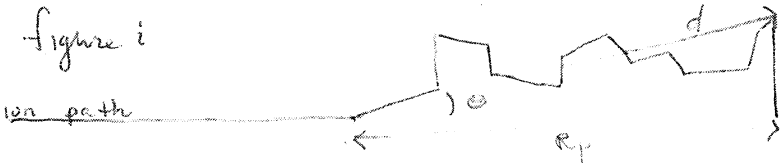

Projected Range

An experimentally measured range is not the path length range for most experiments. For a very small diameter ion beam one could get a measure of the vector distance d in figure i if one measured the angular distribution of the recoils. But for common experimental conditions the component of the range projected onto the original ion beam direction is closer to what is measured ($\bar{R}_p$ in figure 2). To compare these measured ranges with LSS predictions, a path length correction is applied to get from $\bar{R}_p$ to $\bar{R}$.

Range distribution

The range is an average quantity of sorts, depending on the final distribution of the recoils. This distribution arises from Straggling: each recoil ion experiences a different collisional-energy loss pattern along its path and consequently not all ions of starting energy E travel the same distance. If the distribution is gaussian, half the recoils go farther than $\bar{R}$ and half go less. The projected range, $\bar{R}_p$ is analogously an 'average'.

Straggling Behavior

The extent of straggling in a stopping medium is dependent on the initial ion recoil energy (figure ii)

figure ii
(LSS figure 6)

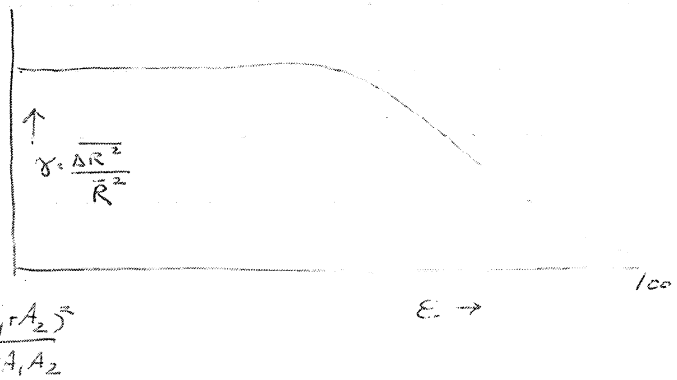

At low initial energies, where nuclear stopping dominates the energy loss process, the straggling converges to a <u>constant fraction</u> of the total range. When electronic stopping becomes the major factor in the energy loss process, the straggling drops off dramatically. Note that figure ii is not a differential curve.

Straggling is usually characterized by a straggling parameter ρ where $\rho^2 = \overline{R^2} - \bar{R}^2 = \overline{\Delta R^2}$, the variance of the distribution.

For a gaussian, $\pm 2.6\sigma$ about the mean value includes the total distribution.

B. Limitations from range behavior applied to catcher foil experiments

I would like now to make a general application of range behavior for catcher foil type experiments. In one of this type of experiment an ion beam passes through and is stopped in a row of stacked catcher foils.

If the ion beam is monoenergetic, the LSS theory will generally

give to good accuracy (~ 20 %) the expected projected range and straggling for a single component stopping medium.

The total catcher foil thickness is selected to catch all recoils. If the distribution is expected to be gaussian the total catcher thickness should be at least $\bar{R}_p + 2.6\,\sigma_{gauss}$ as illustrated in figure iii

figure iii

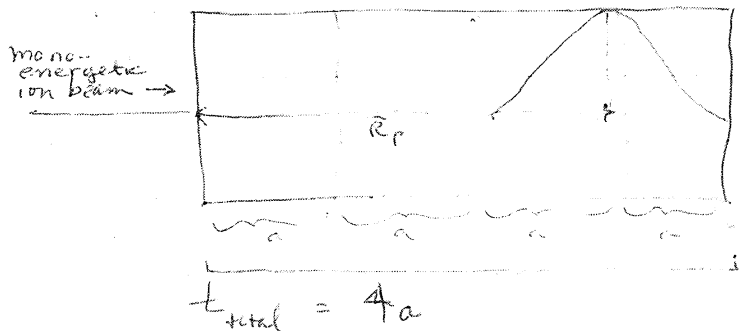

4 catchers of thickness a

If the beam is not monoenergetic, as is the case for ions recoiling out of a target, the situation seen in figure iv results. ~~(for ions dominated by nuclear stopping process)~~

figure iv

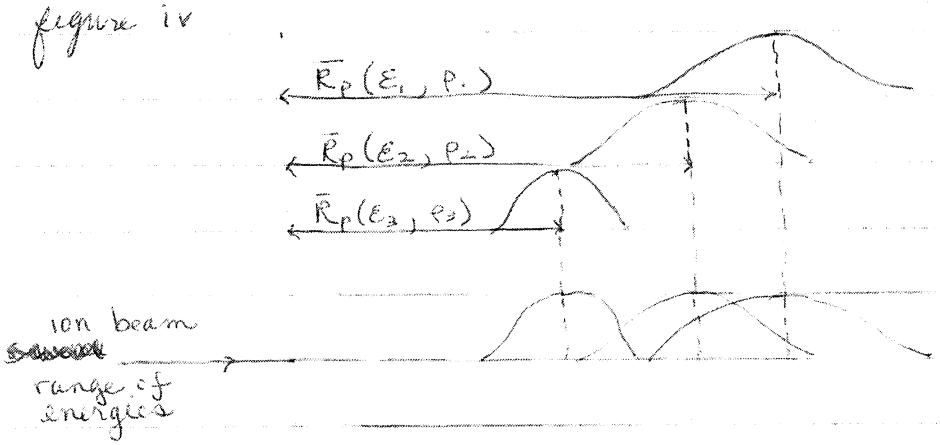

iv A representative energies

ε_i = energy
ρ_i = straggling parameter

iv B Straggling packet overlapping

Using a very thin target (thin compared to the range of the ion in the target material) minimizes the ion energy distribution and as a result concentrates the range of straggling packets into one region of the catcher. Then the measured range and straggling will be closest to the value expected of the monoenergetic beam.

C. Discussion of basic applicability of LSS theory to this work

~~LSS predictions for this work; other experiment applications of range and catcher concepts~~

1. Basic calculation of range variables $\bar{R}, \bar{R}_p, \rho$

For a single component stopping medium the LSS theory expresses the range and energy of an ion projectile as dimensionless quantities.

$$\rho = R N M_2 (4\pi a^2) \frac{M_1}{(M_1+M_2)^2} \qquad \varepsilon = E \frac{a M_2}{Z_1 Z_2 e^2 (M_1+M_2)}$$

R = ion range along its total path length
N = scattering centers per unit volume in the stopping medium
a = radius parameter (screening parameter)
E = projectile ion energy
Z_1, M_1 = projectile nuclear charge, mass
Z_2, M_2 = medium nuclear charge, mass

A Thomas-Fermi type interaction is assumed between the ion and medium atoms for nuclear collisions ($V < V_0 \cong 2.2 \times 10^8$ cm/sec), deflections in the screened coulomb field of the medium.

$$V(r) = \frac{Z_1 Z_2 e^2 a_s^{s-1}}{s r^s} \qquad a_s \approx .8853 a_0 Z^{-1/3}$$

s = ~~an constant~~ adjustable constant

At higher energies electronic interactions dominate the energy loss process. The electronic stopping is assumed to be proportional to $\varepsilon^{1/2}$ (velocity proportional stopping region $v < v_1 = v_0 Z_1^{2/3}$). LSS measures this effect on the range in terms of a parameter k,

$$\frac{d\varepsilon}{d\rho} = \left(\frac{d\varepsilon}{d\rho}\right)_{nuclear} + k\,\varepsilon^{1/2}$$

$$k = \xi_e \frac{.0793\, Z_1^{1/2} Z_2^{1/2} (A_1+A_2)^{3/2}}{(Z_1^{2/3}+Z_2^{2/3})^{3/4} A_1^{3/2} A_2^{1/2}} \qquad \xi_e \sim Z_1^{1/6}$$

A_1, A_2 mass number

They derive a series of universal range-energy curves for the k values.

For U^{227} in U^{235} as a representative system $k = .182$. When E is expressed in MeV, "a" in fermis, the masses in a.mu. and $e^2 = 1.44$ MeV-fermis:

$\mathcal{E} = .135$ U^{227} product recoil from 100 MeV protons + ^{235}U

$\mathcal{E} = .76$ U^{227} product recoil from 140 MeV alpha beam + ^{235}U

The values of ρ can be read directly from the LSS graphs

$\rho = .4$ proton interaction recoils

$\rho = 1.7$ alpha interaction recoils

The average range expressed in $\mu g/cm^2$ is given as

$$\bar{R}\,(\mu g/cm^2) = \rho \frac{(M_1 + M_2)^2}{4\pi a^2\,(cm^2)\,(6.02\times10^{17})\,(M_1)}$$

Masses in micrograms

$\bar{R} = 86\ \mu g/cm^2$ proton interaction recoils in U^{235} (pure)

$\bar{R} = 354\ \mu g/cm^2$ alpha interaction recoils in U^{235} (pure)

~~Experimentally, the expected projected range, $\bar{R}_p$, is expected~~

The LSS theory systematically relates the projected range, $\bar{R}_p$, to a parameter

$\mu = \frac{M_s}{M_p}$ M_s = stopping medium mass

M_p = projectile mass

since $\bar{R}_p$ is the outgrowth of scattering effects. (see figure i)

To a rough approximation $\bar{R}/\bar{R}_p = 1 + \mu/3$; figure 8 from LSS is reproduced to show that, at the experimental $\mathcal{E}$ values, $\bar{R}_p$ is not far from being proportional to Energy. (figure v.) Path length correction can be read directly from

this graph. For U^{227} in pure U^{235} $\bar{\rho} = 1.35\,\bar{\rho}_p$ as determined from this graph for 2.4 MeV recoils. By direct proportion then $\bar{R}_p$ is 262 $\mu g/cm^2$.

To get an estimate of the relative straggling expected in pure uranium we can use the LSS approximation that $\frac{\overline{\Delta R^2}}{\bar{R}^2} \approx \frac{\gamma}{6}$ (a) where

$$\gamma = \frac{4M_1M_2}{(M_1+M_2)^2}.$$

In the target-projectile system of this work, at recoil energies just above this work, a considerable reduction in the relative straggling occurs (see LSS figure 6 my figure 11) so that (a) could not be used at higher recoil energies.

Using (a) $\frac{\overline{\Delta R^2}}{\bar{R}^2} = .167$ and $\frac{\overline{\Delta R}}{\bar{R}} = .41$

Using the LSS graphical method of figure 6 gives $\frac{\overline{\Delta R}}{\bar{R}} = .324$

The LSS ~~theory~~ paper does not calculate general curves for the relative straggling in the projected range, $\bar{R}_p$. However, it does give the results for $\mu = 1$, and for this case $\overline{\Delta R^2_p}$ is of the order of $\overline{\Delta R^2}$. For U^{227} in U^{235} under this last assumption $\overline{\Delta R_p} \approx 85\ \mu g/cm^2$. Since $\overline{\Delta R^2_p} = \overline{R^2_p} - \bar{R}^2_p$ is as defined a standard deviation, straggling of recoiling products would occur to varying extents in any target much thicker than 41 $\mu g/cm^2$ of pure U^{235}.

Table 1 gives a summary of relevant LSS parameters for substances of this work for a representative recoil, U^{227}

Table 1

	$\mathcal{E}$ .425 MeV / 2.4 MeV	k	γ	graph $\Delta R^2/\bar{R}^2 / \gamma$	Straggling ρ	$\bar{R}/\bar{R}_p$	$\bar{R}$ $\mu g/cm^2$
U	.135 / .757	.182	1	.117 / .105	.342 / .324	1.35	86 / 354
F	.272 / 1.526	.105	.298	.125 / .110	.193 / .181	1.04	30 / 115
C	.258 / 1.457	.109	.191	.125 / .113	.154 / .147	1.02	25 / 98

The LSS theory was derived for a single component stopping medium. (continued on pg 8)

$\bar{R}_p$

19/6

$\frac{354}{1.35}$ 262.22

UF_4 → 195 $\mu g/cm^2$

$\frac{115}{1.04}$ 110.58

$\bar{R}$ w path length correction → 232 / path correction = ?

Extension of the LSS theory for a multi-component stopping medium is not directly available.

Range predictions for the two-component stopping media of this work are arrived at only under certain ~~([illegible])~~ assumptions. Experimental range work in heavy multi-component stopping media is rare, so that the ~~relative~~ absolute error introduced by the assumptions made is difficult to estimate.

~~[Without a doubt the largest sim dominating uncertainty in the derived σ come from uncertainty in the catcher efficiency]~~

The first assumption made is that the two-component medium range can be expressed as a weighted average of the range in the elements themselves:

$$R_c = \frac{M_c}{X\frac{M_a}{R_a} + Y\frac{M_B}{R_B}}$$

$C = A_X B_Y$

R_i = LSS single component range

M_i = atomic weight

However, when the LSS ε value ~~[illegible]~~ is much different in the two components (ie when the stopping cross sections in both elements ~~are~~ not proportional to the same power of the recoil ion energy + LSS ref) this weighted range value will be in error. From table ~~[illegible]~~ 1 it can be seen that the ε values for the UF_4 target medium ~~are~~ differ by a factor of about two. The work of Domeij and coworkers (DO-64) establishes an approximate ~~upper bound~~ estimate ~~of~~ the error involved in this latter assumption. One of the systems they studied, Xe^{125} in WO_3 is similar to this work when ~~the mass and energy~~ the LSS parameters ε_i, P_i and k_i are calculated. I used The LSS method ~~was used~~ to first calculate pure element ranges of Xe^{125} in W^{184} and O^{16}. Then the weighted range was calculated. ~~Thus~~ This range is larger than the uncorrected measured range by about 35%. The measured

range is more indicative of $\bar{R}_p$ however, and if $\bar{R}_p$ is calculated for Xe^{125} in W and O separately, and then if a new weighted range is calculated, the projected range in WO_3 is in excellent agreement with the measured range (better than 5%).

Alternatively, Application of the path-length correction to the measured range data in WO_3 is not straightforward because of uncertainty in assigning a k and ε value for the two-component substance. In LSS figure 8, however, the path-length correction is seen not to vary much over the ε_i and k_i values of W and O separately. If an "average" correction is read from this graph and the measured range is corrected, the calculated weighted range is less than this corrected range by about 30%. I believe this should establish a reasonable estimate for the error introduced by using the weighted range calculation. The parameter μ for the $WO_3 - {}^{125}Xe$ system is 1.86. For the $UF_4 - U^{229}$ system, the parameter μ is 1.38. According to LSS figure 9, the variation of path length correction with μ in the ε range of analogous to these systems is of the order of 23 - 33% between $\mu = 1$ and $\mu = 2$.

The path length correction for the $UF_4 - U^{229}$ system will be less than the $WO_3 - Xe^{125}$ system. The weighted range then should be closer to the experimental range, whether a projected range is calculated or not.

The second assumption used in this work is that the range straggling can also be estimated by the weighting method used above. The Domeij work did not attempt to compare the straggling of their recoil ions in WO_3 because of the large μ parameters

and the consequent uncertainty in the path-length corrections. Domey quotes an equation for straggling which is valid if weighted range is valid:

$$\frac{\overline{\Delta R_c^2}}{\overline{R_c^2}} = \frac{x\left(\frac{M_A}{R_A}\right)\left(\frac{R_B}{M_B}\right)\frac{\overline{\Delta R_A^2}}{\overline{R_A^2}} + y\,\frac{\overline{\Delta R_B^2}}{\overline{R_B^2}}}{x\left(\frac{M_A}{R_A}\right)\left(\frac{R_B}{M_B}\right) + y} \qquad R \text{ in } \mu g/cm^2$$

Another way of expressing this is

$$\rho_c \left(\frac{\overline{\Delta R_c^2}}{\overline{R_c^2}}\right)^{1/2} = \frac{M_c}{\frac{y M_A}{\rho_A} + \frac{x M_B}{\rho_B}}$$

where ρ, the straggling parameter $= \left(\frac{\overline{\Delta R_c^2}}{\overline{R_c^2}}\right)^{1/2}$

The third assumption made here is that the straggling is gaussian, and that the straggling in the projected range is the same as the true range.

Without these assumptions catcher foil and degrader foil efficiencies could not be calculated, but would need to be measured.

~~(ii) Sample calculation of target, degrader and catcher efficiency~~

Try 2 MeV for plot

for uranium $\mathcal{E} = 2 \cdot (.31765) = .64$

$\rho_{graph} \sim \sim 1.38$

$R = 216 \times 1.38 = 298$

for fluorine $\mathcal{E} = 2 \cdot (.64) = 1.28$

$\rho_{graph} =$

$\mathcal{E} = 1.526 \rightarrow \rho = 2.863_{calc.}$

$\mathcal{E} = 1.28 \rightarrow \rho = 2.401$ proportion assumed Reasonable graphing

$R = 40167 \times 2.401 = 96$

$$\bar{R} = \frac{314}{\frac{79}{96} + \frac{235}{298}} = 199$$

170 μg/cm² UF_4 →

127 μg/cm² U

43 μg/cm² F

What energy just penetrates both –

** Note **

7/4/77 ⇒ these should be taken as F values ? ∴ correction to path length MUST be applied to 85

for Uranium $k = .182$

127 μg/cm² = ρ · 215.85

.59 = ρ

E graph ~ .23

$\mathcal{E} = E \cdot (.31765)$

$E \cong .72$ MeV

for fluorine $k = .105$

1.074 = ρ

43 μg/cm² = ρ · 40.167

E graph ~ .43

$\mathcal{E} = E \cdot (.64)$

$E \cong .67$ MeV

⇓

~ .70 MeV → $\dfrac{314}{\frac{4(19.75)}{43} + \frac{235}{127}} = 85$

Try 1.4 MeV to see if weighted range is 170

for uranium $\mathcal{E} = 1.4 \times .31765 = .445$

ρ graph 1.0

R = 2.6

for fluorine $\mathcal{E} = 1.4 \times .64 = .896$

ρ graph 2.1 (2.08)

R = 84

$\bar{R} = \dfrac{314}{\frac{79}{84} + \frac{235}{216}} = 155$

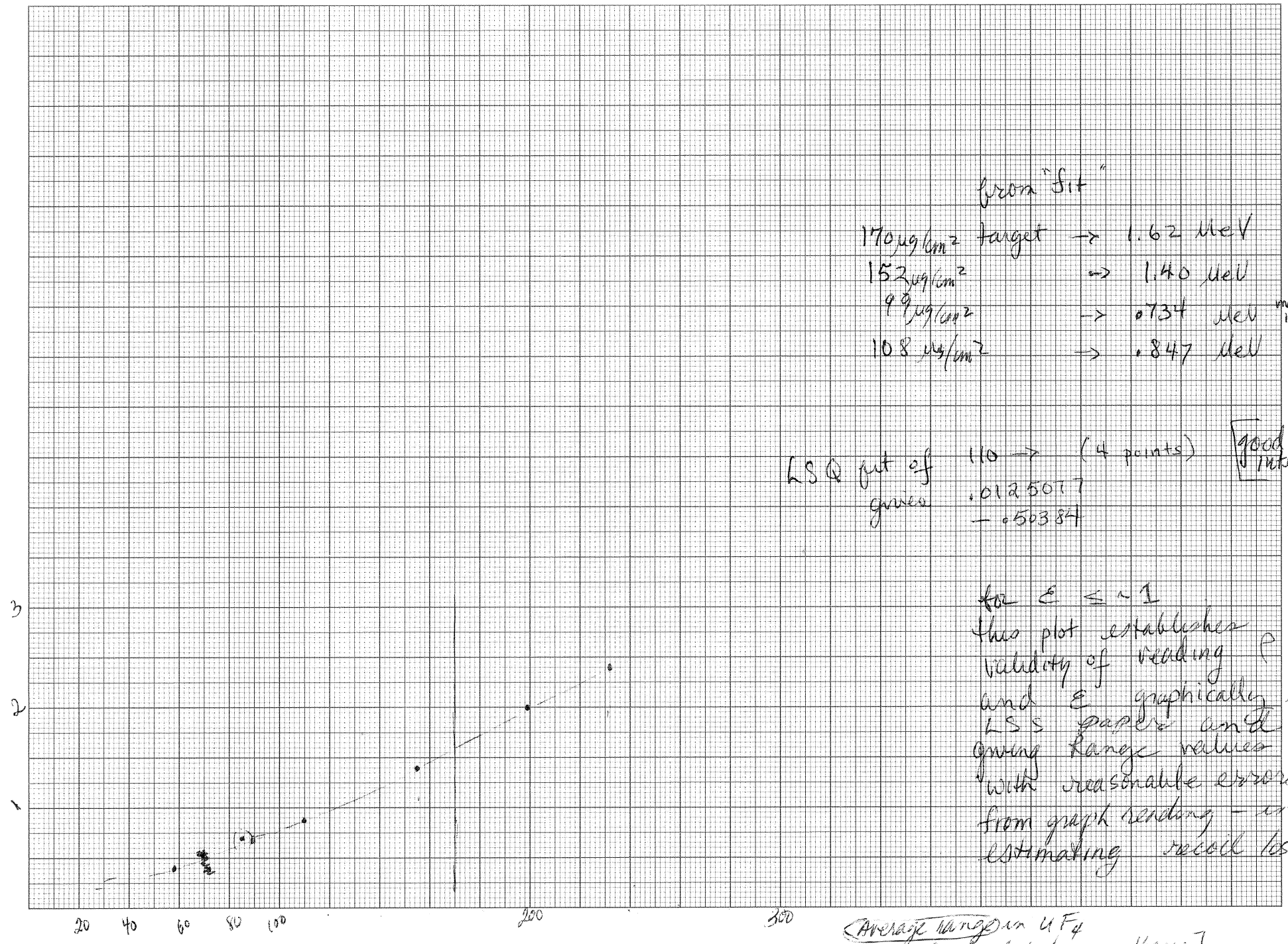

from "fit"

170 μg/cm² target → 1.62 MeV
152 μg/cm² → 1.40 MeV
99 μg/cm² → .734 MeV may be low
108 μg/cm² → .847 MeV

LSQ fit of 110 → (4 points) [good fit internally]
gives .0125077
− .50384

for ε ≤ ~1
this plot establishes validity of reading ρ and ε graphically on LSS paper and giving range values with reasonable errors from graph reading — or estimating recoil losses

(Average range in UF_4
[calculated as in theory])

$$a_1 = \frac{\begin{vmatrix} y_1 & X_{12} & X_{13} \\ y_2 & X_{22} & X_{23} \\ y_3 & X_{32} & X_{33} \end{vmatrix}}{\begin{vmatrix} X_{11} & X_{12} & X_{13} \\ X_{21} & X_{22} & X_{23} \\ X_{31} & X_{32} & X_{33} \end{vmatrix}}$$

Cramers rule

$$y_k = \sum_{j=1}^{n} (a_j X_{kj}) \qquad k = 1, n$$

$$a_j = \frac{|X'(j)|}{|X|}$$

substitute y matrix for jth column in determinant $|X|$ to get $|X'(j)|$

$$|A| = \sum_{k=1}^{n} [A_{jk} \operatorname{cof}(A_{jk})] = \sum_{k=1}^{n} (-1)^{j+k} A_{jk} A^{jk}]$$

$$\operatorname{Cof}(A_{jk}) = (-1)^{j+k} A^{jk}$$

row, column

$$a_1 = \begin{vmatrix} y_1 & x_{12} & x_{13} & x_{14} \\ y_2 & x_{22} & x_{23} & x_{24} \\ y_3 & x_{32} & x_{33} & x_{34} \\ y_4 & x_{42} & x_{43} & x_{44} \end{vmatrix}$$

$$(-1)^{1+1} y_1 \begin{vmatrix} x_{22} & x_{23} & x_{24} \\ x_{32} & x_{33} & x_{34} \\ x_{42} & x_{43} & x_{44} \end{vmatrix}$$

$$(-1)^{1+2} x_{12} \begin{vmatrix} y_2 & x_{23} & x_{24} \\ y_3 & x_{33} & x_{34} \\ y_4 & x_{43} & x_{44} \end{vmatrix}$$

$$(-1)^{1+3} x_{13} \begin{vmatrix} y_2 & x_{22} & x_{24} \\ y_3 & x_{32} & x_{34} \\ y_4 & x_{42} & x_{44} \end{vmatrix}$$

$$(-1)^{1+4} x_{14} \begin{vmatrix} y_2 & x_{22} & x_{23} \\ y_3 & x_{32} & x_{33} \\ y_4 & x_{42} & x_{43} \end{vmatrix}$$

elem	cofactor	coeff.
y_1	$(-1)^{1+1}\left[X_{22}X_{33} - X_{32}X_{23}\right]$	
X_{12}	$(-1)^{1+2}\left[y_2 X_{33} - y_3 X_{23}\right]$	a_1
X_{13}	$(-1)^{1+3}\left[y_2 X_{32} - y_3 X_{22}\right]$	

$$y_1\left[X_{22}X_{33} - X_{32}X_{23}\right] - X_{12}\left[y_2 X_{33} - y_3 X_{23}\right] + X_{13}\left[y_2 X_{32} - y_3 X_{22}\right]$$

If use 4 X 4

ΔJ_{15-16}

$$\frac{\begin{vmatrix} 8386 & .118 & 0 & 0 \\ 5257 & .70 & .118 & 0 \\ 3737 & .186 & .70 & .082 \\ 3751 & 0 & .186 & .79 \end{vmatrix}}{\begin{vmatrix} .96 & .118 & 0 & 0 \\ .187 & .70 & .118 & 0 \\ 0 & .186 & .70 & .082 \\ 0 & 0 & .186 & .79 \end{vmatrix}}$$

$$\frac{2714.49}{0.3328508} = 8155.27$$

$$8386 \begin{vmatrix} .70 & .118 & 0 \\ .186 & .70 & .082 \\ 0 & .186 & .79 \end{vmatrix}$$

$$-.118 \begin{vmatrix} 5257 & .118 & 0 \\ 3737 & .70 & .082 \\ 3751 & .186 & .79 \end{vmatrix}$$

4th should be 3628

a) term 1

AJ 15-16

$$.70 \begin{vmatrix} .70 & .082 \\ .186 & .79 \end{vmatrix} - .118 \begin{vmatrix} .186 & .082 \\ 0 & .79 \end{vmatrix}$$

$$\underbrace{.537748}_{.3764236} \qquad \underbrace{}_{-\ .01733892} \qquad = .35908$$

term 2

$$5257 \begin{vmatrix} .70 & .082 \\ .186 & .79 \end{vmatrix} - .118 \begin{vmatrix} 3737 & .082 \\ 3751 & .79 \end{vmatrix}$$

$$\underbrace{.537748}_{2826.94} \qquad \underbrace{}_{312.068} \qquad = 2514.87$$

$$8386\,(.35908) - .118\,(2514.87) =$$

$$3011.24 \qquad 296.75 \qquad = 2714.49$$

denom

$$.96 \begin{vmatrix} .70 & .118 & 0 \\ .186 & .70 & .082 \\ 0 & .186 & .79 \end{vmatrix}$$

$$-.118 \begin{vmatrix} .187 & .118 & 0 \\ 0 & .70 & .082 \\ 0 & .186 & .79 \end{vmatrix}$$

---

term 1

$$.70 \begin{vmatrix} .70 & .082 \\ .186 & .79 \end{vmatrix} - .118 \begin{vmatrix} .186 & .082 \\ 0 & .79 \end{vmatrix} =$$

as above
.35908

term 2

$$.187 \begin{vmatrix} .70 & .082 \\ .186 & .79 \end{vmatrix} - .118 \begin{vmatrix} 0 & .082 \\ 0 & .79 \end{vmatrix} =$$

$$\underbrace{.187(.537748)}_{.100558876} - 0 = .100558876$$

denom = $.96(.35908) - .118(.100558876)$

= $.3328508$

$$
\begin{aligned}
N_1 &= .96\,X_1 + .118\,X_2 + 0\,X_3 + 0\,X_4 \\
N_2 &= .187\,X_1 + .7\,X_2 + .118\,X_3 + 0\,X_4 \\
N_3 &= 0\,X_1 + .186\,X_2 + .7\,X_3 + .082\,X_4 \\
N_4 &= 0\,X_1 + 0\,X_2 + .186\,X_3 + .79\,X_4
\end{aligned}
$$

solving for X_1

$$
X_1 = \frac{\begin{vmatrix} N_1 & .118X_2 & 0 & 0 \\ N_2 & .7X_2 & .118X_3 & 0 \\ N_3 & .186X_2 & .7X_3 & .082X_4 \\ N_4 & 0 & .186X_3 & .79X_4 \end{vmatrix}}{\begin{vmatrix} .96X_1 & .118X_2 & 0 & 0 \\ .187X_1 & .7X_2 & .118X_3 & 0 \\ 0 & .186X_2 & .70X_3 & .082X_4 \\ 0 & 0 & .186X_3 & .79X_4 \end{vmatrix}}
$$

$$
X_1 = \frac{N_1 \begin{vmatrix} .7X_2 & .118X_3 & 0 \\ .186X_2 & .7X_3 & .082X_4 \\ 0 & .186X_3 & .79X_4 \end{vmatrix} - .118X_2 \begin{vmatrix} N_2 & .118X_3 & 0 \\ N_3 & .7X_3 & .082X_4 \\ N_4 & .186X_3 & .79X_4 \end{vmatrix}}{\text{DENOM}}
$$

numerator $= N_1 \left\{ .7X_2 \begin{vmatrix} .7X_3 & .082X_4 \\ .186X_3 & .79X_4 \end{vmatrix} - .118X_3 \begin{vmatrix} .186X_2 & .082X_4 \\ 0 & .79X_4 \end{vmatrix} \right\}$

$$
-.118X_2 \left\{ N_2 \begin{vmatrix} .7X_3 & .082X_4 \\ .186X_3 & .79X_4 \end{vmatrix} - .118X_3 \begin{vmatrix} N_3 & .082X_4 \\ N_4 & .79X_4 \end{vmatrix} \right\}
$$

expanding:

$$
N_1 \left\{ .7X_2 \left(\overset{.53775\,X_3X_4}{.553\,X_3X_4 - .01525\,X_3X_4} \right) - .118X_3 \left(.14694\,X_2X_4 - 0 \right) \right\}
$$

$$
-.118X_2 \left\{ N_2 \left(.53775\,X_3X_4 \right) - .118\,X_3 \left(.79\,N_3X_4 - .082\,N_4X_4 \right) \right\}
$$

X_1 continued

$$N_1 \left\{ .376425\, X_2 X_3 X_4 - .017339\, X_2 X_3 X_4 \right\}$$

$$- .118\, X_2 \left\{ .53775\, N_2 X_3 X_4 - .09322\, N_3 X_3 X_4 + .009676\, N_4 X_3 X_4 \right\}$$

$$N_1 \left\{ .359086\, X_2 X_3 X_4 \right\}$$

$$- \left\{ .06345\, N_2 X_2 X_3 X_4 - .0110\, N_3 X_2 X_3 X_4 + .001142\, N_4 X_2 X_3 X_4 \right\}$$

numerator =

$$X_2 X_3 X_4 \left\{ .359086\, N1 - .06345\, N2 + .0110\, N_3 - .001142\, N_4 \right\}$$

3011 333 41 4.3

271456

figure X_5 only using 5×5

$$X_5 = \frac{\begin{vmatrix} .96 & .118 & 0 & 0 & 8386 \\ .187 & .70 & .118 & 0 & 5257 \\ 0 & .186 & .70 & .082 & 3737 \\ 0 & 0 & .186 & .79 & 3751 \\ 0 & 0 & 0 & .13 & 2583 \end{vmatrix}}{\text{denom determ}}$$

numerator =

$$.3309\,N5 - .05835\,N4 + .01571\,N3 - .00432\,N2 + .000084\,N1$$

$$.33285 - .05639$$

denom (.33285)

$$N5 - .1694\,N4$$

evaluation of neumerator

$$(-1)^2 \cdot .96 \begin{vmatrix} .76 & .118 & 0 & N_2 \\ .186 & .70 & .082 & N_3 \\ 0 & .186 & .79 & N_4 \\ 0 & 0 & .13 & N_5 \end{vmatrix}$$ term 1

$$(-1)^3 \cdot .118 \begin{vmatrix} .187 & .118 & 0 & N_2 \\ 0 & .70 & .082 & N_3 \\ 0 & .186 & .79 & N_4 \\ 0 & 0 & .13 & N_5 \end{vmatrix}$$ term 2

$$(-1)^4 \cdot 0 \begin{vmatrix} & & & \\ & & & \\ & & & \\ & & & \end{vmatrix}$$

$$(-1)^5 \cdot 0 \begin{vmatrix} & & & \\ & & & \\ & & & \\ & & & \end{vmatrix}$$

$$(-1)^6 \cdot N_1 \begin{vmatrix} .187 & .70 & .118 & 0 \\ 0 & .186 & .70 & .082 \\ 0 & 0 & .186 & .79 \\ 0 & 0 & 0 & .13 \end{vmatrix}$$ term 3

4×4 determin. eval.

term 1

$$(-1)^2 \; .70 \begin{vmatrix} .70 & .082 & N_3 \\ .186 & .79 & N_4 \\ 0 & .13 & N_5 \end{vmatrix}$$

$$(-1)^3 \; .118 \begin{vmatrix} .186 & .082 & N_3 \\ 0 & .79 & N_4 \\ 0 & .13 & N_5 \end{vmatrix}$$

$$(-1)^4 \; 0 \begin{vmatrix} & & \\ & & \\ & & \end{vmatrix}$$

$$(-1)^5 \; N_2 \begin{vmatrix} .186 & .70 & .082 \\ 0 & .186 & .79 \\ 0 & 0 & .13 \end{vmatrix}$$

getting actual numbers

$$(-1)^2 .70 \left\{ (-1)^2 .70 \left(.79 N5 - .13 N4 \right) + (-1)^3 .082 \left(.186 N5 - 0 N4 \right) + (-1)^4 N_3 \left(.186 \times .13 - 0 \times .79 \right) \right\}$$

$$(-1)^3 .118 \left\{ (-1)^2 .186 \left(.79 N5 - .13 N4 \right) + \underbrace{\cancel{(-1)^3 .082 \left(0 N5 - 0 N4 \right)}}_{0} + \underbrace{\cancel{(-1)^4 N3 \left(-0 \times .79 + 0 \times .13 \right)}}_{0} \right\}$$

$$(-1)^5 N_2 \left\{ (-1)^2 .186 \left(.186 \times .13 - 0 \times .79 \right) + \underbrace{\cancel{(-1)^3 .7 \left(-0 \times .79 + 0 \times .13 \right)}}_{0} + \underbrace{\cancel{(-1)^4 .082 \left(0 - 0 \times .186 \right)}}_{0} \right\}$$

term 1 continued

$$.7\left\{(.553N5 - .091\,N4) - 1(.015252N5 - 0) + .02418\,N3\right\}$$

$$-.118\left\{(.14694\,N5 - .02418\,N4)\right\}$$

$$-N_2\left\{.00449748\right\}$$

final collecting of terms:

$$.37642\,N5 - .0637\,N4 + .016926\,N3$$
$$-.0173389\,N5 + .002853\,N4$$
$$-.00449748\,N2$$

AND

$$\boxed{.35908\,N5 - .06085\,N4 + .016926\,N3 - .004498\,N2}$$

4 x 4 determ eval.

3 2a 2b

term 2

$$(-1)^2 .187 \begin{vmatrix} .70 & .082 & N_3 \\ .186 & .79 & N_4 \\ 0 & .13 & N_5 \end{vmatrix}$$

this determinant is the same as term 1 part 1

$$(-1)^3 .118 \begin{vmatrix} 0 & .082 & N_3 \\ 0 & .79 & N_4 \\ 0 & .13 & N_5 \end{vmatrix} \rightarrow 0$$

$$(-1)^4 \; 0 \; \begin{vmatrix} & & \\ & & \\ & & \end{vmatrix}$$

$$(-1)^5 N_2 \begin{vmatrix} 0 & .70 & .082 \\ 0 & .186 & .79 \\ 0 & 0 & .13 \end{vmatrix} \rightarrow 0$$

$$(-1)^2 .187 \left\{ (-1)^2 .7(.79N5 - .13N4) + (-1)^3 .082(.186N5 - 0N4) + (-1)^4 N_3(.186 \times .13 - 0 \times .79) \right\}$$

$$(-1)^2(.187) \left\{ .553N5 - .091N4 - .015252N5 + .02418N3 \right\}$$

AND

$$\boxed{\begin{array}{lll} .10107N5 & - \; .000595N4 & + \; .0045217N3 \\ .10056 & .017017 & \end{array}}$$

4X4 determ eval

$\boxed{\begin{array}{r} 3 \\ -3a \\ \hline 3b \end{array}}$

term 3

$$(-1)^2 .187 \begin{vmatrix} .186 & .7 & .082 \\ 0 & .186 & .79 \\ 0 & 0 & .13 \end{vmatrix}$$

this determinant is the same as term 1 part 3

$$\cancel{(-1)^3 .7 \begin{vmatrix} 0 & .7 & .082 \\ 0 & .186 & .79 \\ 0 & 0 & .13 \end{vmatrix}} \rightarrow 0$$

$$\cancel{(-1)^4 .118 \begin{vmatrix} 0 & .186 & .082 \\ 0 & 0 & .79 \\ 0 & 0 & .13 \end{vmatrix}} \rightarrow 0$$

$$(-1)^2 .187 \left\{ (-1)^2 .186 \left(.186 \times .13 - 0 \times .79 \right) + \underbrace{\cancel{(-1)^3 \cdot .7 \left(-0 \times .79 + 0 \times .13 \right)}}_{0} + \underbrace{\cancel{(-1)^4 .082 \left(0 - 0 \times .186 \right)}}_{0} \right\}$$

$$(-1)^2 .187 \left(.00449748 \right)$$

AND

$$\boxed{.0000841}$$

final solution collection of numerator terms:

from term 1

$$(-1)^2 .96 \left\{ .35908\,N5 - .06085\,N4 + .016926\,N3 - .0044975\,N2 \right\}$$

$$.344717 \qquad .058416 \qquad .016249 \qquad .0043176$$

from term 2

$$(-1)^3 .118 \left\{ \underset{\substack{.013806 \\ .0118661}}{\overset{.10056}{.10107\,N5}} - \underset{\substack{.00007021 \\ .0020261}}{\overset{.017017}{.00595\,N4}} + .0045217\,N3 \right\}$$

$$.00053356$$

from Term 3

$$(-1)^6 N_1 \left\{ .0000841 \right\}$$

Summing:

$$.344717\,N5 - .058416\,N4 + .016249\,N3 - .0043176\,N2$$

$$- \underset{.011866}{.013806}\,N5 + \underset{.0020261}{.00007021}\,N4 - .00053356\,N3 + .0000841\,N1$$

$\boxed{\text{final}}$

$$.3309\,N5 - .05835\,N4 + .01571\,N3 - .00432\,N2 + .000084\,N1$$

$$.33285 \qquad -.0563899$$

$$x_1 = \frac{\begin{vmatrix} N_1 & .118 & 0 & 0 \\ N_2 & .7 & .118 & 0 \\ N_3 & .186 & .7 & .082 \\ N_4 & 0 & .186 & .79 \end{vmatrix}}{\text{denominator}}$$

$$x_1 \cdot \text{denominator} = N_1 \begin{vmatrix} .7 & .118 & 0 \\ .186 & .7 & .082 \\ 0 & .186 & .79 \end{vmatrix} - .118 \begin{vmatrix} N_2 & .118 & 0 \\ N_3 & .7 & .082 \\ N_4 & .186 & .79 \end{vmatrix}$$

$$= N_1 \left\{ 0.7 \begin{vmatrix} 0.7 & .082 \\ 0.186 & 0.79 \end{vmatrix} - 0.118 \begin{vmatrix} .186 & .082 \\ 0 & .79 \end{vmatrix} \right\}$$

$$- 0.118 \left\{ N_2 \begin{vmatrix} .7 & .082 \\ .186 & .79 \end{vmatrix} - 0.118 \begin{vmatrix} N_3 & .082 \\ N_4 & .79 \end{vmatrix} \right\}$$

$$= N_1 \left\{ 0.7 (.553 - .0153) - 0.118 (0.147) \right\}$$

$$- 0.118 \left\{ N_2 (.553 - .0153) - 0.118 (0.79 N_3 - 0.082 N_4) \right\}$$

$$= N_1 \left\{ (\cancel{0.331}\ \cancel{0.280}\ 0.376 - 0.017) \right\} - 0.118 \left\{ \cancel{0.4}\ 0.534 N_2 - 0.093 N_3 + 0.010 N_4 \right\}$$

$$x_1 \cdot \text{denominator} = 0.359 N_1 - 0.063 N_2 + 0.011 N_3 - 0.001 N_4$$

$$x_1 = 1.078 N_1 - 0.189 N_2 + 0.033 N_3 - 0.003 N_4$$

$$x_2 = \frac{\begin{vmatrix} .96 & N_1 & 0 & 0 \\ .187 & N_2 & .118 & 0 \\ 0 & N_3 & .7 & .082 \\ 0 & N_4 & .186 & .79 \end{vmatrix}}{\text{denominator}}$$

$$x_2 \cdot \text{denominator} = 0.96 \begin{vmatrix} N_2 & .118 & 0 \\ N_3 & .7 & .082 \\ N_4 & .186 & .79 \end{vmatrix} - N_1 \begin{vmatrix} .187 & .118 & 0 \\ 0 & .7 & .082 \\ 0 & .186 & .79 \end{vmatrix}$$

$$= 0.96 \left\{ N_2 \begin{vmatrix} .7 & .082 \\ .186 & .79 \end{vmatrix} - 0.118 \begin{vmatrix} N_3 & .082 \\ N_4 & 0.79 \end{vmatrix} \right\}$$

$$- N_1 \left\{ 0.187 \begin{vmatrix} 0.7 & .082 \\ 0.186 & .79 \end{vmatrix} - 0.118 \begin{vmatrix} 0 & .082 \\ 0 & 0.79 \end{vmatrix} \right\}$$

$$= 0.96 \left\{ N_2 (0.553 - 0.0153) - 0.118 (0.79 N_3 - 0.082 N_4) \right\}$$

$$- N_1 \left\{ 0.187 (0.553 - 0.0153) - 0.118 (0) \right\}$$

$$= 0.96 \left\{ \overset{0.538}{\cancel{0.560}} N_2 - 0.093 N_3 + 0.010 N_4 \right\} - \overset{0.101}{\cancel{0.075}} N_1$$

$$x_2 \cdot \text{denominator} = - \overset{0.101}{\cancel{0.075}} N_1 + \overset{0.516}{\cancel{0.384}} N_2 - 0.0893 N_3 + 0.010 N_4$$

$$\cancel{x_2 = -0.225 N_1 + 1.153 N_2 - 0.2682 N_3 + 0.029 N_4}$$

$$x_2 = -0.303 N_1 + 1.550 N_2 - 0.268 N_3 + 0.029 N_4$$

denominator = 0.333

$$x_3 \cdot \text{denominator} = \begin{vmatrix} .96 & .118 & N_1 & 0 \\ .187 & .7 & N_2 & 0 \\ 0 & .186 & N_3 & .082 \\ 0 & 0 & N_4 & .79 \end{vmatrix}$$

$$= 0.96 \begin{vmatrix} .7 & N_2 & 0 \\ .186 & N_3 & .082 \\ 0 & N_4 & .79 \end{vmatrix} - 0.118 \begin{vmatrix} .187 & N_2 & 0 \\ 0 & N_3 & .082 \\ 0 & N_4 & .79 \end{vmatrix}$$

$$+ N_1 \begin{vmatrix} .187 & .7 & 0 \\ 0 & .186 & .082 \\ 0 & 0 & .79 \end{vmatrix}$$

$$= 0.96 \left\{ 0.7 \begin{vmatrix} N_3 & 0.082 \\ N_4 & 0.79 \end{vmatrix} - N_2 \begin{vmatrix} .186 & .082 \\ 0 & .79 \end{vmatrix} \right\}$$

$$- 0.118 \left\{ 0.187 \begin{vmatrix} N_3 & 0.082 \\ N_4 & .79 \end{vmatrix} - N_2 \begin{vmatrix} 0 & 0.082 \\ 0 & .79 \end{vmatrix} \right\}$$

$$+ N_1 \left\{ 0.187 \begin{vmatrix} 0.186 & .082 \\ 0 & .79 \end{vmatrix} - 0.7 \begin{vmatrix} 0 & .082 \\ 0 & .79 \end{vmatrix} \right\}$$

$$= 0.96 \left\{ 0.7 (0.79 N_3 - 0.082 N_4) - N_2 (0.147 - 0) \right\}$$

$$- 0.118 \left\{ 0.187 (0.79 N_3 - 0.082 N_4) \right\} + N_1 \left\{ 0.187 (.147) \right\}$$

$$= 0.96 \left\{ (0.553 N_3 - 0.057 N_4) - 0.147 N_2 \right\}$$

$$- 0.118 \left\{ 0.148 N_3 - 0.015 N_4 \right\} + 0.027 N_1$$

$$= 0.531 N_3 - 0.055 N_4 - 0.141 N_2 - 0.017 N_3 + 0.002 N_4 + 0.027 N_1$$

$$x_3 \cdot \text{denominator} = 0.027 N_1 - 0.141 N_2 + 0.514 N_3 - 0.053 N_4$$

$$x_3 = 0.081 N_1 - 0.423 N_2 + 1.544 N_3 - 0.159 N_4$$

$$x_4 \cdot \text{denominator} = \begin{vmatrix} .96 & .118 & 0 & N_1 \\ .187 & .7 & .118 & N_2 \\ 0 & .186 & .7 & N_3 \\ 0 & 0 & .186 & N_4 \end{vmatrix}$$

$$= .96 \begin{vmatrix} .7 & .118 & N_2 \\ .186 & .7 & N_3 \\ 0 & .186 & N_4 \end{vmatrix} - 0.118 \begin{vmatrix} .187 & .118 & N_2 \\ 0 & .7 & N_3 \\ 0 & .186 & N_4 \end{vmatrix}$$

$$- N_1 \begin{vmatrix} .187 & .7 & .118 \\ 0 & .186 & .7 \\ 0 & 0 & .186 \end{vmatrix}$$

$$= 0.96 \left\{ 0.7 \begin{vmatrix} .7 & N_3 \\ .186 & N_4 \end{vmatrix} - 0.118 \begin{vmatrix} .186 & N_3 \\ 0 & N_4 \end{vmatrix} + N_2 \begin{vmatrix} .186 & .7 \\ 0 & .186 \end{vmatrix} \right\}$$

$$-0.118 \left\{ 0.187 \begin{vmatrix} .7 & N_3 \\ .186 & N_4 \end{vmatrix} - 0.118 \begin{vmatrix} 0 & N_3 \\ 0 & N_4 \end{vmatrix} + N_2 \begin{vmatrix} 0 & .7 \\ 0 & .186 \end{vmatrix} \right\}$$

$$- N_1 \left\{ 0.187 \begin{vmatrix} .186 & .7 \\ 0 & .186 \end{vmatrix} - 0.7 \begin{vmatrix} 0 & .7 \\ 0 & .186 \end{vmatrix} + .118 \begin{vmatrix} 0 & .186 \\ 0 & \cancel{.186}\ 0 \end{vmatrix} \right\}$$

$$= 0.96 \left\{ 0.7 (0.7 N_4 - 0.186 N_3) - 0.118 (0.186 N_4) + N_2 \underset{.034596}{(0.035)} \right\}$$

$$-0.118 \left\{ 0.187 (0.7 N_4 - 0.186 N_3) \right\} - N_1 \left\{ 0.187 \underset{.034596}{(0.035)} \right\}$$

$$= 0.96 \left\{ 0.49 N_4 - 0.1302 N_3 - \underset{.021954}{0.022 N_4} + \underset{.034596}{0.035 N_2} \right\}$$

$$- 0.118 \left\{ \underset{.1309}{0.131 N_4} - \underset{.03478}{0.035 N_3} \right\} - \underset{.00647}{0.007 N_1}$$

$$= \underset{.00647 N_1}{-0.007 N_1} + 0.4704 N_4 - 0.125 N_3 - 0.021 N_4 + \underset{.0332 N_2}{0.034 N_2} - \underset{.015446}{0.015 N_4} + \underset{.00410}{0.004 N_3}$$

$$x_4 \cdot \text{denominator} = \underset{-0.00647 N_1}{-0.007 N_1} + \underset{+0.0332 N_2}{0.034 N_2} \underset{-0.121 N_3}{-0.121 N_3} + \underset{+0.4549}{0.434 N_4}$$ Subtraction error

$$x_4 = -0.021 N_1 + 0.102 N_2 - 0.363 N_3 + 1.303 N_4$$

$$-0.01944 N_1 + 0.09974 N_2 - 0.36353 N_3 + 1.3667 N_4$$

4129 w vi Hi 1977 data